1-24-2024

Morphodynamic Diversity of Alluvial River Systems in the Upper Yellow River Watershed, Qinghai-Tibet Plateau

Xiwei Guo
Syracuse University

Abstract

Alluvial rivers exhibit diverse forms and dynamic processes based on the physiographic configuration and in response to the interactions between water flow, sediment transport, and channel morphology. The current understanding of the formative and evolutionary processes controlling channel morphology and the dynamics remains incomplete, as it falls short of explaining and predicting a variety of channel forms and processes. Using data derived from remote sensing analysis and field measurement, this dissertation investigates the morphological characteristics, lateral adjustment, and channel-floodplain interactions of meandering and anabranching rivers in a pristine, high-altitude environment in the source watershed of the Yellow River, eastern Qinghai-Tibet Plateau. Through three chapters (i.e., Chapter 2, 3, and 4) that respectively examine meandering channels, meandering river floodplains, and anabranching channels, this dissertation explores the pioneer issues regarding fluvial processes in these systems, demonstrating the morphodynamic complexity embraced in meandering and anabranching systems. In Chapter 2, I characterize meander-bend morphology and propose a quantitative criterion to distinguish compound-form meander bends from simple meander bends. I also quantify the lateral migration of meander bends, examine the relationships between bend morphology and lateral migration, and assess the geomorphic implications of it, highlighting the inherent mechanism of meander-bend evolution through which the planform structures remain stable. In Chapter 3, I characterize hydrologic connectivity and morphological variation of oxbow lakes, an essential geomorphic unit in floodplains of meandering rivers, and find very low hydrologic connectivity between oxbow lakes and the main channel, owing to the unique paleogeographic setting of the study area, using a newly proposed probability-based index for quantifying hydrologic connectivity. In Chapter 4, I scrutinize the dynamic patterns of the

anabranching system and assess their flow efficiency based on five heuristic anabranching structures. The results explicitly suggest that island dynamics and their interactions with channels are the key components for understanding anabranching evolution and stability. Overall, as Chapter 5 concludes, this dissertation provides new insights into the morphodynamic complexity of alluvial channel forms and processes and sets a foundation for future research to serve global and trending needs.

Morphodynamic Diversity of Alluvial River Systems in the Upper Yellow River Watershed, Qinghai-Tibet Plateau

by

Xiwei Guo

B.A., University of Colorado, Boulder, 2015
M.A., University of Texas, Austin, 2017

Dissertation
Submitted in partial fulfillment of the requirements for the degree of
Doctor of Philosophy in Geography

Syracuse University
December 2023

Acknowledgment

I would like to express my deepest appreciation to members of the advising committee: Dr. Peng Gao, Dr. Jake Bendix, and Dr. Jane Read, for their guidance throughout the process of dissertation research, and to all other members of the Department of Geography and the Environment at Syracuse University for their continuous support.

I would also like to thank my parents for their love, understanding, and encouragement, which have been the bedrock of my achievements and will continue to inspire me on future journeys.

Table of Contents

List of Figures

Chapter 1

Chapter 2

Chapter 3

Chapter 4

List of Tables

Chapter 2

Chapter 4

Chapter 1: Introduction

Rivers are a fundamental landform on Earth, which shape valleys, floodplains, deltas, and other landscapes, and change morphology in space and over time (Ashworth and Lewin, 2012; Kleinhans et al., 2014; Church and Ferguson, 2015). As a critical natural resource to the livelihood and well-being of humans, rivers supply fresh water, facilitate navigation, and provide diverse ecosystem services (e.g., Wohl, 2005; Dudgeon et al., 2006). A variety of disasters, such as floods, debris flows, and bank erosion, however, are brought by rivers as well. To minimize these disasters while optimizing their roles as resources, river management has been practiced throughout the history of human civilization. For instance, the Chinese character of "political order" (治), with three waterdrops on the left, originally represents river-channel dredging. This character demonstrates the importance of river management in maintaining peace and prosperity in ancient human societies. Today, with the increasing use of rivers for shipping, hydropower, irrigation, recreation, and other needs, strategic management of rivers becomes more critical than ever (Palmer et al., 2005; Lehner et al., 2011; Wohl et al., 2015). Therefore, developing sustainable plans for river management requires a comprehensive understanding of morphological characteristics and their dynamic responses to variable fluvial processes at multiple spatiotemporal scales.

Alluvial and semi-alluvial rivers can rapidly adjust their channels through changes in bed configuration, channel depth and width, planform property, and channel gradient, exhibiting diverse forms and dynamic processes. Particularly, the dynamic processes involved in planform property include, but are not limited to, width adjustment, lateral migration, avulsion, and bifurcation (e.g., Lane et al., 1996; Bertoldi and Tubino, 2007; Nanson and Huang, 2017). In response to these processes, alluvial channels exhibit various types of planform patterns, which

can be generally categorized as single-thread (e.g., straight and meandering) and multi-thread (e.g., anabranching and braided) channels (Leopold and Wolman, 1957; Rust, 1978; Schumm, 1985; Rosgen, 1994; Van den Berg, 1995; Lewin and Brewer, 2001). Substantial efforts have been made to establish theories (e.g., hydraulic geometry, magnitude and frequency of discharges, and sediment rating curves) interpreting the complex interactions between water flow, sediment transport, and the associated morphological changes of channels. Nonetheless, a thorough understanding of these complex processes has yet to be achieved. For example, the limited recognition of the prevalence of anabranching pattern in alluvial rivers under across the globe might have caused inadequate discernment of fluvial processes involved in multi-channel rivers and on differentiating and predicting channel patterns under various physiographic settings (Latrubesse, 2008; Nanson, 2013; Henriques et al., 2022; Wang et al., 2022). Moreover, the prevailing fluvial processes controlling channel morphology and its dynamics may be interrupted by anthropogenic activities, such as urbanization, deforestation, and dam construction, and such impacts are evidenced to accelerate in recent decades with local and global environmental changes (Surian and Rinaldi, 2003; Gregory, 2006; Latrubesse et al., 2017; Best, 2019). Therefore, one of the biggest challenges in investigating the forms and processes of alluvial rivers is to separate the impacts of human activities from the underlying natural processes on river morphology and its spatiotemporal changes. Therefore, undisturbed rivers that have their banks, beds, and longitudinal profiles remain in pristine conditions potentially provide a "shortcut" for elucidating such natural processes.

Located in the "third pole" of the planet – the Qinghai-Tibet Plateau, the source watershed of the Upper Yellow River has been subjected to very limited anthropogenic forces. It,

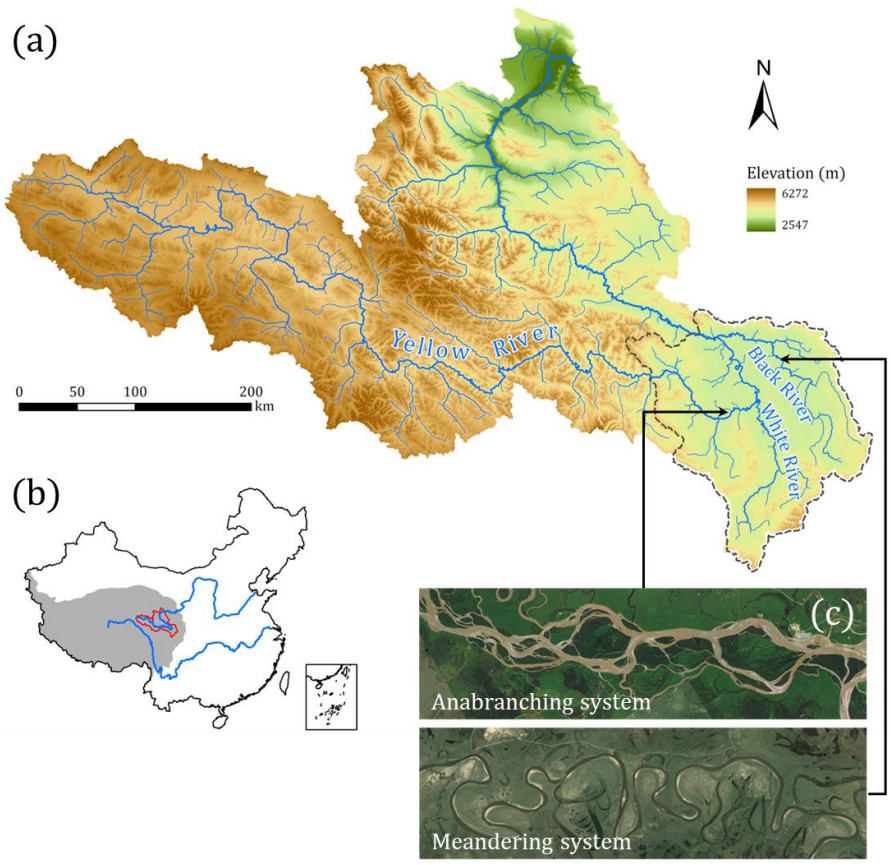

Figure 1.1 Overview of the study area. (a) Topography of the source watershed of the Upper Yellow River and the Zoige Basin (dotted outlined area); (b) Locations of the source watershed of the Upper Yellow River (red outlined area) and the Qinghai-Tibet Plateau (grey area) in China; (c) Planform views (Google Earth images) of the anabranching system in the mainstream of the Upper Yellow River and the meandering system in the Black River in the Zoige Basin.

therefore, provides an opportunity for us to examine fluvial processes and the corresponding morphological responses of rivers under natural conditions. Specifically, the Upper Yellow River (Fig. 1.1a) originates from the Bayan Har Mountains, then flows eastwards until reaching the "First Great Bend" in the Zoige Basin western China. Surrounded by the orographic-uplifted Minshan Mountains to the south, the Guoluo Mountains to the west, the Amne-Machin Mountains to the north, and the Dieshan Mountains to the east, the Zoige Basin (Fig. 1.1a) is a relatively flat area with the mean elevation of 3,400 m. The basin once was a giant lake about 37 ka ago and gradually collapsed and drained due to headward incision of the paleo Yellow River

(Chen et al., 1999; Zeng et al., 2017; Wang et al., 2023). Consequently, large extents of peats were fostered due to the extensive growth of herbaceous plants, leading to the modern Zoige Basin with the largest alpine peatland in the world. Alluvial rivers developed thereafter vary greatly in size, shape, and hydrogeomorphic properties. They generally fall into two major categories: meandering and anabranching rivers (Fig. 1.1c). In particular, meandering rivers are developed along many first-order tributaries of the Upper Yellow River, including its largest tributaries (i.e., the Black and the White Rivers; Fig. 1.1a) in the source watershed, while anabranching rivers are mainly distributed along the mainstream of the Upper Yellow River within the basin (Fig. 1.1a). Previous work has demonstrated that the transition from one type of alluvial channel into another in the source watershed is mainly controlled by the channel gradient, vegetation distribution, and valley width (Li et al., 2013; Yu et al., 2014), while detailed analysis of the morphodynamic characteristics of each type of alluvial system has not been conducted.

Globally, knowledge about the distinction of meandering rivers from other alluvial patterns, especially the braided ones has been built upon decades of studies based on field measurements, observations from remotely sensed data, flume experiments, and numerical simulations (Leopold and Wolman, 1957; Schumm, 1985; Smith, 1998; Lewin and Brewer, 2001; Mueller and Pitlick, 2014). The well-known threshold of these two river types was proposed by Leopold and Wolman (1957), which may be defined as $S = 0.06Q^{-0.44}$, where S and Q denote channel gradient and bankfull discharge in ft^3/s, respectively. This threshold illustrates the physiographic difference between meandering and braided channels in that the latter tends to be developed in steeper valley settings than the former for a given range of river discharges. Later, Schumm (1985) argued that the transport mode of sediment is a major control

of alluvial channels. Along this line, he classified the rivers into suspended load-dominated ones that have relatively small width/depth ratios and large channel sinuosity (i.e., the meandering rivers), bedload-dominated ones having larger width/depth ratios and greater channel multiplicity (i.e., braided pattern), as well as the mixed type. Numerous subsequent studies have demonstrated that many rivers can be featured by both types of sediment loads (Eaton et al., 2010; Nicholas, 2013; Wohl, 2019). Furthermore, it is not uncommon to find multiple types of channel pattern developed in the same reaches of natural rivers.

Although the fluvial processes driving the changes of meandering rivers, including bank erosion (e.g., Darby et al., 2002; Gao et al., 2021), point bar formation (e.g., Nanson, 1980; Mason and Mohrig, 2019), and the resultant channel lateral migration and meander cutoff (e.g., Constantine and Dunne, 2008; Van Dijk et al., 2012; Donovan et al., 2021), have been substantially investigated, there still remain many unknown issues, such as modeling lateral migration rate of meander bends, the processes associated with compound-form bends, and intra-stage morphodynamics of abandoned meander bends (Hudson et al., 2012; Hooke, 2013).

The prevalence of anabranching systems in global rivers and their morphodynamic characteristics have apparently been overlooked, which is primarily due to the common coexistence of anabranching pattern and other patterns development in many rivers, as well as the scarcity of anabranching pattern in small rivers. Generally, anabranching rivers are known to differ from braided ones in that the former may maintain the multithread pattern at the bankfull condition and have greater stability than the latter (e.g., Nanson, 2013; Rhoads, 2020). However, no consensus has been reached thus far on the process-based mechanisms that catalyze morphological stability of anabranching rivers. Specifically, although theoretical explanations based on channel hydraulics highlight a greater stability of “simple” anabranching pattern that

develops fewer channels (i.e., ≤ 4; Huang and Nanson, 2007; Eaton et al., 2010; Carling et al., 2014), natural anabranching rivers with more complex morphology are widely identifiable in rivers around the world, including the anabranching reach in the Upper Yellow River.

To address these scientific gaps, this dissertation aims to characterize the key morphological and morphodynamic properties involved in the meandering and anabranching systems in the study area and reveal the underlying processes through the lens of fluvial geomorphology. The dissertation is organized as follows: Chapter 2 examines morphological characteristics and lateral migration of the meandering reach of the Black River; Chapter 3 evaluates hydrologic connectivity and morphological responses to the variable hydrologic regime of oxbow lakes developed in the floodplain adjacent this meandering reach; Chapter 4 dives into the morphodynamic characteristics and the associated evaluation of channel stability of the anabranching reach along the main channel of the Upper Yellow River.

Chapter 2: Morphological characteristics and lateral changes of the meandering systems[1]

2.1 Introduction

Meandering rivers encompass a broad spectrum of single-threaded channels that exhibit various sinuous planform patterns (Leopold and Wolman, 1960; Schumm, 1985; Hooke, 2013). They are typically developed in alluvial environments and repeatedly migrate over floodplains (Hooke, 1984; Howard, 1992; Nicoll and Hickin, 2010). A river channel may be defined as "meandering" when its sinuosity is greater than 1.3-1.5, although a single, clear threshold value of sinuosity is hard to be determined because it is scale-dependent (Chang, 1984; Ebisemiju, 1994). Meandering channels may increase their sinuosity by lateral migration and decrease it by cutoff (Ikeda et al., 1981; Hickin and Nanson, 1984; Constantine and Dunne, 2008; Güneralp and Rhoads, 2009). Spatial and temporal patterns of meanders are controlled by hydrogeomorphic properties of channels and floodplains, which arise from complex interactions among river flow, sediment transport, channel morphology, and floodplain characteristics (Ferguson, 1975; Dietrich et al., 1979; Anthony and Harvey, 1991; Simon and Collison, 2002; Perucca et al., 2007; Hooke, 2013; Constantine et al., 2014, Schwendel et al., 2015).

Research on forms and processes of meandering channels includes empirical and theoretical analyses for explaining and predicting patterns of meander morphology and its changes at multiple spatial and temporal scales (Stølum, 1996; Güneralp et al., 2012; Hooke, 2013; Church and Ferguson, 2015). While empirical studies aim to characterize meander processes from different aspects, such as bank erosion, bar formation, cutoff, and, more

[1] This chapter has been published in:
Guo, X., Gao, P., & Li, Z. (2021). Morphological characteristics and changes of two meandering rivers in the Qinghai-Tibet Plateau, China. *Geomorphology*, *379*, 107626. https://doi.org/10.1016/j.geomorph.2021.107626

generally, lateral migration (e.g., Nanson, 1980; Thorne, 1991; Frothingham and Rhoads, 2003; Constantine et al., 2014; Li and Gao, 2019a), theoretical approaches rely on experimental or numerical models to simulate morphodynamic processes involved in meander evolution (e.g., Ikeda et al., 1981; Zolezzi and Seminara, 2001; Darby et al., 2002). Many of these studies highlighted hydrologic processes in controlling channel morphological adjustment (e.g., Dietrich, 1987; Markham and Thorne, 1992), whereas others focused on revealing kinematic linkages between bend morphology and migration (e.g., Parker et al., 1983; Hickin and Nanson, 1984; Hudson and Kesel, 2000; Hooke, 2007). Experimental and modeling outcomes are typically supported by in-situ measured data and/or planform morphology of specific meandering rivers (e.g., Howard and Knutson, 1984; Lancaster and Bras, 2002), which lead to an enduring limitation: the findings lack generalization (Güneralp and Marston, 2012). The main reason causing this limitation is that repetitively measuring meander channel morphology and its temporal changes is labor-intensive and thus could not be widely deployed in practice. For instance, it is well known that bend migration is not only controlled by intensified shear stress along the outer bank but also affected by bar development as the latter changes flow structure (Seminara, 2006). Yet, measuring these hydraulic parameters and bend morphology over time is pragmatically difficult because of the obvious logistic challenges, though there have been very limited studies on detailed velocity distribution in channel cross-sections and spatial variations of bank properties along a meander bend (Frothingham and Rhoads, 2003; Zinger et al., 2013; Konsoer et al., 2016). Therefore, using satellite imagery to effectively extract bend morphology over various spatial and temporal ranges, and to understand how meander planform patterns are tied to its lateral migration is still popular in current research frontiers (Hooke and Yorke, 2010;

Ollero, 2010; Gilvear and Bryant, 2016; Schwenk et al., 2017; Guo, et al., 2019; Ielpi and Lapôtre, 2019).

Studies in the past five decades have advanced our knowledge in: 1) quantifying bend geometry using morphological metrics such as bend amplitude, wavelength, and curvature (e.g., Magdaleno and Fernández-Yuste, 2011; Yousefi et al., 2016); 2) determining diverse trajectories of bend migration using a typology of bend change (e.g., Hooke and Harvey, 1983; Morais et al., 2016); 3) understanding the lag between locations of maximum bend curvature and migration rate, and their relationships (Nanson and Hickin, 1983; Güneralp and Rhoads, 2009; Sylvester et al., 2019). Nonetheless, it is far from reaching general models that enable the prediction of the evolution of meandering rivers under various environments. There are still two missing pieces in our current understanding of meandering rivers with regards to river environments and the complexity of river planform. First, though meandering rivers with complex planform structures have been noted and studied (e.g., Frothingham and Rhoads, 2003; Gautier et al., 2007; Hooke, 2013), their patterns of channel morphology and dynamics are not fully understood yet. Second, meandering rivers in temperate and tropical lowland environments have been extensively investigated, but little attention has been paid to those developed in high-elevation environments where the hydrological regime, land cover, and other hydrogeomorphic factors may be different.

In this study, we investigated morphological characteristics and dynamic changes of two meandering rivers with complex planform structures in the Upper Yellow River Watershed, located in eastern Qinghai-Tibet Plateau (QTP) of western China (Fig. 1.1a). Particularly, we attempted to achieve three objectives: 1) characterizing channel planform morphology of the two meandering rivers; 2) revealing patterns of channel morphological and morphodynamic changes;

3) assessing geomorphological differences between the two rivers and among other meandering rivers in the world.

2.2 Materials and methods

2.2.1 Study area

Sourced from the Bayan Har Mountains in northeastern QTP, the Upper Yellow River runs for about 600 km until arriving at the "First Great Bend" where the two main tributaries, the Black and the White rivers converge (Fig. 2.1b). The contributing areas of the two rivers form the Zoige Basin whose mean elevation is approximately 3,400 m. The Zoige Basin has a relatively flat topography surrounded by high mountains formed around 14 million years ago due to orographic activities (Nicoll et al., 2013). The basin is filled with lacustrine deposits that are at least 30 m deep (Chen et al., 1999), allowing local rivers to develop alluvial channels. The Zoige basin has a typical highland climate and is strongly influenced by the East Asian Monsoon that brings precipitation during the summer months. The Black and the White rivers both originate from the Minshan Mountains and generally flow northward through the Zoige Basin with the former situated in the north and the latter in the south (Fig. 2.1b). Their drainage areas are 7,600 and 5,500 km^2, respectively, and their mean annual discharges at the outlets are 58 and 56 m^3/s, respectively.

This study focused on the middle and lower reaches of the two rivers (i.e., the lower Black River and the lower White River) where meandering channels are extensively developed. Their floodplains are featured by ample oxbow lakes and are covered by uniformly distributed peat or grass. Specifically, the studied reach of the Black River starts at the first upstream confluence where the Requ River joins the Black River in the Town of Dazhasi and ends at the

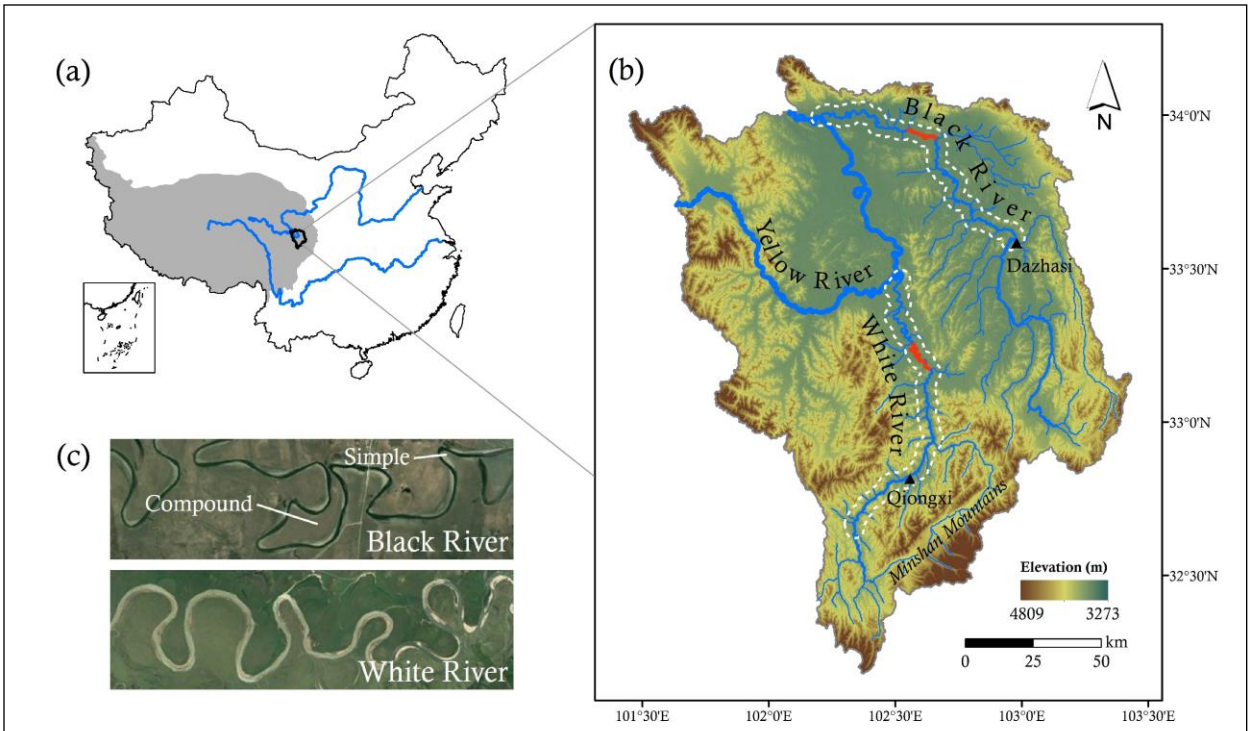

Figure 2.1 Overview of the study area. (a) Qinghai-Tibet Plateau (the shaded area) and the Zoige Basin (the outlined area) in China; (b) Geomorphology of the Zoige Basin and locations of the studied reaches (within dotted lines); (c) Plan view of a selected section of each studied river (their locations are marked in red in b) and examples of simple and compound bends in the Black River.

outlet of the Black River (Fig. 2.1b). The total channel length is approximately 240 km. For the White River, we studied the lowermost 190 km reach before it enters the Upper Yellow River (Fig. 2.1b). The reach-averaged sinuosity of the lower Black and White rivers are 2.03 and 1.63, respectively, though their local channel segments commonly have higher sinuosity (> 2.0). Their average channel widths are 86 and 91 m, respectively. The lower Black River develops many compound bends with convoluted loops that form highly sinuous channels, whereas the lower White River has fewer compound bends but more mid-channel and lateral bars, especially near the downstream end (Fig. 2.1c). The average channel gradients are 0.09‰ and 0.4‰ for the studied reaches of the Black and the White rivers, respectively. Lateral migration and cutoff are the predominant processes shaping their planform structures with the latter dominated by neck cutoff. Both studied reaches are gravel-bedded and have comparable grain size distributions in

channel banks and beds. Banks along the two studied reaches have a two-layer vertical structure with the top one comprised of soil-vegetation (peat or grass) mixture and the lower one comprised of fine sand and silt (the average median particle size is 89 μm based on analysis of particle size distribution from several field-collected samples) that are graded into the bank toe formed by fine gravels. Because the top mixed layer has a much higher resistance to fluvial erosion than the lower layer does, channel banks often form cantilever arms. Therefore, cantilever failure due to continuous fluvial erosion is the key mechanism of bend evolution in the Zoige Basin (Li and Gao, 2019a).

The two studied reaches largely remain undisturbed. Human activities in the Zoige Basin are primarily grazing. Along the main channels of the two rivers, the only two towns, Qiongxi (Hongyuan County seat) and Dazhasi (Zoige County seat), have a population of around 10,000 in each. The greatest environmental change within the Zoige Basin over the past few decades was wetland degradation, which was mainly attributed to the excavation of artificial ditches between the 1960s and 1990s that had drained 57.7% of peatland areas as of 2015 and gully erosion on hillslopes (Qiu et al., 2009; Li et al., 2018; Li and Gao, 2019b; Li et al., 2019). In general, channels of the two rivers largely remain in pristine conditions.

2.2.2 Methods

2.2.2.1 Data acquisition and error assessment

Using Landsat Thematic Mapper (TM) and Operational Land Imager (OLI) data with a spatial resolution of 30 m, we extracted channel planform morphology in 1986 and 2017. The data selected were acquired in the summer when cloud cover was minimal and the water level was high, such that meander bends along the reaches may be clearly identified. Since the rate of

channel migration in the studied reaches was relatively small, an observation from our preliminary study, the selected satellite imagery of 1986 and 2017, spanning over 31 years, was sufficient to capture changes of meander bends. Because several segments of the channels in both studied reaches (accounting for less than 5% of total channel lengths) were not identifiable due to cloud cover in data acquired in 1986, an additional TM image obtained in summer 1990 was used for compensation. The satellite images were then imported into ArcGIS where channel banks and centerlines were digitized. The bank lines were digitized according to the identified vegetation boundaries along the channels that best represent channel bankfull width (e.g., Winterbottom, 2000; Frias et al., 2015; Donovan et al., 2019). These vegetation boundaries were determined using the Normalized Distribution Vegetation Index (NDVI) based on a threshold of 0.2 (Bertoldi et al., 2011; Henshaw et al., 2013) such that areas with pixel values smaller than the NDVI threshold were identified as river channels. This included both water surfaces and bars. Channel centerlines were then delineated based on identified bank lines.

There are two main types of uncertainties associated with data acquisition and processing in this study. The first was the registration error from the original satellite images, which could be viewed in the metadata. The Root Mean Square Error (RMSE) for data registration was 6.95 and 7.83 m for the 1986 and 2017 images, respectively. These errors accounted for less than 10% of the average channel width for both studied reaches. The second may arise during the process of channel digitization, which in this study was assessed by calculating the mean lateral displacement of a section of channel bank from 50 times of re-digitization under the same scale (Downward et al., 1994). We found that the digitizing error was 2.3 m (±0.65) under the scale of 1:10,000. The total error (E_t) could be subsequently calculated by:

$$E_t = \sqrt{{E_1}^2 + {E_2}^2}$$

where E_1 and E_2 denote registration and digitizing errors, respectively. In this study, the calculated E_t was 7.32 and 8.16 m for the images of 1986 and 2017, respectively. In this study, therefore, any linear distance of channel morphology and lateral change less than 10 m was neglected and treated as zero.

2.2.2.2 Bend identification and morphometric analysis

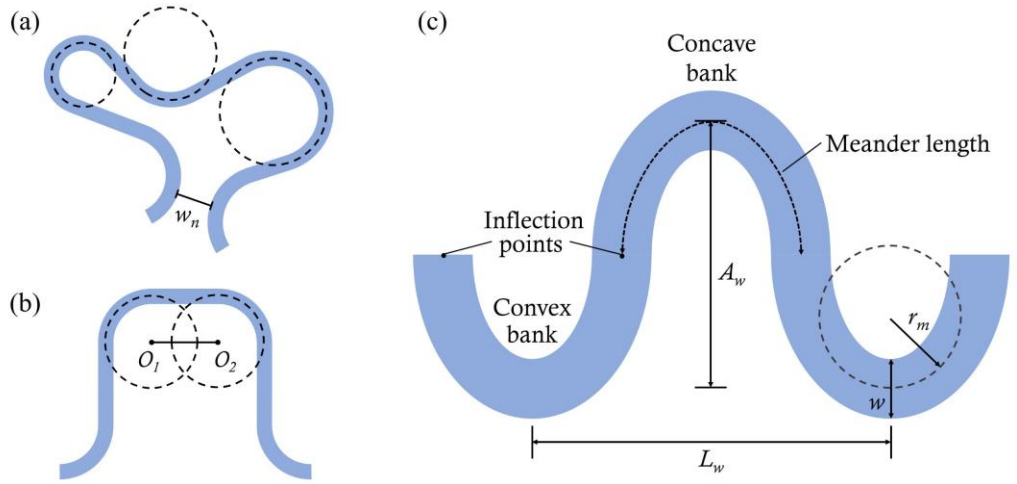

Figure 2.2 Bend morphology and morphometric parameters. (a) Identification of a compound bend when bend neck is present; (b) Identification of a compound bend when bend neck is not present. Shapes of the compound bends are based on Figure 1H and 1P in Brice (1974); (c) Definition of morphometric parameters in an ideal sine-curved meander bend.

Meander bends were identified based on channel centerlines at the initial condition of the study period (i.e., 1986). A bend was identified where there is an arc of at least 60° along the channel centerline (Brice, 1974). All qualified arcs were subsequently classified as either simple bends or sub-bends of compound bends. While a simple bend only contains one qualified arc, a compound bend contains multiple qualified arcs adjacent to each other. A potential problem associated with the classification of meander bend morphology is that quantitatively distinguishing compound bends from simple bends is difficult. For instance, a given channel segment with multiple qualified arcs may be identified as a single compound bend that involves

multiple sub-bends or as multiple simple bends developed in a row. Therefore, we defined that a compound bend may be identified in two conditions: 1) a bend neck (the narrowest part of the bend) is present and the neck width (w_n) is smaller than ten times the average channel width (w) at the neck (Fig. 2.2a); 2) if a bend neck is not present, the radii of qualified arcs (O_1, O_2, etc.) are located on the same side (i.e., the left or right bank) of the channel and the distance between any two adjacent radii is less than ten times of average w at bend apices (Fig. 2.2b). In the first condition, all qualified arcs beyond the bend neck are identified as sub-bends of the compound bend, as marked by dotted circles. This distance threshold (i.e., 10w) was determined based on our preliminary study of the meander bends. Although it may be subjective, it was sufficient for effective bend classification in the lower Black and White rivers.

The planform morphology of each bend was then characterized using bend amplitude (A_w) and wavelength (L_w) (Magdaleno and Fernández-Yuste, 2011) (Fig. 2.2c), which capture the degree of bend elongation and widening, respectively. Both parameters were normalized with w of each bend apex. For compound bends, A_w was measured from the farthest sub-bend and was normalized by the average w at bend apices of all sub-bends in the compound bend. Both A_w and L_w were used to compare statistically between the two types of bends (i.e., simple and compound) and between the two rivers. The parameters were also plotted against longitudinal distance, which was measured in downstream direction as valley length, rather than the channel length. Radius of curvature of meander bends (r_m) was measured for all identified bends by drawing circles that fit the arcs previously used for bend identification (e.g., Brice, 1974; Hooke, 1984; Nicoll and Hickin, 2010) (Fig. 2c). For compound bends, r_m was measured for each individual sub-bend. Meander bend curvature (r_m/w) was then calculated by normalizing r_m with w at bend apices.

2.2.2.3 Analysis of channel morphological changes

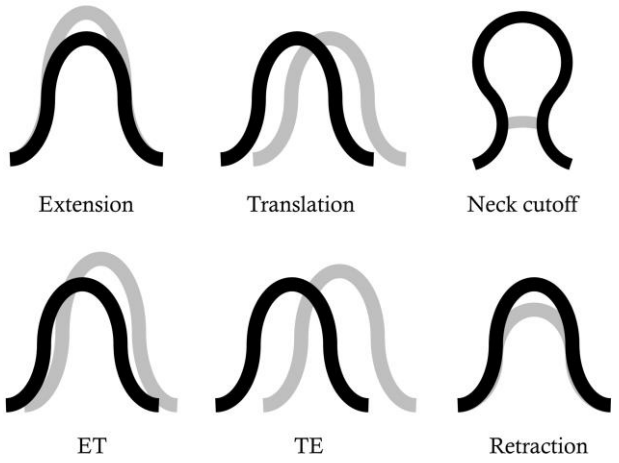

Figure 2.3 Major types of meander-bend change observed in the studied reaches of the Black and the White rivers. The black and the grey lines indicate the initial and final positions of the same channel, respectively.

Morphological changes of the studied reaches were characterized based on the typology (Hooke and Harvey, 1983; Hooke, 1984) describing relative positions of the same bend in the beginning (i.e., 1986) and ending (i.e., 2017) year (Fig. 2.3). By superimposing the two extracted centerlines and viewing the positional changes of each bend (sub-bends), we classified patterns of bend changes into four main categories: extension, translation, cutoff, and retraction (Fig. 2.3). Besides, a significant amount of bends in both reaches exhibited a pattern that combined both extension and translation. To reflect their differences with pure extension and pure translation, we created two more categories: extension with translation (ET) and translation with extension (TE). In particular, ET reflected the change of a bend that had migrated for a greater distance in the transverse direction (i.e., towards the floodplain) than in the longitudinal direction (i.e., downstream along the channel), whereas TE represented the change of a bend that had migrated for a greater distance longitudinally than transversely. Other than these types of bend changes, meander bends that involved lateral changes of large, semi-vegetated bars or islands were marked as “conditional” cases in the classification. These large bars and islands were rare in both studied reaches due to the dominant single-thread characteristic of meandering channels.

Meander morphological changes have also been commonly described by calculating the lateral migration rates of meander bends (Hickin and Nanson, 1984; Casado et al., 2016; Alber and Piégay, 2017). We measured lateral migration of all bends between 1986 and 2017 as the maximum displacement along the superimposed channel centerlines of each bend, including each sub-bend. A migration distance less than 10 m was considered as zero due to potential errors described before. For bends that changed by translation, the lateral migration was measured by linking points with a similar local curvature in each bend because it best reflected dynamic patterns of meander-bend change. In the studied reaches, the maximum migration typically occurred at or immediately downstream of bend apices. The 31-year total migration was then normalized with *w* and was statistically summarized among different types of bend change and between the two studied reaches. Because this study only involved one time period (i.e., 1986-2017) for both studied reaches, we used total migration distance over the 31-year study period for assessment. Migration distances of meander bends that changed by extension, translation, ET, and TE were then plotted against bend curvature to examine their relationships.

2.2.2.4 Analysis of morphodynamic patterns

In this study, morphodynamic patterns referred to spatial distributions of erosion and deposition in meander bends along the two studied reaches. Particularly, an area outside the bank boundary of 1986 but within the boundary of 2017 was considered an erosional area (A_e), while that within the bank boundary of 1986 but outside of the boundary of 2017 was considered a depositional area (A_d). Any individual area of erosion or deposition smaller than 100 m^2 or with an average width of smaller than 10 m was neglected owing to the potential uncertainties described before. A_e and A_d were not measured for bends that changed by cutoff and irregular

change. We calculated total A_e and A_d, their mean values, and coefficient of variation (*CV*). We also used the ratio of erosion to deposition (A_e/A_d) of each bend to examine reach-scale morphodynamic patterns with $A_e/A_d > 1$ indicating an erosion-dominated pattern and $A_e/A_d < 1$ indicating a deposition-dominated pattern. For meander bends without deposition (i.e., $A_d = 0$), we manually set $A_d = 1$ to assure that the ratio was mathematically meaningful.

2.3 Results

2.3.1 Bend morphology

Table 2.1: Summary of bend identification in the studied reaches.

		Black River	White River
		Number of bends	Number of bends
Total bends		149	141
Simple bends		99	128
Compound bends		50	13
Compound bends with	Two sub-bends	36	10
	Three sub-bends	9	3
	Four sub-bends	5	0

There were 149 meander bends identified in the lower Black River and 141 bends identified in the lower White River. In the former, 99 were simple bends and the remaining 50 were compound. In the latter, however, 128 bends were simple and only 13 were compound (Table 2.1). Among the compound bends in both studied reaches, the majority had two sub-bends, making up 72% (i.e., 36 out of 50) and 77% (i.e., 10 out of 13) of the total in the lower Black and White rivers, respectively. The number of compound bends with three sub-bends accounted for 18% (i.e., 9 out of 50) and 23% (i.e., 3 out of 13) in the lower Black and White rivers, respectively. Only in the lower Black River were there five compound bends with each had four sub-bends fostered, accounting for 10% (i.e., 5 out of 50) of total compound bends in the studied reach. In addition to the presence of more sub-bends, the lower Black River also exhibited a cluster pattern for compound bends. Among the 50

compound bends, 40 were distributed next to one another, forming several compound bend clusters with each containing two to six compound bends. By contrast, compound bends in the lower White River were sporadically located over the whole reach and did not exhibit any cluster pattern.

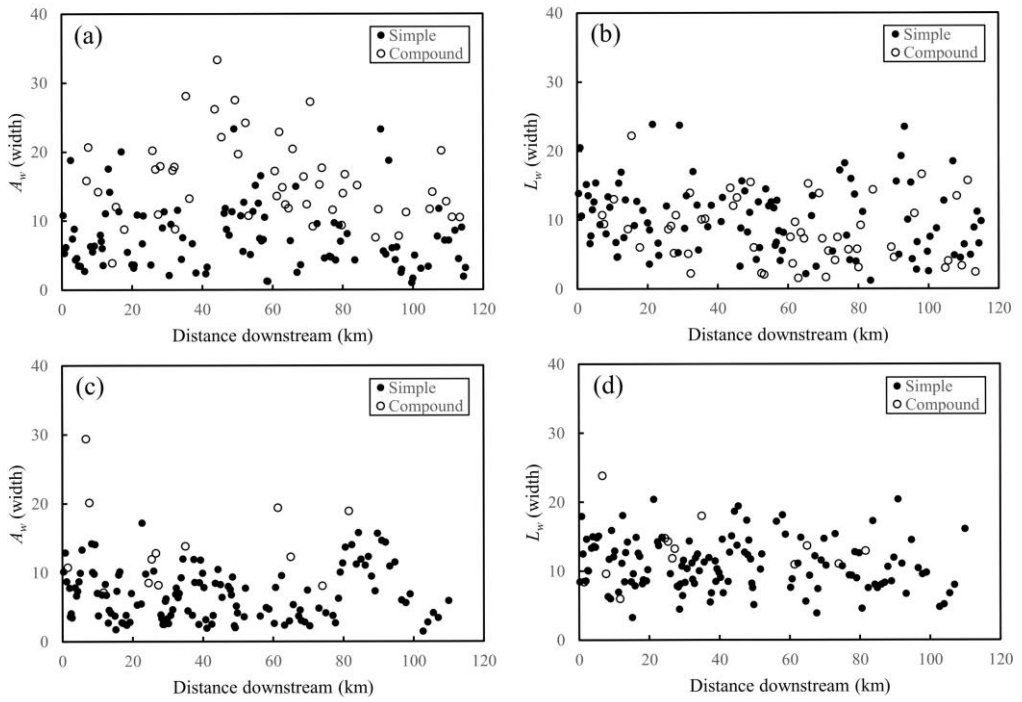

Figure 2.4 Longitudinal distributions of width-normalized A_w and L_w of simple and compound bends in the studied reaches of the Black River (a & b) and the White River (c & d).

In the lower Black River, A_w of simple bends ranged between 1 and 23.3 widths with the mean value of 7.6 widths and *CV* of 0.62. A_w of compound bends ranged between 3.9 and 33.3 widths with the mean value of 15.7 widths and *CV* of 0.39 (Fig. 2.4a), showing that A_w of simple bends was significantly smaller than that of compound bends ($p < 0.01$), but had greater variability than that of compound bends. In the lower White River, A_w ranged between 1.4 and 17.2 widths for simple bends and between 7.1 and 29.3 widths for compound bends. The mean A_w and *CV* were 6.8 widths and 0.54, respectively, for simple bends, and 13.9 widths and 0.44, respectively, for compound bends (Fig. 2.4c). Although A_w of simple and compound bends in the

lower White River were also significantly different ($p < 0.05$), the difference was relatively less, compared to that between simple and compound bends in the lower Black River.

By contrast, L_w did not differ significantly ($p > 0.05$) between simple and compound bends in both studied reaches. In the lower Black River, L_w ranged between 1.2 and 23.8 widths for simple bends and between 1.5 and 22.2 widths for compound bends. The mean L_w and *CV* were 10.1 widths and 0.49, respectively, for simple bends and 8.4 widths and 0.56, respectively, for compound bends (Fig. 2.4b). In the lower White River, L_w ranged between 3.3 and 20.4 widths for simple bends and between 6 and 23.8 widths for compound bends. The mean L_w and *CV* were 11 widths and 0.33, respectively, for simple bends and 13 widths and 0.33, respectively, for compound bends (Fig. 2.4d).

2.3.2 Morphological change

With each sub-bend of compound bends counted independently for analysis of bend morphological change, there were in total 218 bends in the lower Black River and 157 bends in the lower White River involved (Table 2.2). It was interesting to note that both rivers had a significant amount of bends that did not have traceable changes, which were 34 and 22, accounting for 16% and 14% of total bends in the lower Black and White rivers, respectively. In both rivers, extension was the most common mode of bend change, which accounted for 46% of bends in the lower Black River and 49% in the lower White River. Translation was also common in both studied reaches, taking 18% of the total bends in the lower Black River and 9% in the lower White River. All cases of translation in the two reaches involved bends that migrated towards the downstream direction. ET and TE, as the combination of bend extension and translation, occurred in a number of bends in both studied reaches, taking up about 8% and 7%,

Table 2.2: Summary of types of meander-bend change in the studied reaches. Each sub-bend of compound bends was analyzed independently for bend change.

Types of bend change	**Black River**	**White River**
	Number of bends	Number of bends
Total bends incl. sub-bends	218 (100%)	157 (100%)
Extension	100 (45.9%)	77 (49.0%)
Translation	39 (17.9%)	14 (8.9%)
Extension with translation	18 (8.3%)	5 (3.2%)
Translation with extension	15 (6.9%)	10 (6.4%)
Cutoff	1 (0.5%)	9 (5.7%)
Retraction	5 (2.3%)	3 (1.9%)
Conditional extension	2 (0.9%)	2 (1.3%)
Conditional retraction	3 (1.4%)	N/A
Translation with retraction	1 (0.5%)	N/A
Irregular change	N/A	15 (9.6%)
No change	34 (15.6%)	22 (14.0%)

respectively, of bends in the lower Black River. By contrast, about 3% and 6% of bends in the lower White River changed by the form of ET and TE, respectively.

In addition to extension, translation, ET, and TE, other types of bend change were rarer in the lower Black River but more common in the lower White River. From 1986 to 2017, the lower Black River only had one case of bend cutoff, whereas the lower White River had nine cases of cutoff that accounted for 6% of total bends in the studied reach (Table 2.2). There were also 15 cases in the lower White River classified as “irregular change”, which mostly occurred in bends that shared a portion of channel segments with the bends changed by cutoff. Morphological changes of those bends with “irregular change” therefore could not be classified into any of the identified modes. Moreover, retraction, translation with retraction, and bends impacted by lateral changes of bars and islands, marked with “conditional”, were relatively rare, in total accounting for 5% and 3% of all bends in the lower Black and White rivers, respectively.

Total migration distances from 1986 to 2017 were statistically summarized among the four major types of meander-bend change: extension, translation, ET, and TE (Fig. 2.5). In both studied reaches, bends changed by translation migrated significantly faster than those changed by extension ($p < 0.05$). The average total migration distances were 0.30 and 0.74 widths for bends

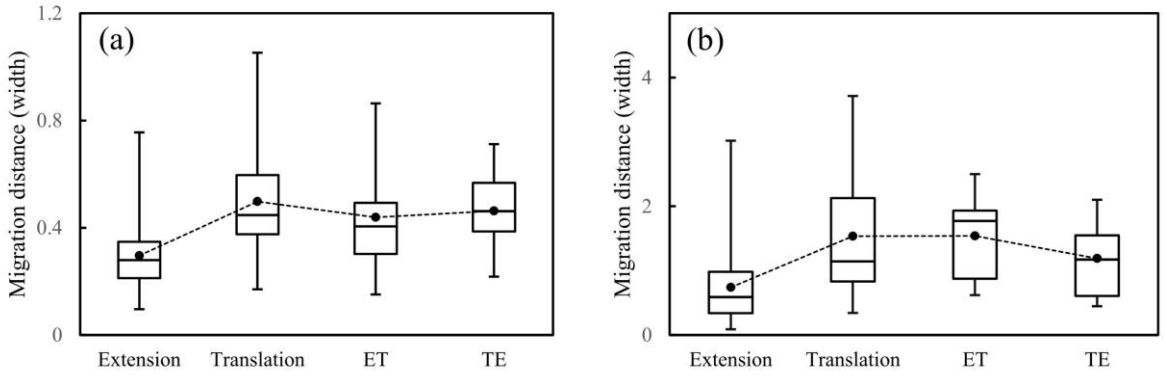

Figure 2.5 Statistical distributions (boxes show percentiles and whiskers show the maximum and minimum values) and mean values (dark dots) of width-normalized total migration distance among the four major types of meander-bend change in the studied reaches of the Black River (a) and the White River (b).

that changed by extension in the lower Black and White rivers, respectively, whereas the respective values for bends changed by translation in the two reaches were 0.50 and 1.50 widths. Therefore, the average migration distance of bends changed by translation was about 67% and 103% higher than that of bends changed by extension in the lower Black and White rivers, respectively. Migration distances of bends changed by ET and TE, in general, fell between those of pure extension and translation in both studied reaches, although in the lower White River the mean migration distance of bends changed by ET was as much as that of bends changed by translation (Fig. 2.5). Overall, meander bends in the lower White River tended to migrate much faster than bends in the lower Black River. On average, the total migration distance of bends in the lower White River was 147%, 206%, 250%, and 159% greater than those of the bends in the lower Black River for bends that changed by extension, translation, ET, and TE, respectively.

For bend that changed by extension and translation, multiple lateral migration rates were associated with a given value of r_m/w (Fig. 2.6). However, the range of variation increased first with increasing r_m/w, until it reached between two and three, and then decreased for the rest of r_m/w values. This pattern may be characterized by a single-mode parabolic envelop (black dotted

lines) showing that bend migration reached the maximum when r_m/w = 2-3 in both studied reaches. In addition, bends that changed by ET and TE were blended into those of the previous two types and followed similar patterns (Fig. 2.6).

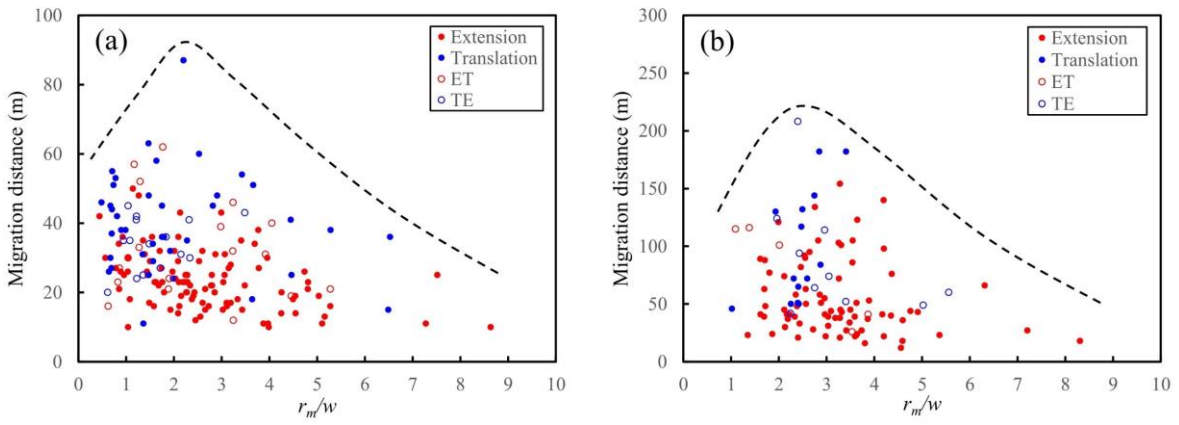

Figure 2.6 Relationships between migration distances from 1986 to 2017 of meander bends that changed by the four major modes of bend changes in the studied reaches of the Black River (a) and the White River (b) and r_m/w with the envelope curves.

2.3.3 Morphodynamic patterns

From 1986 to 2017, the total A_e and A_d in the lower Black River were 2.6 and 3 km^2, respectively. For all individual bends along the lower Black River, values of A_e varied within a limited range between zero and 0.04 km^2 with the mean value of 0.012 km^2 and *CV* of 0.58 (Fig. 2.7a). By contrast, with the mean of 0.014 km^2 and *CV* of 0.89, the longitudinal distribution of A_d in the lower Black River oscillated more widely with higher values prevailed in the downstream portion of the reach. The higher degree of variation for A_d was mostly caused by a few spikes representing substantial deposition in these bends. Some of the bends with larger A_d (i.e., > 0.06 km^2) were changed by conditional retraction triggered by the closure of secondary branches previously separated from the main channels by central bars. In general, locations of high and low A_e values were in phase with those of A_d, indicating that lateral migration was primarily

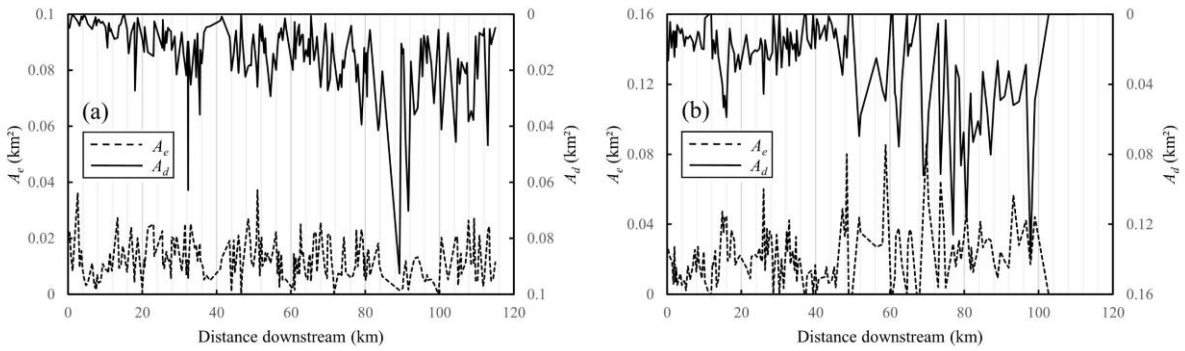

Figure 2.7 Longitudinal patterns of A_e and A_d in the studied reaches of the Black River (a) and the White River (b).

achieved by bend lateral movement that involved erosion and deposition to occur separately on the banks (Fig. 2.7a).

In the lower White River, while the general oscillating patterns of A_e and A_d were similar to those found in the Black River, the degree of oscillation tended to increase longitudinally along the reach (Fig. 2.7b). Values of both A_e and A_d were constrained in a relatively small range with the mean A_e and A_d of 0.021 and 0.019 km^2, respectively, in the first 50 km. Many spikes were present in the rest downstream portion of the reach, leading to the increased mean values of A_e and A_d (i.e., 0.032 and 0.055 km^2, respectively). Over the entire reach, the total value of A_e and A_d were 3.3 and 4.1 km^2, respectively. The mean A_e and A_d were 0.024 and 0.031 km^2, with their *CV*s of 0.65 and 0.82, respectively. It was signified that deposition was the dominant pattern in the studied reach of the White River and that lateral movement was generally greater in the lower White River than that in the lower Black River, a finding consistent with patterns of bend migration.

Longitudinal patterns of A_e/A_d in the two studied reaches suggested a non-linear decreasing trend in both reaches (Fig. 2.8). Although the relationship was featured by a discernable degree of scatter and different decreasing ranges, both reaches showed an erosion-dominated pattern in the upstream portion and a deposition-dominated pattern downstream. In

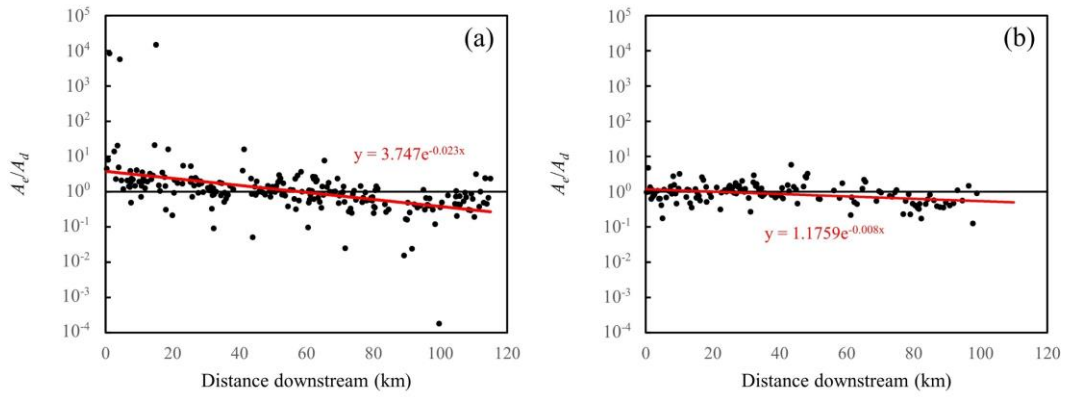

Figure 2.8 Longitudinal patterns of ratio A_e/A_d in the studied reaches of the Black River (a) and the White River (b).

the Black River, the turning point for the dominant morphodynamic pattern (i.e., from erosion to deposition-dominated) was about 60 km, the midpoint of the studied reach, indicating a spatially balanced morphodynamic pattern within the reach (Fig. 2.8a). By contrast, with the turning point for morphodynamic pattern located much more upstream, the lower White River exhibited a strong deposition-dominated trend (Fig. 2.8b).

2.4 Discussions

2.4.1 Relationship between bend curvature and channel migration

The results on the lower Black and White rivers showed that bend migration rates were nonlinearly related to bend curvature (r_m/w) with the migration maxima that occurred around r_m/w = 2.2 and 2.6, respectively for the two rivers (Fig. 2.6). Accordingly, bends with both smaller and greater curvatures than the critical value tended to migrate more slowly. This pattern was in accord with findings reported in many other meandering rivers (e.g., Hickin and Nanson, 1975; Nanson and Hickin, 1983; Hooke, 1997), which further confirmed the long-standing assertion that bend migration tended to reach the peak in bends with medium curvatures, represented by the value of r_m/w around three (Hickin, 1978). It should be noted that the

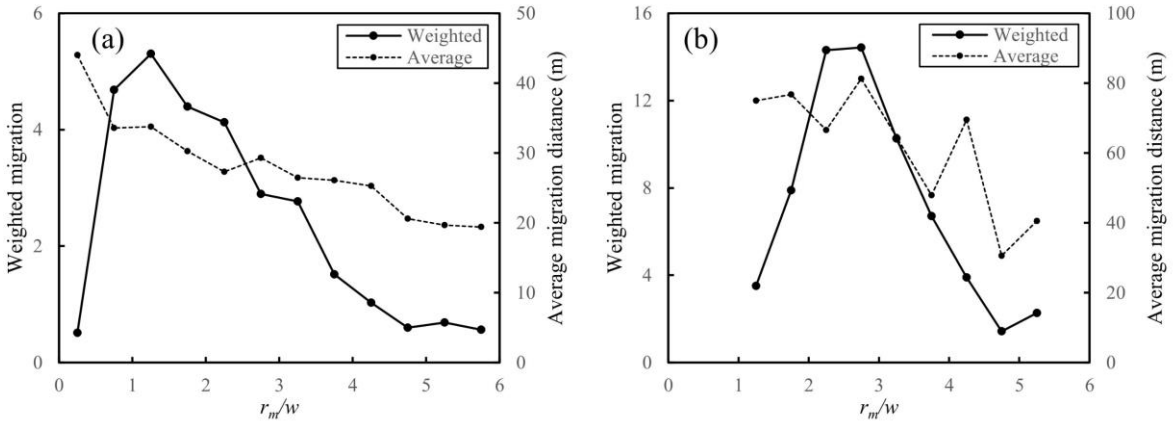

Figure 2.9 Average and weighted average migration distances of meander bends that changed by extension, translation, ET, and TE from 1986 to 2017 in the studied reaches of the Black River (a) and the White River (b). Both measures were calculated for every 0.5 increment of r_m/w, starting from 0 for the Black River and from 1 for the White River. Bend curvatures greater than 6 in the Black River and greater than 5.5 in the White River were summarized in the 5.5-6 and 5-5.5 intervals, respectively. Weighted average migration was calculated based on the proportion of the bend number in each class interval to the total number.

relationship between bend curvature and migration rate was obtained from meander bends regardless of their migration modes (e.g., extension and translation). Although earlier modeling studies had supported this conceptual generalization (e.g., Howard and Knutson, 1984), evidence from field studies indicated that this nonlinear pattern between bend curvature and migration rates in fact existed as an envelope covering a wide range of migration rates for a given r_m/w (Hudson and Kesel, 2000, Nicoll and Hickin, 2010, Hooke, 2013; Finotello et al., 2019), as shown in Figure 2.6. This pattern between bend curvature and migration rates suggested that meander bends with medium bend curvature were likely to be most capable of eroding banks and reworking floodplains because tightened bends with very high curvature (small r_m/w values) could cause increased flow resistance and partially offset the degree of erosion on the outer banks (Bagnold, 1960; Hickin and Nanson, 1984; Blanckaert and Graf, 2001).

When accounting for the percentage of bends in each r_m/w class interval (every 0.5 of r_m/w value, starting from 0 for the Black River and from 1 for the White River) regarding the total number of bends and calculating the weighted average in each r_m/w interval, we reproduced

a curve similar to the classic envelope for both studied reaches (Fig. 2.9). However, by taking a simple average of migration rates for each class interval of r_m/w, we found that bend migration was, in general, monotonically and inversely related to the curvature with larger migration distance associated with larger curvature (small r_m/w values). This quasi-monotonic and inverse relationship indicated that bends with higher curvature tended to migrate at higher rates, which was supported by a recent study on the meandering tributaries in the Amazon River (Sylvester et al., 2019).

We believe that this apparent discrepancy revealed a fundamental mechanism of bend migration. As a bend tightens with increasing curvature (decreasing r_m/w values), migration of the bend apex is less affected by that of its upstream positions because the bend has short spatial memory (Güneralp and Rhoads, 2009). Thus, a bend with higher curvature (smaller r_m/w) may migrate faster. On the other hand, as bend curvature increases, there may be a higher probability of initiating cutoff to eliminate the entire bend along the meandering channels or triggering compound-form development to stabilize the original bend, suggesting that for a given meandering reach, the number of bends with greater curvature (smaller r_m/w) tends to be fewer than that of bends with smaller curvature (greater r_m/w). This may be perceived as an inherent mechanism of river meandering by which the planform of meander bends stabilizes. Moreover, the peak in the envelope curve that emerged for r_m/w in the range between two and three suggested that the balance between increased flow resistance and fluvial erosion could reach a level leading to the maximum migration rate, although most bends with r_m/w between two and three could not reach this level (Fig. 2.6). Therefore, bend migration is controlled by bend curvature in a complex way that has not been fully understood yet.

2.4.2 Comparison of bend migration rates between the two studied reaches and with other meandering rivers

Meander bends involved in this study exhibited several distinct morphological characteristics between the lower Black and White rivers. First, the lower Black River had significantly more compound bends by both the absolute number (i.e., 50) and the percentage in all bends (i.e., 34%) than the lower White River (i.e., 13 and 9%) (Table 2.1). Also, the compound bends in the lower Black River tended to be more complex with more sub-bends and were distributed in clusters. Second, though both A_w and L_w of the compound bends remained generally unchanged along the two studied reaches with higher variations in the Black than in the White River (Fig. 2.4), the two studied reaches showed significantly different longitudinal trends of w. While w of the lower Black River only showed a gradual, constant increase throughout the whole reach from about 50 m at the upstream end to about 100 m at the outlet of the river (i.e., 120 km), w of the lower White River increased gradually in the first 40 km but then rose drastically in the lower half of the reach (i.e., after 60 km) (Fig. 2.10), showing a strong tendency of widening before the river reached to the outlet to join the Upper Yellow River. Third, the lower White River migrated at a much faster rate than that of the lower Black River. Within the

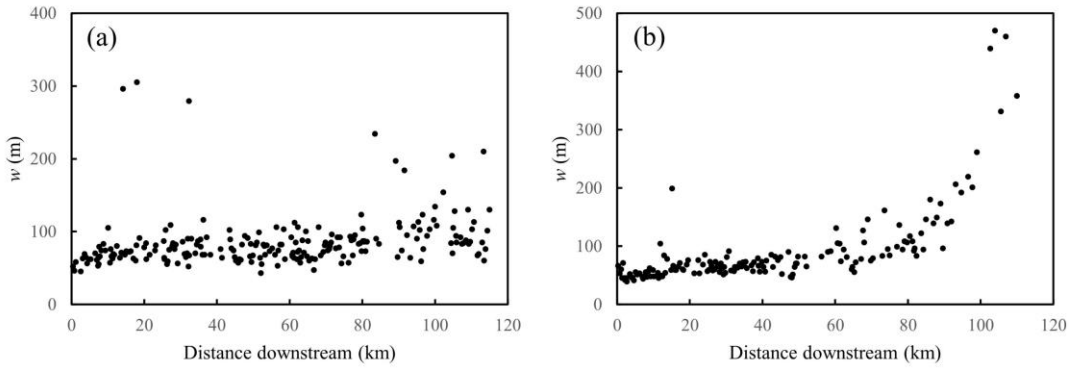

Figure 2.10 Longitudinal patterns of channel widths (w) in the studied reaches of the Black River (a) and the White River (b).

studied period, the mean width-normalized migration distance of bends that changed by extension and translation in the lower White River were 2.5 and 3.1 times, respectively, the migration distance of the lower Black River (Fig. 2.5). Lastly, only one cutoff occurred in the lower Black River, whereas nine such cases occurred in the lower White River.

Since that the two studied reaches are located in the same area with identical climatic settings and similar hydrogeomorphic properties in terms of the channel size, mean discharge, grain size, and land cover, channel gradient marks the most significant difference between the two studied reaches. Additionally, though the annual mean discharges of the two rivers were close, the mean annual maximum discharges were 198 and 304 m^3/s for the lower Black and White rivers, respectively. It follows that the maximum unit stream power in the lower White River (13.1 W/m^2) was significantly higher than that of the lower Black River (2.0 W/m^2). Therefore, stream power is likely the critical external factor resulting in high migration rate and more frequent meander cutoff in the lower White River, as corroborated in many other meandering rivers (Gautier et al, 2007; Nicoll and Hickin, 2010; Hooke, 2013).

On average, meander bends that changed by extension, translation, ET, and TE had the migration rate of 0.011 and 0.028 widths/year for the lower Black and White rivers, respectively. To compare with other meandering rivers worldwide under different hydrogeomorphologic settings, we summarized the mean and maximum width-normalized migration rates reported from previous studies (Table 2.3). Those rivers vary greatly in their environmental settings and sizes, such that they represent sufficiently a wide range of natural meandering rivers in the world. We found that lateral migration of the lower Black and White rivers were in the group of rivers with low rates. In particular, the lower Black River had almost the lowest migration rate, suggesting the slow evolution of the channels and floodplains in this area. Meanwhile, this

Table 2.3: Comparison of width-normalized channel migration rate with meandering rivers worldwide.

	Mean migration (widths/year)	Max migration (widths/year)	Average *w* (m)	How migration was measured	Reference
Black River	0.011	0.034	86	Maximum	This paper
White River	0.028	0.12	91	Maximum	This paper
Beni River	0.055	0.25	600	Unclear	Gautier et al. (2007)
Lower Mississippi	0.028	0.077	1600	Maximum	Hudson and Kesel (2000)
Tarim River	0.1	2.3	260	Maximum	Li et al. (2017)
Dane River	0.04	0.07	15-20	Unclear	Hooke (2007)
Sacramento River	0.01	0.05	374	Unclear	Micheli et al. (2004)
Canadian Rivers	0.019	0.068	21-288	Maximum	Nicoll and Hickin (2010)
Luangwa River	<0.1	0.22	100-200	Maximum	Gilvear et al. (2000)
Mamoré River	0.05	>0.05	300-500	Average	Constantine et al. (2014)
Solimões–Amazon River	0.005	0.03	>2000	Maximum	Mertes et al. (1996)

comparison is complicated by the inconsistency of the measured migration rates in the selected rivers, which was derived from: 1) whether width-normalized migration was used; 2) whether lateral migration was measured for entire meandering reaches or only for meander bends; 3) whether the maximum or the average migration distance within the entire course of each bend was used to represent migration distance of the bend for studies focusing on bend-based migration. Nonetheless, given that meander bends with no lateral migration were not included and that the maximum distance of each bend was used in this study to calculate the mean migration rate of all associated bends in each river, the fact that lateral migration rates in the lower Black and White rivers were generally low, in comparison with those in other parts of the world, sustained.

2.5 Conclusions

This study revealed morphological characteristics and patterns of meander-bend changes for two highly convoluted meandering reaches developed in the Zoige Basin within the Qinghai-Tibet Plateau, the highest plateau in the world. These meandering channels were largely undisturbed, providing an opportunity for examining meander morphology and changes controlled by natural fluvial processes. We found that both the Black River and the White River exhibited a tendency of complex planform structures that favored the development of compound bends. This tendency was especially obvious in the Black River with its compound bends accounting for more than one third of total bends. Furthermore, the studied reach of the Black River exhibited relatively slow bend migration and fewer cutoffs than that of the White River, which may be explained by its considerably smaller stream power.

Analysis of bend morphological changes and morphodynamic patterns in the two studied reaches demonstrated that extension, translation, and their combination were the dominant modes of bend change. However, bends that changed by translation tended to migrate at faster rates than those changed by extension. Both reaches had greater areas of deposition than erosion, although both exhibited a transition from an erosion-dominated pattern in the upstream portion into a deposition-dominated pattern in the downstream portion. The relation between bend curvature and migration rates revealed a similar pattern to that of many meandering rivers in other regions, highlighting an envelope curve that shows a peaked migration rate for bends with medium curvatures, commonly between two and three. However, the average migration rates calculated for each class interval of bend curvature showed a quasi-monotonic relationship with bend curvature. Thus, the frequency of bends with similar curvature but different migration rates may alter this envelope relationship, suggesting the complex responses of bend migration to bend planform morphology. The comparison of migration rates with other meandering rivers

worldwide showed that the Black and the White rivers were at the higher end of a spectrum of meandering rivers in the world with regards to the complexity of river planform structure. Our results provided new insights into developing complete theories for explaining and predicting bend migration and meander evolution.

Chapter 3: Hydrologic connectivity and morphologic variation of oxbow lakes in the meandering system of the lower Black River[2]

3.1 Introduction

Oxbow lakes are abandoned channel sections commonly seen in meandering river floodplains as relics of meander-bend cutoff (Liverpool and Edwards, 1995; Stølum, 1996; Constantine and Dunne, 2008). They produce ecologically crucial aquatic environments for sustaining a great diversity of habitats (Miranda, 2005; Bhattacharya et al., 2016), and are an important geomorphic unit of fluvial systems. Oxbow lakes can signify hydrogeomorphic properties of river channels (Poff et al., 1997; Constantine et al., 2010; Hudson et al., 2012; Dieras et al., 2013; Constantine et al., 2014), preserve the threshold morphology of meander bends prior to cutoff (Weihaupt, 1977; Stølum, 1998), and archive the history of overbank floods (Wolfe et al., 2006; Toonen et al., 2012; Ishii and Hori, 2016; Shen et al., 2021). Therefore, their morphology, evolution, and hydrologic interactions with the active main channels have drawn considerable attention in fluvial geomorphology, river engineering, stream ecology, and sedimentology. Oxbow lakes created from meander cutoffs may experience diverse evolutionary processes with a variety of planform morphology (Bai and Wang, 2014; Li et al., 2017; Konsoer et al., 2016). As such, their lifespan varies from a few years to centuries (e.g., Gagliano and Howard, 1984; Riquier et al., 2017; Amoros et al., 2000).

The evolution of oxbow lakes is generally classified into four consecutive stages: active meander-bend (Stage I), cutoff (Stage II), lacustrine (Stage III), and terrestrial (Stage IV) phases (Gagliano and Howard, 1984; Wren et al., 2008; Richards and Konsoer, 2020). Among them,

[2] This chapter has been published in:
Guo, X., Gao, P., & Li, Z. (2023). Hydrologic connectivity and morphologic variation of oxbow lakes in a pristine alpine fluvial system. *Journal of Hydrology*, 129768. https://doi.org/10.1016/j.jhydrol.2023.129768

Stage II begins when (chute or neck) cutoff occurs and usually lasts between one and ten years, during which the former main channel is gradually transformed from an open waterbody that constantly receives water, sediment, and nutrient from the main channel into an isolated lacustrine environment due to plug bar formation at the entrance (i.e., inlet) and exit (i.e., outlet) of the lake (Gagliano and Howard, 1984; Hooke, 1995; Richards et al., 2022). The development of plug bars plays a vital role in the isolation process that is controlled by the morphodynamic properties of the channel, such as sediment supply and diversion angle (Constantine et al., 2010; Dieras et al., 2013; Ishii and Hori, 2016; Dépret et al., 2017; Li and Gao, 2019a). A large diversion angle, often formed by neck cutoff, may promote rapid development of plug bars at the lake entrance, which subsequently reduces the supply of the coarse-material loads (i.e., bed load) to the abandoned channel. Conversely, a small diversion angle, normally associated with chute cutoff, causes a slower formation of plug bars, allowing the abandoned channel to receive more coarse materials from the active channel. Stage III starts from the isolation of the lake, during which the oxbow lake may only reconnect to the main channel when "overbank" floods occur. Sedimentation within the lake would continuously infill the oxbow lake, allowing for vegetation encroachment that eventually leads to a complete terrestrialization of the oxbow lake, namely Stage IV. With the oxbow lake gradually transformed from the lacustrine setting into a terrestrial environment, the sediment source gradually switches from the exogenous-dominated supply (from the main channel by overbank flows) to the endogenous-dominated deposition due to the reduced frequency of overbank flows (Gautier et al., 2007; Richards et al., 2022). Hydrologically, oxbow lakes in Stage III receive water from a variety of sources, including direct precipitation, overland flow through the catchment upslope of the lakes, surface water supply (i.e., hydrologic connection between the lake and channel), and groundwater recharge.

Depending on the rate of lake sedimentation, the duration of Stage III may last for a wide range of periods among different fluvial settings (e.g., Gagliano and Howard. 1984; Dieras, 2013; Kobus et al., 2016).

Thus far, the fluvial processes associated with the early two stages (i.e., Stages I and II) have been extensively studied (e.g., Constantine and Dunne, 2008; Grenfell et al., 2012; Dieras et al., 2013; Sylvester et al., 2019), whereas limited understanding has been established about the intra-stage evolutionary processes for oxbow lakes in Stage III. Specifically, although oxbow lakes in this stage are known to undergo an overall shrinking trend given continuous lake infilling (e.g., Wren et al., 2008; Constantine et al., 2010; Ishii and Hori, 2016), the dynamics of lake morphology in response to variable hydrologic conditions of the main channel remain elusive. Therefore, a quantitative assessment of their morphologic responses to fluctuations of river discharge over a short period (i.e., intra-annual), is still needed for revealing and inferring the driving processes involved in the long-term shrinking trend. Additionally, hydrologic connectivity, a concept used for characterizing hydrologic interactions between hydrological elements (e.g., oxbow lakes and channels) (Freeman et al., 2007; Bracken et al., 2013), highlights streamflow pulses in generating water and sediment interactions between channels and oxbow lakes (e.g., Junk et al., 1989; Wainwright et al., 2011), especially for newer lakes (Hudson et al., 2012). However, this concept bears different meanings in different quantification approaches and mostly relies on the presence of surface water connection, which omits hydrologic processes other than surface water in controlling oxbow lake hydrology. The relations between hydrologic connectivity and oxbow lake variation under a variable hydrologic regime have yet to be explored either. Therefore, a full understanding of the evolutionary processes of

oxbow lakes requires the answers to the question: how does the hydrogeomorphology of oxbow lakes respond to a variable hydrologic regime of the neighboring meandering channel?

In this study, we seek to provide the answers by 1) characterizing the morphology of oxbow lakes in relation to the active channel, 2) quantifying their morphologic variations in response to variable hydrologic conditions, and 3) revealing variable degrees of hydrologic connectivity among oxbow lakes under variable flow conditions in a pristine meandering reach. Finally, we, based on the collected samples of lake deposits, illustrate processes revealed by morphologic properties of the oxbow lakes and examine the long-term evolution of the meandering river floodplain.

3.2 Study area

The Zoige Basin is located on the northeastern edge of the Asian "water tower" and the world's third pole – the Qinghai-Tibet Plateau (Fig. 3.1a). With a mean elevation of 3,400 m, the basin has a relatively flat topography surrounded by high mountains, including the Minshan Mountains – the origin of the studied Black River (Fig. 3.1b). As a unique area in the Qinghai-Tibet Plateau, the Zoige Basin fosters the world's largest alpine peatland, which was formed by lacustrine deposits of a paleolake that collapsed and drained 37 ka before present (Chen et al., 1999; Nicoll et al., 2013; Zeng et al., 2017; Wang et al., 2023). With a cold alpine climate (Dwc in Köppen Classification), the basin has an annual mean temperature of 0.7 ℃ and an annual mean precipitation of 645 mm (Li et al., 2014). Most precipitation occurs in summer due to the prevalent East Asian monsoon, making the Zoige Basin one of the moistest regions in the Qinghai-Tibet Plateau. The land cover of the basin is dominated by herbaceous plants, including grassland, peatland, and a mixture of both. Although human disturbances are limited due to the

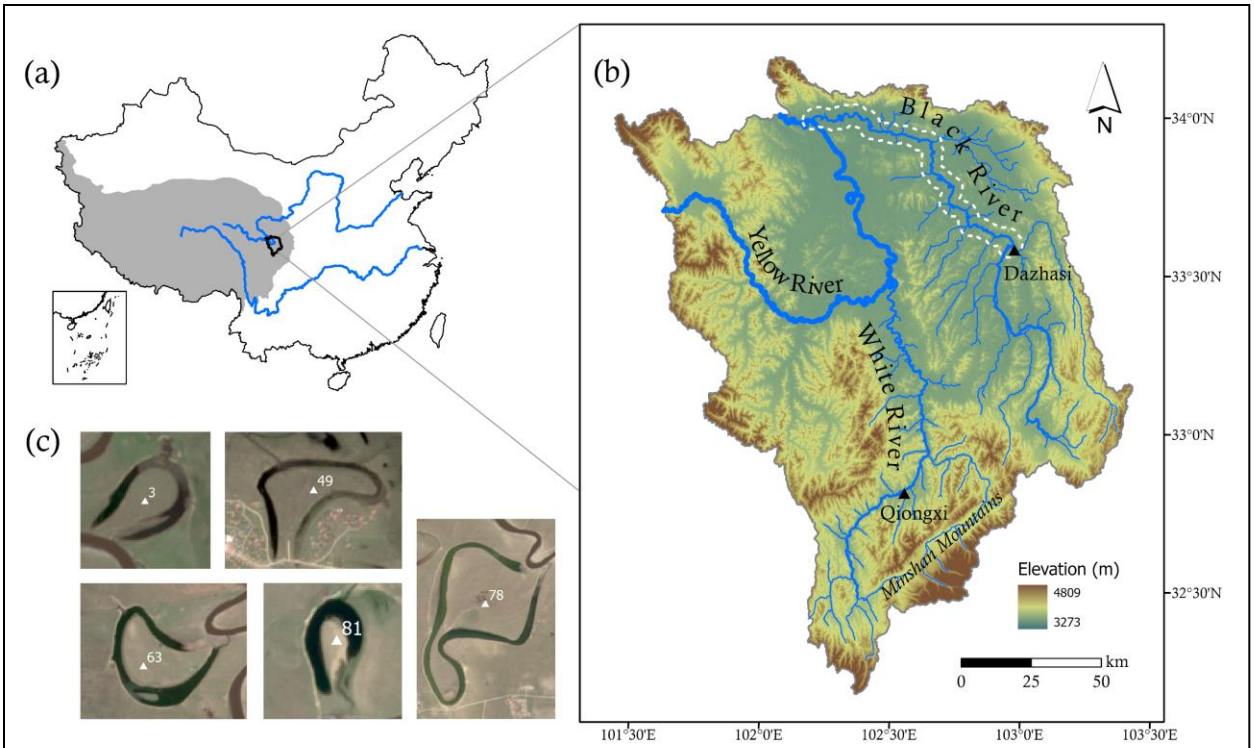

Figure 3.1 Overview of the study area. (a) Locations of the Qinghai-Tibet Plateau (shaded area) and the Zoige Basin (outlined area) in China; (b) Topography of the Zoige Basin and stream networks of two major tributaries of the Yellow River in the Zoige Basin: the Black and the White rivers. The study reach ("lower Black River") is indicated by the white dotted buffer line; (c) Snapshots of typical oxbow lakes developed in the lower Black River (images courtesy of Sentinel-2).

harsh living condition, peatland degradation is still evident in the upstream hillslopes possibly related to the excavation of artificial ditches and gully erosion over the past five decades (Qiu et al., 2009; Li and Gao, 2019b; Li et al., 2020).

The Black River is the largest tributary of the Upper Yellow River in its source region (Fig. 3.1b), with a drainage area of 7,600 km^2 and a mean annual discharge of 58 m^3/s. The middle and lower reaches of the river develop highly sinuous meandering patterns, which are primarily characterized by extensively developed point and scroll bars, compound bends, and oxbow lakes (Fig. 3.1c). Precipitation is the major water source of streamflow in the region, followed by late-spring snowmelt and groundwater supply. This study focuses on oxbow lakes developed along a 120-km reach of the downstream Black River from the town of Dazhasi, the seat of the Zoige County (hereafter referred to as the "lower Black River"). The reach-averaged channel gradient,

width, and sinuosity are 0.09 ‰, 86 m, and 2.03, respectively. Channel banks of the lower Black River typically constitute a two-layer structure, with the upper layer having a cohesive vegetation-soil mixture layer and the lower layer comprising fine sand and silt. Consequently, cantilever arms can be easily formed as the lower layer is subject to continuous fluvial erosion, leading to bank collapse once the threshold is reached. This fluvial-mass failure mechanism dominates the rates of bank retreat and meander-bend evolution (e.g., Gao et al., 2021; Yang et al., 2023). Because the cycle of bank collapse takes time (usually several years), meander bends in the reach evolve slowly, giving rise to a mean rate of lateral migration at bend apices of 0.011 width/year. Meander cutoff, dominated by neck cutoff, has occurred only three times over the last 40 years (Guo et al., 2021; Li et al., 2023).

3.3 Methods

3.3.1 Hydrological analysis

Characterizing morphologic variations and hydrologic connectivity of oxbow lakes is built upon the hydrologic conditions of the main channel of the lower Black River. Flood frequency analysis was conducted using the record of annual peak discharges (1980-2020) obtained from the Zoige gauge station (33.595°N, 102.536°E) near the town of Dazhasi. Among the commonly used probability density functions (Chow et al, 1988), the lognormal function is proven to best fit the discharge data. The constructed flood frequency curve was subsequently used to determine discharges of given recurrence intervals (RIs). By matching the available satellite images with the calculated recurrence intervals (see details in the following section), four representative hydrologic conditions were selected, which are the mean annual discharge (Q_{am} = 27.1 m^3/s, assuming the recurrence interval is 0.1), the discharge with 1-year recurrence interval (Q_1 = 53.7

m^3/s), the discharge with 10-year recurrence interval (Q_{10} = 256.3 m^3/s), and the record-high discharge (equivalent to the discharge with about 45-year recurrence interval; Q_{45} = 376.0 m^3/s), respectively.

3.3.2 Remote sensing acquisition and analysis

A total of 86 oxbow lakes were identified along the lower Black River for this study A total of 86 oxbow lakes were identified along the lower Black River for this study using high-resolution (< 10 m) images from Google Earth. These lakes encompass all abandoned channels preserved within the floodplains that are identifiable by their presence of water or the desiccated beds and remaining banks. We used sequential Sentinel-2 imagery, with a spatial resolution of 10 m, to extract oxbow lake morphology based on water extents under the four flow levels reported above. We were unable to find satellite images that correspond to other flow levels (e.g., discharges with 5-year and 20-year RIs) due to the instantaneous peaks of these high flows that are unable to be captured by the sensor given its revisit time, as well as the prevailing cloud cover during the rainy season. For each image, we generated water masks for oxbow lakes by visual interpretation, assisted by the Modified Normalized Difference Water Index (MNDWI), a widely used spectral index for water delineation based on green and shortwave infrared bands (e.g., Xu, 2006; Rokni et al., 2014; Singh et al., 2015). The planform morphology and the temporal changes of each oxbow lake were subsequently extracted and determined in ArcGIS Pro. Potential uncertainties may arise from the registration of the original data and errors associated with digitizing subjectivity (Downward et al., 1994; Lea and Legleiter, 2016; Donovan et al., 2019). The total error, calculated as the square root of the sum of the squares of the individual error, remains < 10 m for this study using the same methods as what we adopted

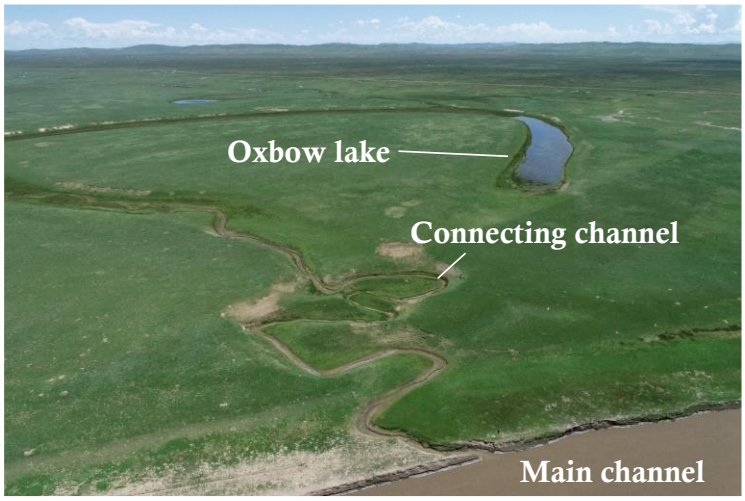

Figure 3.2 A drone photo, taken in summer 2022, over a connecting channel in the study reach. Discharge of the main channel is in between the annual mean and 1-year flows, and the limited water within the connecting channel flows from the oxbow lake into the main channel.

for the digitization of river channels of the lower Black River and the Upper Yellow River (Guo et al., 2021, 2023).

The planform morphology of oxbow lakes can be described using static and dynamic metrics. Specifically, static metrics are based on the shapes of oxbow lakes and their spatial relationships with the main channel, regardless of their surface water levels. They include 1) simple or compound oxbow lakes; 2) oxbow lakes with and without connecting channels; 3) the shortest distance between an oxbow lake and the main channel (D_C); and 4) the distance between the two entrances (i.e., inlet and outlet) of an oxbow lake (D_L). Specifically, a simple oxbow lake must contain one former meander bend defined as an arc > 60°, while a compound oxbow lake should involve multiple former bends as defined by Guo et al. (2021). A connecting channel, which was also referred to as "tie channel" or "tributary channel" (e.g., Dietrich et al., 1999; Rowland et al., 2005; 2009), is a smaller channel connecting an oxbow lake to the main active channel (Fig. 3.2), which could be easily detected in Google Earth. Both D_C and D_L were measured based on the remaining banks and beds of the former channel identifiable in Google Earth, which are not affected by water-level fluctuations of the lakes. The value of D_L is the distance between the two ends of the oxbow lake centerline, whose minimum value should approximate the width of the main channel at the time when the oxbow lake was formed by neck

cutoff. The dynamic metrics capture the changes in oxbow-lake planform morphology at different water levels, which include lake length, width, and area defined by water masks. Under the record-high flow (i.e., Q_{45}), many oxbow lakes were completely inundated, making their morphology unidentifiable. In this case, we assigned a very large value for their area (1 km^2), length (10 km), and width (1 km) to make them distinct from other non-inundated oxbow lakes.

For each selected oxbow lake, we performed linear regression analysis between lake areas at the four flow levels and their corresponding recurrence intervals. The established model is generally strong with statistical significance. The slope of each model (S^*) reflects the rate of change in area for each oxbow lake, with a greater S^* indicating a higher rate of lake expansion with increasing discharge in the main channel.

Hydrologic connectivity generally describes the transport of water and materials involved in the hydrologic cycle (Freeman et al., 2007; Bracken et al., 2013). For oxbow lakes, the hydrologic connectivity is referred to as the degree to which oxbow lakes reconnect to river channels, which is a critical process controlling the geomorphic and ecologic properties of meandering river floodplains (Miranda, 2005; Glińska-Lewczuk, 2009; Riquier et al., 2017; Wang et al., 2020; Szewczyk et al., 2022). Here we quantify the hydrologic connectivity of the studied oxbow lakes based on surface water connection along a path between an oxbow lake and the adjacent main channel, which must be clearly observed from the remotely sensed images. According to our preliminary investigation, hydrologic connectivity of the studied oxbow lakes remains low even under relatively high flows (i.e., $> Q_{am}$ but $< Q_2$) in summer. To quantify it, we proposed a probability-based index for hydrologic connectivity, *PHC*, which is defined as:

$$PHC = 1/RI$$

where the *RI* of each oxbow lake is the magnitude of the main-channel discharge under which the lake is hydrologically connected to the main channel. For example, an oxbow lake with *PHC* = 1 (i.e., *RI* = 1) means the lake connects to the main channel at discharges ≥ Q_1, and an oxbow lake with *PHC* = 0.022 (i.e., *RI* = 45) means the lake connects to the main channel only at Q_{45} or higher discharges while remaining disconnected at the other three lower flow levels. For oxbow lakes that remain disconnected from the main channel at all four flow levels, we assigned a very large *RI* value (i.e., 100, which means *PHC* = 0.01) to make them distinct from others.

3.3.3 Field-data acquisition and analysis

To compensate for the limitations of planform morphology derived from remotely sensed data, we collected vertical samples of bed deposits in two oxbow lakes during fieldwork in the summers of 2021 and 2022. Two sediment cores were collected in an oxbow lake for particle-size analysis (Cores #1 & 2; see section 5.3 for details and the relevant discussion) and two more sediment cores were collected in two different oxbow lakes for dating analysis (Cores #3 & 4; see section 5.4 for details and the relevant discussion). Specifically, Cores #1 and #2 are both 120 cm deep, while Cores #3 and #4 are 140 and 100 cm deep, respectively. All cores were sliced into sequences of 5 cm sections, which were subsequently preprocessed and analyzed using a laser diffraction particle size analyzer for particle-size analysis (at Hohai University, China) and gamma spectrometry for ^{137}Cs dating (at Chengdu Institute of Mountain Hazards and Environment, Chinese Academy of Sciences).

3.4 Results

3.4.1 Characterizing planform morphology of oxbow lakes

Most of the 86 identified oxbow lakes (72%) are located in the floodplain next to the upstream half section of the study reach (from the upstream end, Dazhasi, to the mid-point of the reach, see Fig. 3.1b). These lakes are typically clustered in the areas where the main channel contains highly convoluted meander bends, demonstrating the correlation between the production rate of oxbow lakes and meandering-channel sinuosity (Constantine and Dunne, 2008).

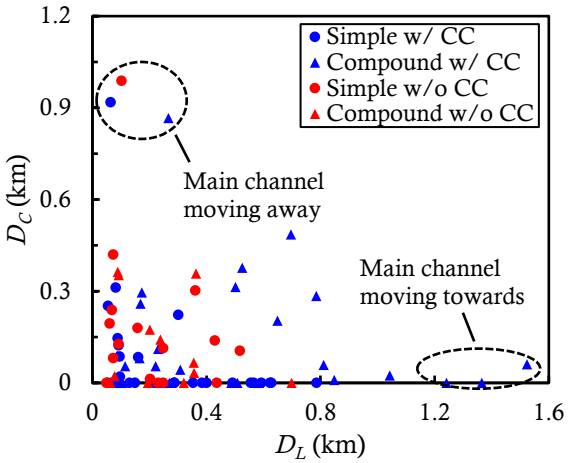

Figure 3.3 Relationship between D_C and D_L for oxbow lakes in simple/compound morphology and with/without connecting channels (CC).

Among all 86 oxbow lakes, 39 are located right next to the main channel (i.e., $D_C = 0$), while the rest have variable distances from the main channel, with the mean D_C = 0.22 km and the maximum D_C = 0.99 km (Fig. 3.3). Because oxbow lakes in the study reach were predominately formed by neck cutoff, they should have the initial D_L of no more than one channel width (i.e., < 100 m). Their subsequent evolution follows different pathways, leading to a variety of the current D_L ranging from < 100 m to 1.52 km, with a mean value of 0.34 km (Fig. 3.3). By plotting D_L against D_C, we show that some oxbow lakes seem to have two types of unusual morphologic relationships, with the first type having small D_L but very large D_C and the second type being characterized by large D_L but small D_C. The first type is possibly the consequence of a relatively fast lateral shifting of the main channel away from the oxbow lakes that made the oxbow lakes unable to receive sufficient sediment from the main

channel for infilling. The second type suggests the lateral migration of the main channel moving towards the oxbow lakes engulfing the original lake entrances.

The studied oxbow lakes exhibit two main morphologic characteristics: the distinction of compound lakes from simple ones, and the prevalence of connecting channels between lakes and channels. Particularly, compound lakes account for nearly 49% (i.e., 42/86) while simple ones take about 51% (i.e., 44/86) of the total number of lakes. Compared with the proportion (i.e., 34%) of meander bends that display compound forms in the same study reach (Guo et al., 2021), the larger proportion of compound oxbow lakes suggests a higher likelihood of compound form development in meander bends as a way, other than cutoff, to achieve relative stability while consuming energy. The compound oxbow lakes also exhibit significantly ($p < 0.05$) larger D_L (i.e., 0.43 km on average) than that (i.e., 0.25 km on average) of the simple ones, though their D_C do not differ significantly.

For the second characteristic, we find that the majority (i.e., 58/86) of oxbow lakes have developed small channels connecting the lake and the main channel. With a mean width generally of 10 m, these channels were commonly formed at lake inlets or outlets where previously developed plug bars were cut through to drain water from the oxbow lakes when the flow stage of the main channel is lower than the water level of the oxbow lakes. Occasionally, they can become pathways to transfer water and sediment from the main channel into the oxbow lakes during high flows, thereby initiating surface water connection between the two geomorphic units. The connecting channels of the studied oxbow lakes are commonly sinuous and rarely connect with tributaries of the Black River in the watershed upslope to the oxbow lakes. Oxbow lakes with connecting channels have significantly ($p < 0.05$) larger D_L (i.e., 0.39 km on average) than those without connecting channels (i.e., 0.23 km on average) (Fig. 3.3), suggesting the

morphologic similarity between oxbow lakes with compound forms (compound lakes are larger in D_L than simple ones) and those with connecting channels. Their D_C values, however, do not differ significantly. Among the 58 oxbow lakes with connecting channels, thirty-two developed connecting channels at the lake inlet, twenty created them at the lake outlet, and six lakes generated them on both sides. The variable locations of the connecting channels indicate the complex interactions among the main channel hydraulics, the lake diversion angle, the shortest path, and the hydrologic connectivity of oxbow lakes in controlling the formative and evolutionary patterns of the connecting channels. Moreover, the connecting channel seems to favor compound oxbow lakes over simple ones, which is likely related to the greater size and more water volume of the compound oxbow lakes.

3.4.2 Morphologic variations of oxbow lakes under variable hydrologic conditions

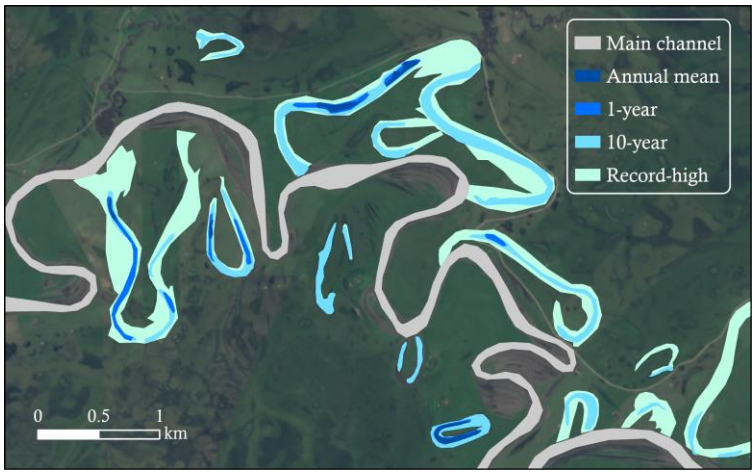

Figure 3.4 Oxbow lake variations in water extents at the four referencing flow levels in a sample reach.

Although oxbow lakes gradually shrink in size because of continuous sediment infilling after their plug bar formation (i.e., the end of Stage II), their planform morphology is found to vary greatly in the intra-annual scale with fluctuating flow levels (Fig. 3.4). Generally, the oxbow lakes along the lower Black River show expansion with the increase of river discharge, leading to greater potentials for the lakes to connect to the main channels via surface water. However, the magnitudes of morphologic changes among the oxbow

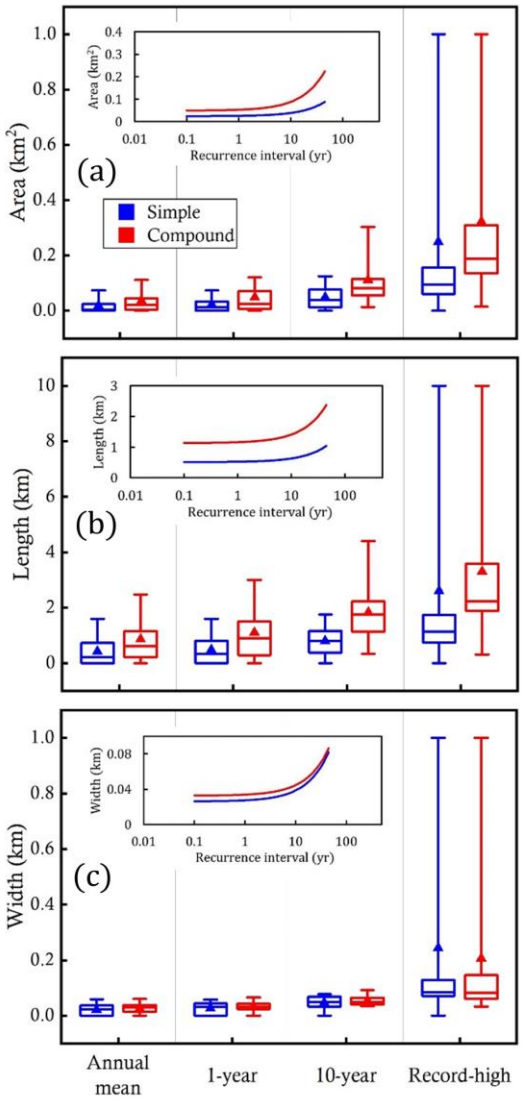

Figure 3.5 Oxbow lakes with connecting channels: statistical distributions of morphologic variations of (a) lake area, (b) length, and (c) width at the four flow levels. The inserted figures show linear regression lines of overall increasing trend of each parameter that does not include inundated lakes at record-high flow.

lakes under different flow levels are different based on their morphologic characteristics described previously (Figs. 3.5 and 3.6).

The length and area of compound lakes are significantly ($p < 0.05$) larger than those of simple lakes at all four flow levels, as indicated by the linear regression lines and median values in Figures 3.5 and 3.6. These differences also increase with the water discharge of the main channel. Nonetheless, lake widths between simple and compound ones do not differ significantly at all flow levels, suggesting that the two types of oxbow lakes have similar rates of transverse deposition. Similarly, oxbow lakes with connecting channels have significantly larger ($p < 0.05$) lengths and areas at all four flow levels than the lakes without connecting channels (Figs. 3.5 and 3.6), whereas their widths are statistically identical, especially at Q_{10} and Q_{45}. These morphologic distinctions reveal that connecting channels are preferable to develop in larger oxbow lakes and that the formation and evolution of the connecting channels are controlled not only by the magnitude and sediment concentrations of sediment-laden flows from the main channel but by the morphologic responses of oxbow lakes.

Therefore, it is important to specify the hydrologic conditions when describing the morphologic variations of oxbow lakes.

Overall, for all 86 oxbow lakes in the study reach, their lengths and widths increase with the water discharge of the main channel (Figs. 3.5 and 3.6), with the mean length of 0.475, 0.580, 1.123, and 1.465 km (not including completely inundated lakes) and the associated mean width of 0.019, 0.022, 0.049, and 0.079 km for Q_{am}, Q_1, Q_{10}, and Q_{45}, respectively. Furthermore, lake width increased faster by magnitude than lake length when the discharge of the main channel $\geq Q_{10}$, suggesting a more rapid widening of the oxbow lakes possibly due to the occurrence of (lake) overbank flows under very large flows. The faster expansion of lake width due to overbank flow is highlighted at Q_{45} (Fig. 3.4).

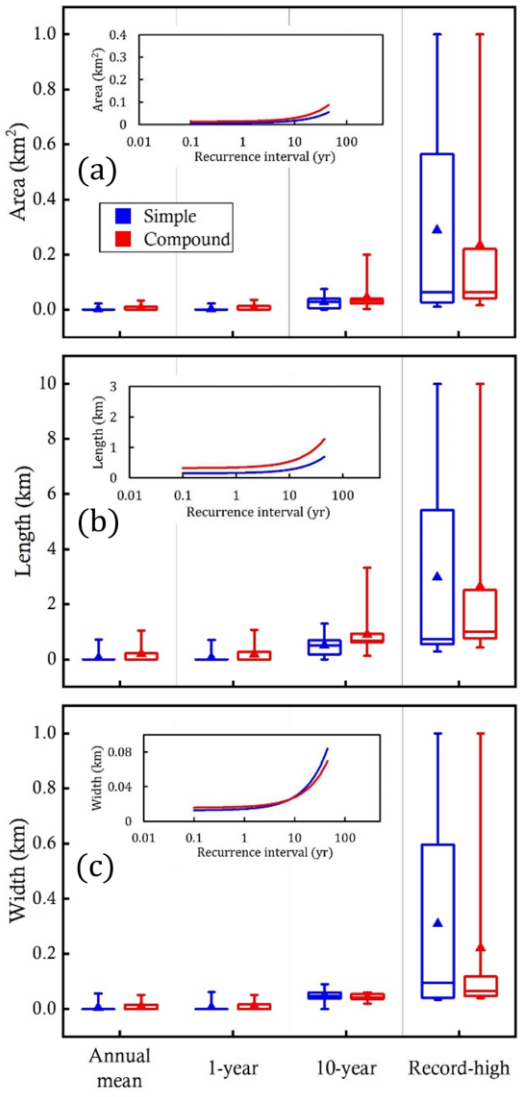

Figure 3.6 Oxbow lakes without connecting channels: statistical distributions of morphologic variations of (a) lake area, (b) length, and (c) width at the four flow levels. The inserted figures show linear regression lines of overall increasing trend of each parameter that does not include inundated lakes at record-high flow.

The record-high flow (Q_{45}) that occurred in July 2018, with the discharge nearly 13 times greater than Q_{am}, marks an unprecedented hydrologic condition in the observed history of the lower Black River. Under such flow, the length, width, and area of all oxbow lakes increased dramatically (Figs. 3.5 and 3.6),

causing the mean area of all oxbow lakes at the record-high flow 5.4-fold greater than that of the lakes at Q_{am}. The total inundated area along the study reach was 85.3 km^2, which was 4.5-fold greater than the water-surface area of the channel at Q_{am}. The inundation was particularly extensive in the floodplains along the upstream section of the study reach, causing 15 oxbow lakes to be completely inundated, such that they are unable to be identified from the satellite images. In the downstream section of the study reach, morphologic variations of the oxbow lakes were limited, and no lake was completely inundated even at the record-high flow level. This contrast demonstrates the spatial heterogeneity of channel-floodplain interactions in the study reach.

The degree of morphologic change (S^*) of the oxbow lakes ranges between about zero and 0.014, which averages at 0.0023. Oxbow lakes with compound forms and connecting channels are found to have significantly ($p < 0.05$) larger S^* than those having simple forms and without connecting channels, respectively (Fig. 3.7), which indicates higher magnitudes of expansion of the oxbow lakes in the former types. The general pattern between S^* and D_C can be expressed as a simple reciprocal function, in which S^* decreases swiftly before $D_C \approx 0.12$ and then decreases with much lower rates for greater D_C (Fig. 3.7a). The relationship between S^* and D_L is highly scattered but can be

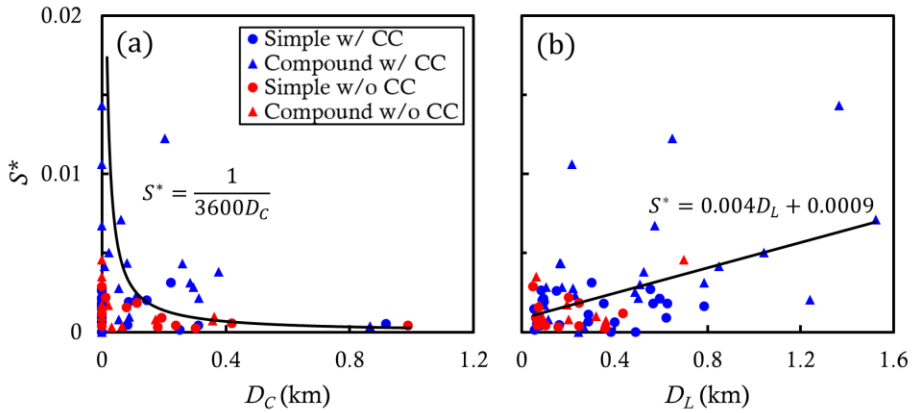

Figure 3.7 S^* relationships with D_C (a) and D_L (b) of all studied oxbow lakes except the inundated ones at record-high flow. Oxbow lakes are classified based on their morphology. The general S^*– D_C trend can be approximated by the equation noted in (a). CC denotes connecting channel.

described by a statistically significant linear trend with three outliers whose S^* are much higher (Fig. 3.7b).

3.4.3 Hydrologic connectivity of the oxbow lakes

Hydrologic connectivity of the studied oxbow lakes using the proposed approach (*PHC*) ranges from 0.01 (never connected to the main channel among the four flow levels) to 10 (always connected to the main channel among the four flow levels), with the majority of lakes having their *PHC*s of 0.02 and 0.1 (71 out of 86 oxbow lakes; Fig. 3.8). These trends suggest that for most oxbow lakes, there is no hydrologic connection with the main channels at Q_{am} and Q_1, which reflects a very inactive hydrologic interaction between the oxbow lakes and their adjacent main channel in the lower Black River. By contrast, early studies have reported comparatively higher intra-annual hydrologic connectivity of oxbow lakes in other regions (e.g., Junk et al., 1989; Hudson et al., 2012).

Among all 86 oxbow lakes, fourteen (16.3%) were never hydrologically connected to the main channel (i.e., *PHC* = 0.01) (Fig. 3.8). These oxbow lakes are either far away from the main channel or separated from the main channel by adequate plug bars or higher channel banks, leading to their complete isolation even at Q_{45}. Thirty (34.9%) oxbow lakes, which are mostly located in the upper section of the study reach, are only hydrologically connected to the main channel at Q_{45} while remaining disconnected at the other three

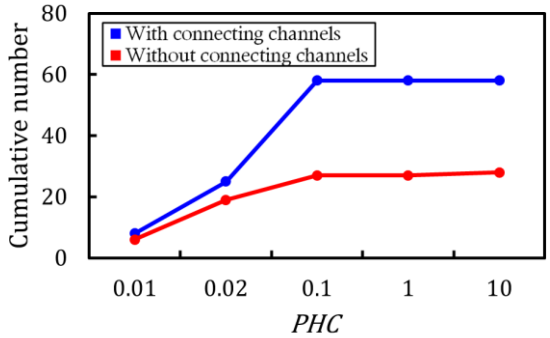

Figure 3.8 Cumulative number of oxbow lakes with different hydrologic connectivity (*PHC*), classified by whether the connecting channel is fostered at lake entrances.

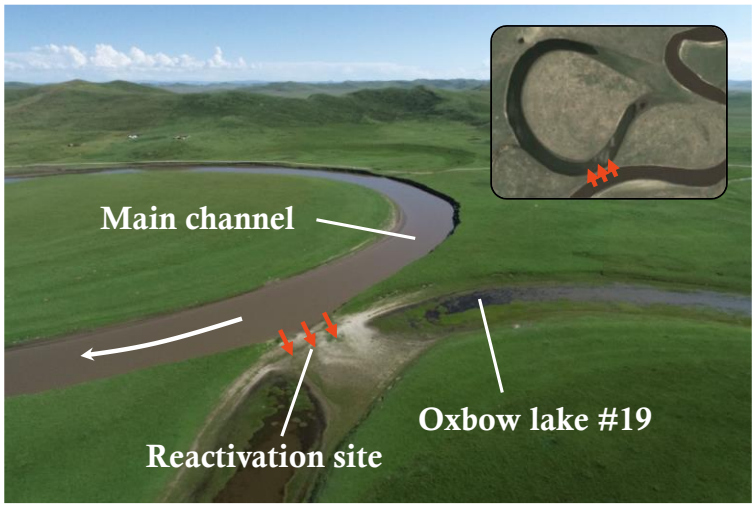

Figure 3.9 A drone photo, taken in summer 2022, over oxbow lake #19 reactivated by the lateral-shifting main channel. The red arrows indicate direction of lateral migration and the white arrow indicate flow direction. The planform view of the lake and the main channel is provided in the upper right (Google Earth image).

water levels (i.e., *PHC* = 0.02). Additionally, 41 (47.7%) lakes have *PHC* = 0.1, indicating that they can be hydrologically connected to the main channel at Q_{10} and greater. Interestingly, while no oxbow lake has *PHC* = 1 (start to achieve hydrologic connection at Q_1), there exists one lake (i.e., Lake #19; Fig. 3.9) that remains hydrologically connected with the main channel at all four water levels (i.e., *PHC* = 10). Its high degree of hydrologic connectivity is caused by the lateral shifting of the main channel that reactivated the previously isolated oxbow lake, exemplifying the strong, but infrequent, effect of the lateral migration of the main channel on oxbow lake evolution. For all studied oxbow lakes, while no correlation was found between *PHC* and D_L, their *PHC* and the associated D_C exhibit a negative correlation, suggesting that D_C may infer the hydrologic connectivity of oxbow lakes (Fig. 3.10). The oxbow lakes with connecting channels have considerably higher hydrologic connectivity (the average times, among the four flow levels, is 1.43) than those without connecting channels (the average time is 1.18). Thus, whether a connecting

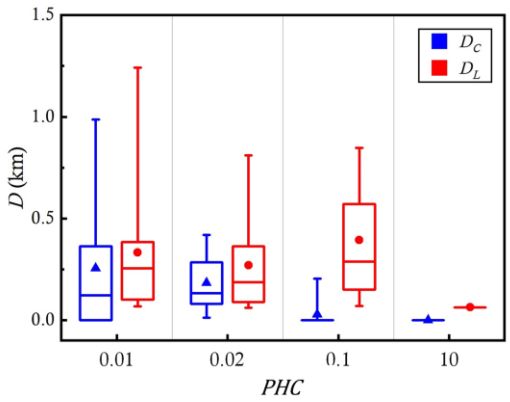

Figure 3.10 Statistical distributions of D_C and D_L, classified by the calculated hydrologic connectivity (*PHC*).

channel is developed or not may be another morphologic indicator for the hydrologic connectivity of the studied oxbow lakes.

3.5 Discussion

3.5.1 The nature of hydrologic connectivity of oxbow lakes

As a critical hydrogeomorphic and ecologic property of oxbow lakes, hydrologic connectivity has been characterized and quantified using a variety of approaches, including classifying connecting patterns between lakes and channels, determining the threshold discharge, estimating the frequency and magnitude of floods that induce connectivity, and interpreting the depositional patterns of oxbow lake infills (e.g., Dembkowski and Miranda, 2011; Hudson et al., 2012; Philips, 2013; Shen et al., 2021). However, there are no consistent metrics that can be used for directly comparing the degrees of hydrologic connectivity among various oxbow lakes in floodplains of different fluvial systems. The probability-based index, *PHC*, proposed in this study quantifies the variable degrees of hydrologic connectivity of the studied oxbow lakes in terms of recurrence interval – a common hydrological concept that is comparable among rivers in any region. Although our results are site-specific, the index *PHC* is transformable for quantifying the hydrologic connectivity of oxbow lakes in other fluvial systems with different hydrologic regimes.

In our case, oxbow lakes in the floodplain of the lower Black River exhibited extremely low hydrologic connectivity with most lakes remaining disconnected from the main channel at Q_{am} and Q_1 (Fig. 3.8). By contrast, many oxbow lakes in lowland floodplains reported in the literature have higher hydrologic connectivity, (e.g., Miranda, 2005; Hudson et al., 2012; Czuba et al., 2019). Oxbow lakes with comparably low hydrologic connectivity may include the

artificially regulated ones in highly populated areas, such as the floodplain of the middle Yangtze River (i.e., the Jingjiang Reach) where the embankment had significantly deactivated channel-floodplain interactions (e.g., Xia et al., 2016; Yang et al., 2017).

The low hydrologic connectivity of the studied oxbow lakes is likely attributable to the unique fluvial setting of the lower Black River. Numerous studies have demonstrated that tributaries of the Upper Yellow River, including the Black River, were subject to the knickpoint incision due to intense channel downcutting induced by the combined climatic and tectonic movements since the collapse of the Zoige paleolake 37 ka before present (e.g., Chen et al., 1999; Wang et al., 2013; Liu et al., 2021; Wang et al., 2023). Consequently, the lower Black River becomes an underfit river (Davis, 1913; Beaty, 1990; Srivastava et al., 2014), in which the flows can rarely reach the bankfull stage under the prevailing hydrologic regime (Li and Gao, 2019a). This fact explains the scarcity of large-area inundation in the study reach and why it may only occur at the unprecedented record-high peak flow.

3.5.2 Interactions between hydrologic connectivity and morphologic variations of oxbow lakes

Oxbow lakes in the study reach are found to increase in size (i.e., length, width, and area) as discharges increase in the main channel (Figs. 3.4-3.6), although their hydrologic connectivity is relatively low (Fig. 3.8). It follows that the expansion of the lakes was not always caused by surface water supplied via the lake-channel connection, but more by direct precipitation on the oxbow lakes and upslope overland flow draining into the lakes during various storm events. Therefore, the hydrologic connectivity of oxbow lakes is not the only mechanism driving dynamic changes of oxbow lakes. One missing piece might be the role of groundwater in oxbow

lake variations during the prolonged non-rainfall periods. The high spatial and temporal variations of groundwater levels in the study area suggest that the impact of groundwater on oxbow lakes could be complex (Li and Gao, 2020), which awaits more field-based data.

Although the connecting channels between the studied oxbow lakes and the main channel may promote hydrologic connectivity, their presence does not signify continuous hydrologic connectivity all year round. Indeed, we observed in the field that the connecting channels commonly remain desiccated or have a very limited amount of water flowing from the oxbow lakes to the main channel during a significant portion of the year, including some higher-flow periods when the main channel discharge exceeds Q_{am}. In these periods, hydrologic connectivity should not be considered to occur because 1) oxbow lakes do not receive channel water under these hydrologic conditions due to the higher water stage of the oxbow lake than that of the main channel, and 2) the major portion of the connecting channels remains desiccated. The conditions characterized by the stage differences between the studied oxbow lake and the main channel is unique from those observed in large fluvial settings, especially in large anabranching systems where the hydrologic connectivity is generally high given the synchronous water stages between the main channel and floodplain lakes (e.g., Hu et al., 2015; Park and Latrubesse, 2017; Park, 2020). Additionally, the actual longitudinal profile of connecting channels (i.e., oxbow-lake-end higher than main-channel-end) commonly developed in the study reach seems to differ from those of "tie channels" (i.e., main-channel-end higher than oxbow-lake-end) formed by sediment-laden flows from the main channel, suggesting distinct formative mechanisms and hydrologic patterns of the connecting channels in the lower Black River from previously studied "tie channel" or "tributary channel" (Dietrich et al., 1999; Rowland et al., 2005, 2009).

The higher S^* associated with oxbow lakes in compound forms (Fig. 3.7) is likely attributed to their larger areas that allow more desiccated lakes beds to be inundated from a lower flow (e.g., Q_{am} and Q_1) to a higher flow (e.g., > Q_{10}). Similarly, the higher S^* associated with oxbow lakes that develop connecting channels may be related not only to their greater areas but to the higher hydrologic connectivity, which enabled relatively active water supply from the main channel via surface water connection. The fact that a larger D_C correlates with generally a smaller S^* (Fig. 3.7a) and a smaller *PHC* (Fig. 3.10) demonstrates that D_C is an important morphologic index for inferring morphologic variation and hydrology of oxbow lakes. Moreover, the generally higher S^* associated with small D_C but large D_L (Fig. 3.7) highlights greater morphologic variation occurring in the oxbow lakes that are prone to lateral migration of the main channel (see Fig. 3.3).

By linking the mean S^* to *PHC* for all studied oxbow lakes, a general positive correlation can be found (Fig. 3.11). For *PHC* < 0.1, the increase of *PHC* may lead to linearly increased mean S^*, suggesting that morphologic changes of oxbow lakes are more sensitive to *PHC* when its degree is relatively low. When *PHC* > 0.1, even a greater increase of *PHC* would not cause a significant increase of the mean S^*, implying that higher degrees of hydrologic connectivity have a very limited impact on morphologic changes of oxbow lakes. It should be noted that this trend is only based on one data point at *PHC* = 10. The apparently limited impact might suggest that hydrologic connectivity is merely one driving force that controls morphologic variations of oxbow lakes.

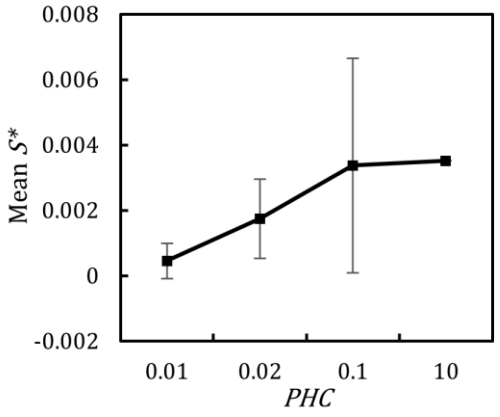

Figure 3.11 Mean S^* and the associated standard deviation (whisker bars) of the oxbow lakes in each class of *PHC*.

3.5.3 Impact of main channel migration on oxbow lake evolution

The production of an oxbow lake in the floodplain of a meandering river relies on the flow regime of the meandering river and its key morphodynamic properties, such as the channel sinuosity and the rates of sediment transport and lateral migration (Constantine and Dunne, 2008; Hooke, 2013). In fully developed oxbow lakes (i.e., in Stage III), sedimentation patterns may still be influenced by the diversion angle between the lake inlet and the main channel (Fisk, 1947; Constantine et al., 2010; Schwendel et al., 2018). However, the diversion angle could continuously change owing to the evolution of oxbow lakes and meandering channels, which in turn affects the rate and pattern of sedimentation in oxbow lakes. Furthermore, as plug bars grow to the elevation that disconnects the oxbow lake from the main channel, the in-lake sedimentation will be much less dependent on the diversion angle. In this study, we examine these changes through the spatial relationships between oxbow lake and the main channel.

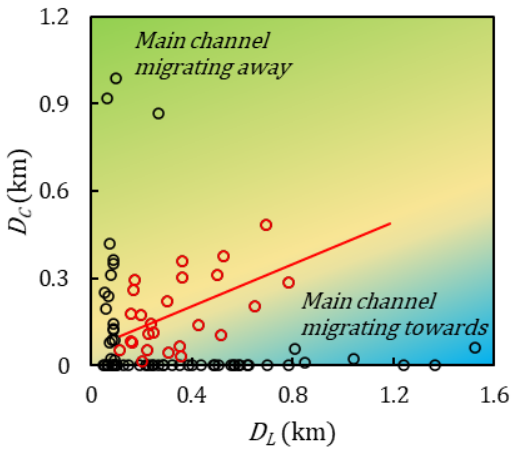

Figure 3.12 The $D_C - D_L$ relationship replotted based on Fig. 3.5, showing the oxbow lakes likely undergoing sedimentation with little or no lateral migration of main channels (red dots and the associated regression), the ones with entrances eroded by main channels migrating towards them (blueish area), and the ones with relatively faster migration of the main channels away from them than their sedimentation rates.

Values of D_L and D_C of an oxbow lake in their initiation (i.e., after the emergence of plug bars) stage ought to be about one channel width (i.e., < 100 m) and zero (unidentifiable from the remotely sensed data), respectively. Subsequently, both D_L and D_C should increase over time because the development of plug bars leads to the gradual retreat of oxbow lake entrances (before reaching

the position of the peak D_L), resulting in a positive correlation between the two (i.e., the red points in Fig. 3.12). This relationship holds when the rate of the lateral migration of the main channel is much less than that of in-lake sedimentation. However, many oxbow lakes follow two different spatial relationships, with one having very small D_L but large D_C and the other showing very small (including zero) D_C but large D_L (Fig. 3.12). In the first relationship, the oxbow lakes remain largely in their original sizes without notable in-lake sedimentation but are distant from the main channel due to its laterally migrating away from the lakes. In the second one, the oxbow lakes are located right next to the channels, but their inlets are distant from the outlets because the main channel migrates towards them. These two different processes of channel migration affect the evolution of oxbow lakes differently, with the former reducing the degree of hydrologic connectivity and the latter enhancing it. The absence of a general D_L-D_C relationship (Fig. 3.12) suggests the important role of lateral migration of the main channel in oxbow lake evolution, as highlighted in previous studies (Gagliano and Howard, 1984; Erskine et al., 1992; Richards et al., 2022).

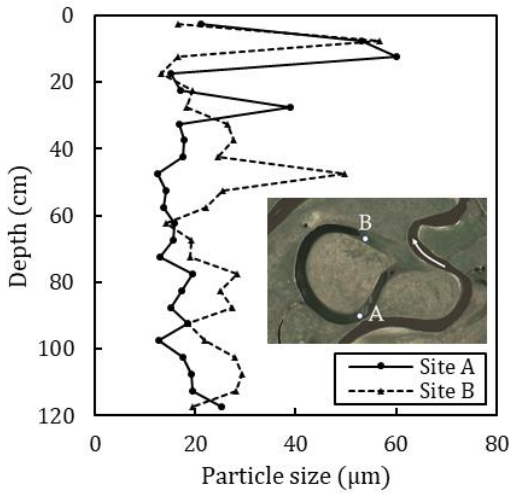

Figure 3.13 Near-surface (120 cm deep) profiles of median particle size collected at the reactivation site (Site A) and the opposite site (Site B) in oxbow lake #19.

Interestingly, the evolution of oxbow lakes may also be uniquely disturbed by direct contact of the main channel in positions away from the inlet and outlet where plug bars do not exist, resulting in the "reactivation" of the lake. As exemplified by oxbow lake #19 (Fig. 3.9), this process significantly intensifies the hydrologic connectivity of the oxbow lake by allowing water

in the main channel to move into the oxbow lake more frequently, making it the only case with *PHC* = 10 among all studied oxbow lakes.

The sediment core (Core #1) collected at Site A where the lake was reactivated shows notable fine-particle (D_{50} ranges between 11 and 23 μm) layers below the level of 30 cm from the surface and two peaks of coarser particles ($D_{50} \approx 58$ and 39 μm, respectively) in the shallower layers of 10-15 cm and 25-30 cm deep (Fig. 3.13). The two peaks may be attributable to the record-high flow in 2018, during which the higher flows caused rapid deposition of coarse sediments within the lake, and the pre-2018 event that triggered the "reactivation" of the oxbow lake, respectively. At Site B, the deep-layer (below the 30 cm level from the surface) deposits are slightly courser than those at Site A, possibly because site B was prone to the incoming flow from the main channel before the oxbow lake was reactivated. Two peaks in D_{50} ($D_{50} \approx 52$ and 45 μm, respectively) are present at the layers of 5-10 cm and 45-50 cm below the surface of Site B as well (Fig. 3.13), which may also be related to the same events as described in Site A but underwent different sedimentation rates. This unique case suggests that, although the reactivation event does not occur frequently in the lower Black River, its impact on the sedimentation patterns and the resultant evolutionary trajectory of the oxbow lake is significant. In the future, with the continuous growth of the natural levee of the main channel and the formation of a new plug bar near Site A, this oxbow lake will likely undergo a reduced rate of sedimentation, while the main channel will continue to erode the lake.

3.5.4 Implications for floodplain evolution of meandering rivers

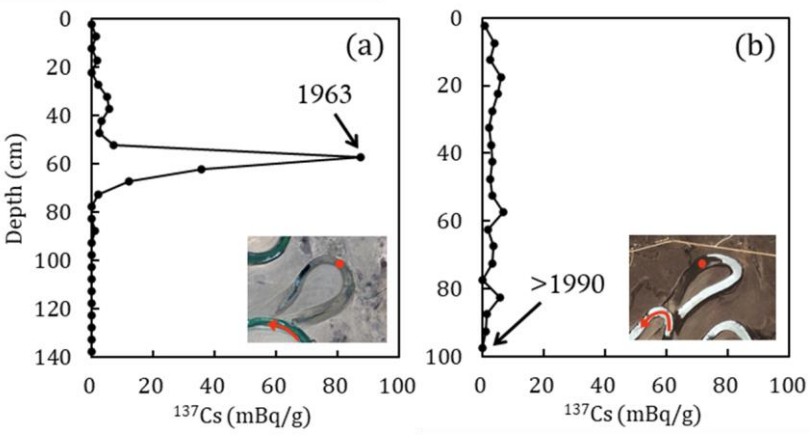

Figure 3.14 Near-surface (up to 140 cm deep) profiles of ^{137}Cs activity collected at inner parts of oxbow lakes #3 (a) and #48 (b).

Lateral migration of river channels, overbank sediment deposition, and production and sedimentation of oxbow lakes are the key processes controlling the evolution of floodplains of meandering systems (e.g., Hooke, 2013; Constantine et al., 2014; Ielpi et al., 2022, 2023). In order to assess the sedimentation rate of oxbow lakes in the study reach, we collected bed deposits of two oxbow lakes (i.e., #3 and #48) formed at different times. Specifically, according to satellite records, oxbow lake #3 was possibly formed more than 50 years ago, which has a D_C of zero and a D_L of 0.13 km (relatively small), whereas oxbow lake #48 was formed in the early 1990s. Because the peak concentration of ^{137}Cs can be accurately dated to the year 1963 for lake deposits in East Asia due to the maximum global fallout from atmospheric nuclear tests (He et al., 1996; Lan et al., 2020), we found the 1963 peak in ^{137}Cs for oxbow lake #3 and estimated its post-1963 average sedimentation rate of about 0.99 cm/year (Fig. 3.14a). For oxbow lake #48, the absence of a prominent peak in ^{137}Cs indicates that its formation time must be later than 1963 (Fig. 3.14b), which is consistent with our observation from the satellite images. Given that the deepest layer (i.e., the layer of 95-100 cm below the surface) may not reach the bottom of post-cutoff deposits, a minimum sedimentation rate of about 4.8 cm/year can be calculated based on the total depth of the sediment core and the earliest possible year of deposition at the 95-100 cm layer.

Clearly, the dramatic difference in sedimentation rate between the two oxbow lakes illustrates a fast-to-slow transition of sedimentation rate of oxbow lakes as they evolve, which is in accord with the patterns seen in typical lowland rivers of various sizes (e.g., Wren et al., 2008; Ishii and Hori, 2016; Shen et al., 2021). Although oxbow lakes in the lower Black River generally exhibit low hydrologic connectivity and very infrequent overbank flows, the significant amount of in-lake sedimentation compared with oxbow lakes in other fluvial systems reported (e.g., Erskineet al., 1992; Citterio and Piégay, 2009; Ishii and Hori, 2016), may still be contributed from the occasional hydrologic connection to the main channels during high-magnitude flow pulses (e.g., Q_{10} and Q_{45}).

The spatiotemporal variations of the channel migration determine dynamic patterns of not only oxbow lake infilling but floodplain reworking (e.g., Mertes et al., 1996; Gautier et al., 2007). In the lower Black River, the estimated rate of the channel migration at apices of meander bends averages at 0.011 widths/year with a maximum of 0.034 widths/year. This is an extremely slow rate compared to those of most meandering rivers worldwide (Guo et al., 2021). The low migration rate would be equivalent to a recycling period of > 8,000 years for the river's alluvial plain (assuming the valley width is approximately 90 times the channel bankfull width). While this recycling period is considerably longer than those of other studied meandering reaches (e.g., Mertes et al., 1996; Gautier et al., 2007; Aalto et al., 2008; Vayssière et al., 2020), it could even be longer due to the spatially uneven rates of channel migration, the occurrence of meander cutoffs, and the long-term (centennial to millennial) climatic and physiographic changes. The extensive peatland preserved within the valley of the Black River best demonstrates the limited impact of channel migration on floodplain reworking.

Overall, the floodplain of the lower Black River is characterized by inactive reworking of the meandering channel, infrequent but pulsed sedimentation patterns within oxbow lakes, and very rare overbank sedimentation in floodplains without oxbow lakes. Although floods equivalent to the 2018 record-high flow, which caused dramatic sedimentation across inundated areas within the floodplains, can rarely occur based on the observable history, the possibility of occurrence is likely to increase soon under the prevailing warming, wetting, and polarizing trends of climate change in the Qinghai-Tibet Plateau (Zhou and Zhang, 2021; Yao et al., 2022). This may eventually lead to more rapid sedimentation via overbank flow and channel migration across floodplains due to intensified fluvial erosion, which collectively contribute to a more dynamic floodplain of the lower Black River.

3.6 Conclusions

Although there is a consensus that the evolution of oxbow lakes involves four stages, including the meander-bend, cutoff, lacustrine, and terrestrial phases, knowledge of the processes controlling morphologic variation of oxbow lakes at Stage III and its relation to hydrologic connectivity remains limited. In this study, we examine a group of pristine oxbow lakes in a highly sinuous meandering reach in the Upper Yellow River watershed by characterizing their morphology and hydrologic connectivity and revealing the key processes driving the intra-stage evolution of the oxbow lakes. We find that the development of compound forms and connecting channels are the main morphologic characteristics of the oxbow lakes and that the distance between the oxbow lake and the main channel (D_C) correlates positively with the distance between oxbow lake entrances (D_L) when the lateral migration of the main channel is inactive. Their relationship may be complicated when the main channel is locally more active, which

could lead to distinct evolutional trajectories of the oxbow lakes in their lacustrine phase (i.e., Stage III).

Using four hydrologic benchmarks based on flood frequency analysis and remotely sensed data, we observe consistent expansion of the oxbow lakes with increasing discharges of the main channel. The expansion is mainly attributable to increased length at flows < Q_{10}, and to increased width at flows > Q_{10}. The rate of morphologic variation (S*) of the oxbow lakes correlates negatively and nonlinearly with D_C, while positively and linearly with D_L, suggesting that the lateral migration of the main channel enhances the magnitude of oxbow lake expansion. Their expansion is persistent with increasing river discharge, regardless of whether the oxbow lake connects to the main channel via surface water. This demonstrates that oxbow lake hydrology is not only controlled by hydrologic connectivity but by direct precipitation and supply of hillslope overland flow. Moreover, the existing approaches conceptualizing hydrologic connectivity based on surface water connection ignore the potential impact of groundwater interactions between oxbow lakes and main channels, which awaits future investigations derived from field data.

A new probability-based index (*PHC*) that can potentially be used for oxbow lakes in other fluvial systems is proposed to quantify the degree of hydrologic connectivity of oxbow lakes. The studied ones are found to have low hydrologic connectivity, which can be inferred from D_C and connecting-channel presence. The low degree of hydrologic connectivity is caused by the climatic and tectonic-driven channel downcutting of the Upper Yellow River. With the slow migration of the meandering channel, a comparatively inactive floodplain of the lower Black River is maintained.

Chapter 4: Morphodynamic characteristics of the complex anabranching system in the Upper Yellow River and the implications for anabranching stability[3]

4.1 Introduction

Anabranching rivers contain multiple channels separated by relatively stable islands of nearly up to the bankfull stage (Nanson and Knighton, 1996; Makaske, 2001; Ashworth and Lewin, 2012) and have now been considered a formal type of channel planform along with meandering, braided, and straight channels (Rust, 1978; Schumm, 1985; Latrubesse, 2008; Carling et al., 2014, Rhoads, 2020). In recent decades, with the increasing availability and accessibility of remotely sensed data for remote regions, anabranching rivers have been observed in various physiographic settings globally (Jain and Sinha, 2003; Latrubesse, 2008, 2015; Nanson, 2013; Liu et al., 2016; Mendoza et al., 2016).

Many efforts have been made to understand how anabranching rivers are formed and why they are sustained (e.g., Nanson and Knighton, 1996; Latrubesse and Franzinelli, 2005; Eaton et al., 2010). It is now well acknowledged that the formation of anabranches may be achieved by flow division from in-channel accretion (in-channel process) or channel incision across floodplains (off-channel process). The former involves channel bar accretion, which may occur when the width/depth ratio is large and discharge variability is high, promoting sediment deposition and bar emergence (Nicolas et al., 2013; Morón, 2017), while the latter involves an avulsion process facilitated by cohesive banks and vertical aggradation of channel beds that forcedly transforms floodplain portions into islands (e.g., Smith and Smith, 1980; Tooth and

[3] This chapter has been published in:
Guo, X., Gao, P., & Li, Z. (2023). Morphodynamic characteristics of a complex anabranching system in the Qinghai-Tibet Plateau and the implications for anabranching stability. *Journal of Geophysical Research: Earth Surface*, 128, e2022JF006788. https://doi.org/10.1029/2022JF006788

Nanson, 1999; Kleinhans et al., 2013; Słowik, 2018). Consequently, anabranching channels may exhibit diverse planform patterns, and islands created by these processes vary greatly in shape, size, and morphodynamic properties (Brizga and Finlayson, 1990; Knighton and Nanson, 1993; Liu et al., 2016).

Irrespective of the diverse planform patterns involved, anabranching rivers are generally regarded as stable river systems (Thorne, et al., 1997; Eaton et al., 2010; Nanson, 2013). Although riparian vegetation has been broadly accepted as a critical exogenous factor that maintains the stability of anabranching channels, especially smaller channels (Tooth et al., 2008; Jansen and Nanson, 2010; Yu et al., 2014), their stability has also been interpreted through the lens of flow efficiency (sediment-transport capacity per unit of stream power), which views anabranching development as the result of self-adjustments for enhanced flow efficiency in overloaded systems (Nanson and Huang, 1999; Jansen and Nanson, 2004; Huang and Nanson, 2007). When assessing the number of channels associated with the most stable form of anabranching rivers, previous studies have revealed that anabranching rivers with ≤ 4 channels tend to be optimal planforms for transporting the maximum amount of sediment (Huang and Nanson, 2007; Eaton et al., 2010; Nanson, 2013; Carling et al., 2014). This is indeed evidenced by many natural anabranching rivers, such as the Amazon, lower Yangtze, and Orinoco Rivers (Latrubesse, 2008; Mendoza et al., 2016; Han et al., 2018), where the number of cross-sectional channels rarely exceeds four. However, cases of anabranching rivers containing more channels (hereafter referred to as complex anabranching rivers/systems) broadly exist in nature as well and include the lower Paraná River, the Amur River (Lewin and Ashworth, 2014; Leli et al. 2020), and wandering gravel-bed anabranching rivers (Rhoads, 2020), where the complex morphology is not only embodied by more channels but also by the continuous development of

the multichannel pattern along the river courses. The long-lasting morphological complexity of these rivers suggests that channel numbers might fall short of effectively characterizing the stability of anabranching systems.

Islands are an integral component of anabranching channels, although the role islands play in maintaining anabranching stability has largely been neglected. Studies of islands in alluvial rivers mainly derive from the framework of island formation by Osterkamp (1998), which classifies the origins of islands into eight categories. For anabranching rivers, previous investigations of islands have focused on their morphological characteristics, formation, and underlying hydrological and climatic properties (e.g., Komar, 1983; Wende and Nanson, 1998; Tooth and Nanson, 1999; Meshkova and Carling, 2013; Leli et al., 2020; Gautier et al., 2021). Recently, Leli et al. (2020) further examined the morphological and sedimentological properties of islands with various planform patterns formed by different processes in the anabranching Paraná River. Nonetheless, these studies have drawn little attention to temporal changes in islands, which may be crucial for understanding the morphodynamic characteristics of anabranching rivers because island dynamics provide direct evidence for morphological adjustments of anabranching channels and enable the evaluation of interactions between islands and channels. Thus, understanding island morphodynamics is essential for fully understanding the fluvial processes and morphological responses of anabranching rivers.

This paper investigates a complex anabranching system in the Upper Yellow River of the Qinghai-Tibet Plateau, where channel splitting and islands are extensively fostered, to explore the role of island dynamics in the evolutionary processes of anabranching rivers. To unravel the morphodynamic characteristics of islands, channels, and their interactions, we document the morphological characteristics of islands and channels in this anabranching system, determine

spatiotemporal patterns of lateral adjustments, and assess the linkages between island and channel dynamics. Finally, based on the actual morphological characteristics of the studied anabranching system, we use a simplified model to predict sediment transport capacity and highlight the critical role that islands and their dynamics play in the evolutionary processes and stability of this anabranching system.

4.2 Study site

The Yellow River originates from the Bayan Har Mountains in the Qinghai-Tibet Plateau and flows eastward until arriving at its "First Great Bend" in the Zoige Basin (Fig. 4.1a), a broad and flat area with a mean elevation of 3,400 m. The basin contains the largest alpine peatland area in the world, which was formed by lacustrine deposits of an ancient lake that drained approximately 12,000 years ago due to river capture (Chen et al., 1999; Zeng et al., 2017). Later, the lakebed was gradually exposed, allowing alluvial channels to form. The study area has a moist and cool highland climate and is heavily impacted by the East Asian monsoon, which brings abundant precipitation in the summer. The annual mean temperature is 0.7 ℃, and the annual mean precipitation level is 645 mm (Li et al., 2014). The basin is mostly covered by herbaceous plants except on islands in the anabranching system of the Upper Yellow River, where *Salix atopantha*, a woody shrub endemic to the Qinghai-Tibet Plateau, grows extensively (Fig. 4.1c). Over the past decades, the Zoige Basin has been subject to a warmer and drier climate due to global environmental change (Hu et al., 2015). This change, together with intensified anthropogenic activities, particularly gully and upstream-channel erosion, has caused continuous wetland degradation (Li et al., 2015; Zhang et al., 2016; Li and Gao, 2019).

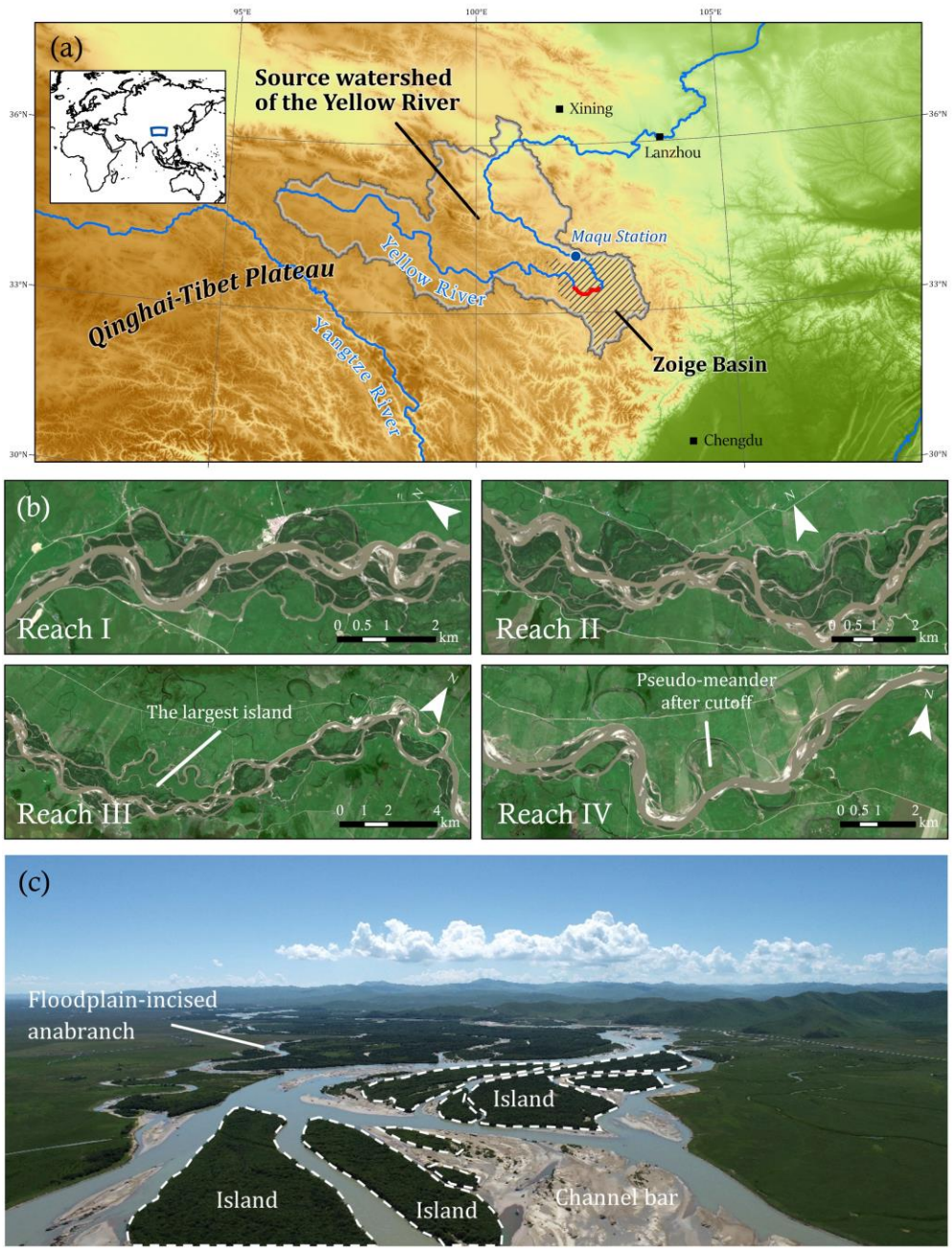

Figure 4.1 Overview of the study area. (a) Locations of the MAS (red line), the Zoige Basin (hatched area), and the source watershed of the Yellow River (outlined area) with elevation set as the background; (b) Planform views of the four studied reaches (Sentinel-2 images). Flows from the left to the right; (c) A bird's-eye view of an anabranching section in Reach II taken in the summer of 2021 using a drone. Water flows away from the camera.

The studied anabranching system ("Maqu Anabranching System" or "MAS") is approximately 56 km long and situated in the core area of the Zoige Basin in Maqu County,

Gansu Province of western China. The system starts immediately after the river enters the central part of the Zoige Basin, where it flows through a wide valley and has a gentle channel gradient. The average channel gradient is 0.5‰, and the median bed grain size is approximately 4.5 mm (Li et al., 2013). The annual mean discharge from 1980-2017 was 437 m^3/s at the Maqu gauge station (Fig. 4.1a). The average total channel width (containing islands, w_{to}) and active channel width (without islands, w_{ac}) are approximately 1,500 m and 480 m, respectively. We divide the anabranching system into four reaches (Reaches I to IV; Fig. 4.1b) based on differences in morphological characteristics. Reach boundaries are determined by nodal points along the river with no island to ensure that no boundary is crossed by a single island. Reach I is located most upstream with a total length of 11 km and contains rounded islands and a few small (narrow) anabranches likely formed by floodplain incision. Reach II immediately downstream of Reach I is 12 km long and has a more complex anabranching pattern (Fig. 4.1b and c). The lower portion of this reach includes several large islands separated from floodplains by small anabranches. Similarly, the 21 km-long Reach III is characterized by several large, elongated islands, including the largest island in the MAS (Fig. 4.1b). The anabranching structure of this reach is characterized by islands of various sizes and diverse types of asymmetric bifurcations. Reach IV is the most downstream reach and is 12 km long with the lowest degree of channel multiplicity. The lower section of this reach contains a large pseudomeander, which progressively dried out during the study period (Fig. 4.1b). Its meandering planform is also revealed by the sinuous channel relics and scroll bars within the surrounding floodplains.

4.3 Data and methods

4.3.1 Data acquisition and processing

We downloaded sequential Landsat Thematic Mapper (TM) and Operational Land Imager (OLI) images of a 30-m spatial resolution acquired between June and September of each year from 1986-2017 from the Earth Explorer repository (https://earthexplorer.usgs.gov/). Data acquired only during the summer months are initially selected to ensure sufficient vegetation cover in the study area for accurate channel delineation. We then select those with no impact of cloud cover over the studied reaches and set the time interval for sequential image analysis as approximately eight years. This interval is determined based on our preliminary study of channel changes, which indicated that lateral adjustments of islands and channels may be best identified from satellite images approximately eight years apart. Consequently, five sets of data, collected in 1986, 1994, 2001, 2009, and 2017, are selected and processed in ArcGIS to delineate islands and channels.

The determination of channel boundaries (i.e., riverbanks) and island extents (i.e., island banks) relies on vegetation lines that best indicate waterbody edges in bankfull conditions (Winterbottom, 2000; Donovan et al., 2019; Guo et al., 2021). To delineate the vegetation boundary, we calculate the normalized distribution vegetation index (NDVI) for each pixel over the study area and adopt 0.2 as the threshold level to differentiate channels (no or limited vegetation) from floodplains (Bertoldi et al., 2011; Henshaw et al., 2013). This method treats potentially exposed channel bars as part of channel areas, which best avoids uncertainties caused by the impacts of varying water stages on channel extents. Channel boundaries and island extents are then digitized for the selected five years based on the NDVI outcomes, and channel areas are extracted by subtracting islands from total areas enclosed by channel boundaries. Using these data, the entire study area can be classified into three general geomorphic units: channels, islands, and floodplains. Among them, the channel unit is further categorized into main channels

(i.e., the widest) and anabranches (i.e., all other narrower channels). The centerlines of the main channels and all anabranches are then delineated according to the positions of river and island banks. In the channel digitization process, narrower anabranches with widths close to the images' pixel size are identified only if they consist of fully continuous (including diagonal connection) "channel" pixels (i.e., NDVI < 0.2) or if each section of discontinuity does not exceed three pixels in length. Islands are defined as areas separated from floodplains by channels, with each comprising at least nine adjacent "nonchannel" pixels (i.e., NDVI > 0.2). These data provide the basis for evaluations of temporal changes (initial year – ending year) in islands and channels for four study periods: 1986-1994 (Period 1), 1994-2001 (Period 2), 2001-2009 (Period 3), and 2009-2017 (Period 4). Areas within channels in the initial year that became part of islands or floodplains in the ending year are defined as accretional, while those initially part of islands or floodplains that subsequently evolved into channels in the ending year are defined as erosional.

Potential errors associated with data acquisition and processing come from two major sources: registration and digitizing errors (Downward et al., 1994; Hughes et al., 2006). Specifically, the former is rooted in the original satellite imagery, for which the positional accuracy may be quantified by the root-mean-square error (RMSE). In this study, the selected images have a mean RMSE of 5.53 m with a maximum of 7.83 m. The latter arise from subjective uncertainties emerging during the digitizing process, although numerous studies have reported that digitizing with visual interpretation can produce more accurate results than using automated methods (e.g., Rowland et al., 2016; Donovan et al., 2019). In a recent study of meandering channel dynamics in the same region and based on the same data source, we employed Downward et al.'s (1994) method and reported an average digitization error of 2.3 m

(Guo et al., 2021). Therefore, the total error can be calculated by summing the squares of all individual errors and taking the square root of the sum, resulting in a value of 5.99 m. This error is acceptable, as a measurement displacement of channel boundaries with a magnitude of > 5 m likely represents true channel adjustments in aerial photographs (Gurnell et al., 1994), an absolute value criterion adopted in multiple previous studies (e.g., Gilvear et al., 2000; Winterbottom, 2000; Nicoll and Hickin, 2010).

Daily discharge data of the Upper Yellow River, recorded at Maqu Station (Fig. 4.1a), are used to evaluate the relationships between local hydrological conditions and morphodynamic characteristics of the MAS.

4.3.2 Data analyses

4.3.2.1 Hydrological analysis

Flood frequency analysis is performed by fitting a lognormal distribution to the time series of annual peak discharges for 1986 to 2017. The calculated discharges associated with 1-year (Q_1), 2-year (Q_2), 5-year (Q_5), and 10-year (Q_{10}) recurrence intervals are subsequently used to count the number of days in each year from 1986-2017 and each study period (i.e., Periods 1, 2, 3, and 4) with daily discharges exceeding each of these reference values. When counting days for each study period, we use dates of acquired images as breakpoints rather than the first and last days of a calendar year. This counting led to 2983, 1813, 2927, and 2911 days for each of the four study periods, respectively. Among them, Period 2 (1994-2001) includes a much smaller number of days due to a lack of hydrological data for 1998 and 1999. To rank the four study periods based on their overall hydrological intensities, we use a “hydrological index” that calculates the weighted sum of the proportion of days with a discharge exceeding the respective

reference discharges (Q_1, Q_2, Q_5, and Q_{10}) for each period using five sets of weighting criteria (details and relevant results are provided in the supporting information section). Among the four periods, the one with the highest hydrological index is considered to have the greatest hydrological intensity.

4.3.2.2 Channel morphology and lateral changes

Morphological characteristics of channels in the four studied reaches are quantified using the total channel width (w_{to}), the active channel width (w_{ac}), and the main-channel sinuosity (S_i), as well as the basic morphological parameters, including the number, length, and area of the main channels and anabranches. Specifically, w_{to} and w_{ac} are defined as follows:

$$w_{to} = \frac{A_{to}}{L_v} \tag{4.1}$$

$$w_{ac} = \frac{A}{L_v} \tag{4.2}$$

where A_{to} is the total area enclosed by channel boundaries that include areas of active channels and islands, A is the area of active channels that includes waterbodies and channel bars when the water stage is below bankfull, and L_v is the valley length of each studied reach. S_i is defined as follows:

$$S_i = \frac{L_{mc}}{L_v} \tag{4.3}$$

where L_{mc} is the centerline length of the main channel.

Additionally, we use an "anabranching intensity index" (An_i) to assess the channel multiplicity of each studied reach. The index was derived from the "braid-channel ratio" used for braided channels (Friend and Sinha, 1993), which has been used to characterize the anabranching-braiding reaches of the lower Yellow River (Kong et al., 2020). It is defined as follows:

$$An_i = \frac{L_{mc}+L_{an}}{L_{mc}} \quad (4.4)$$

where L_{an} is the total length of anabranch centerlines in each reach.

Areas of erosion (A_e) and accretion (A_a) are measured based on temporal changes in channel areas. A reach is considered erosion dominated if $A_e > A_a$ and as accretion dominated if $A_e < A_a$.

4.3.2.3 Island morphology and lateral changes

We first assess the island morphology of each studied reach using the basic morphological parameters of islands, including their numbers, perimeters, and areas. Then, we standardize the total island area (A_{is}) by L_v to assess the collective island width (w_{is}) in each studied reach, which is calculated as follows:

$$w_{is} = \frac{A_{is}}{L_v} = w_{to} - w_{ac} \quad (4.5)$$

Lateral changes in islands are classified based on positional differences in their extents between the initial and ending years of the study period (Fig. 4.2). We identify six main types of island change: expansion (EXP), shrinkage (SHK), coalescence (CLS), cleavage (CLV), new island formation (NIF), and elimination (or extinction; EXT). Specifically, EXP refers to an increase in the area of existing islands caused by accretion along island banks, and SHK refers to a decrease in the area of an existing island due to erosion. It should be noted that given that both EXP and SHK were identified by the net areal change of islands, an island changed by EXP may still show a small amount of erosion, and an island changed by SHK may also present local accretion. While CLS refers to the combination of two or more islands due to accretion within anabranches between them, CLV represents the division of an island into two or more smaller islands due to the formation of new anabranches within it. The pair of NIF and EXT represents the formation of new islands and the elimination of existing islands, respectively, with each

potentially being accomplished by either erosion or accretion. Particularly, for NIF, an island may be formed by in-channel accretion (NIFa) or floodplain incision (NIFe). Similarly, EXT may occur with accretion within anabranches (EXTa) by connecting islands to floodplains or with pure erosion to eliminate an entire island (EXTe).

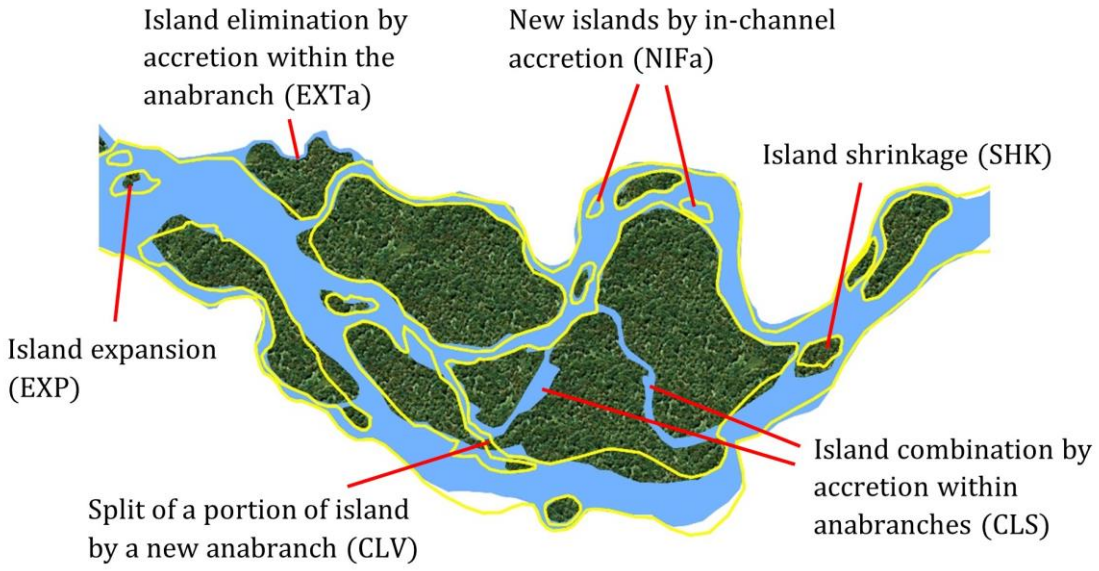

Figure 4.2 Examples of the major types (not including NIFe and EXTe) of island change in a sample section in Reach II. The background indicates channel areas and island extents in 1986 and the yellow outline represents the island extents in 1994.

Overall, accretion-dominated island changes are represented by EXP, CLS, NIFa, and EXTa, whereas erosion-dominated island changes include SHK, CLV, NIFe, and EXTe. We perform statistical analyses for each type based on island areas in the initial year of each study period and measure the total A_e and A_a of the anabranching system resulting from each type of island change.

4.4 Hydrological intensity of the study periods

There were only two days over the entire 31-year period with discharges of > Q_{10}, and both occurred in Period 1. The highest daily discharge was 2,710 m^3/s and occurred in 1989. For

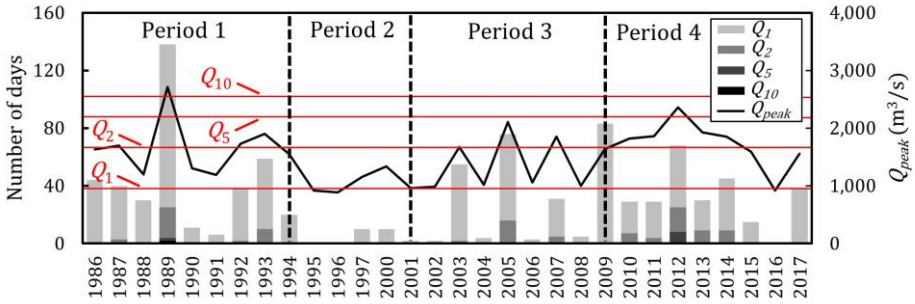

Figure 4.3 Hydrological intensity of the four study periods at Maqu station. Bars represent numbers of days in each year with daily discharges exceeding Q_1, Q_2, Q_5 and Q_{10}, respectively. The curve represents annual peak discharges (Q_{peak}).

Q_5, there were 12 days with greater discharges, with four occurring in Period 1 and eight occurring in Period 4. For Q_2 and Q_1, the numbers of days with greater discharges reached 40 and 385 in Period 1, 0 and 20 in Period 2 (without data for 1998 and 1999), 23 and 204 in Period 3, and 54 and 280 in Period 4, respectively (Fig. 4.3). The results of the hydrological index calculated for the four study periods indicate that Period 1 shows the highest degree of hydrological intensity, followed by Periods 4, 3, and 2 (see the supporting information section for relevant results). This pattern is also consistent with the ranking of the largest discharges (Q_{peak}) in the four study periods (Fig. 4.3).

4.5 Morphological characteristics and lateral changes of channels

4.5.1 Morphological characteristics of channels

Located downstream of a confined valley, the four studied reaches lie within an alluvial valley of variable widths, among which Reach I has the narrowest valley (i.e., 2.65 km) due to its adjacency to the confined upstream section, and Reach III has the widest valley (i.e., 8.21 km). Overall, the anabranching channels in all reaches presented multiyear mean w_{to} and w_{ac} values of 1.07 and 0.49 km, respectively, indicating that the active channels accounted for less than half of the total channel width and thus had abundant space to migrate freely across islands and

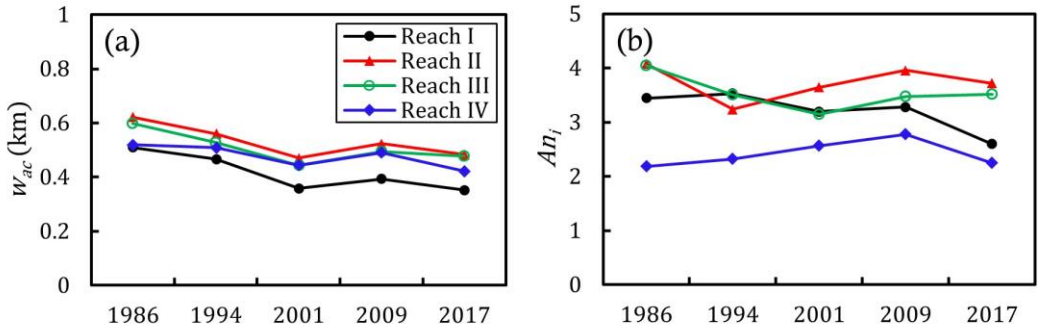

Figure 4.4 Spatiotemporal patterns of (a) the active channel width (w_{ac}) and (b) the anabranching intensity index (An_i).

floodplains. Over the study periods, while w_{to} did not exhibit an explicit temporal trend, w_{ac} underwent an overall decreasing trend in all reaches (Fig. 4.4a), suggesting the prevalence of a channel-narrowing process, except for 2001-2009 (Period 3), when channels notably widened (w_{ac} increased by > 5%) due to severe erosion within the system. Of the four studied reaches, Reach I had the lowest w_{ac}, which was consistent with its relatively narrow valley, and Reach II had the highest w_{ac}, although its valley was narrower than that of Reach III. The relationship between w_{ac} and valley width supports earlier findings showing that anabranching channels tend to develop on wider floodplains (Amos et al., 2008; Latrubesse, 2015; Morón et al., 2017) but also implies that channel width may not always be positively correlated with floodplain width.

The multiyear mean L_{mc} of the anabranching system was 68.22 km, leading to a mean S_i of 1.22 for the entire study period. Clearly, this level of sinuosity was significantly lower than that of meandering channels but was similar to that of other anabranching and braided rivers reported in past studies (e.g., Friend and Sinha, 1993; Frias et al., 2015). Overall, the course of the main channels remained stable in the system except for the occurrence of a "cutoff" of a pseudomeander in Reach IV (Fig. 4.1b), which led to the reach having the highest S_i (i.e., 1.37) among all reaches in 1986 and a reduction in reach-average S_i from 1986-1994 (Period 1) due to the cutoff occurring then. Over the rest of the period (Periods 2-4), S_i displayed a marginal

increase from 1.18 to 1.25, indicating that the main channel slowly evolved into a more sinuous pattern. Reach I, which had the smallest w_{ac}, was also characterized by the lowest multiyear mean S_i (i.e., 1.16), signifying that the planform of the anabranching system was not spatially homogeneous.

The MAS presented a uniquely high degree of channel multiplicity with a multiyear mean An_i of 3.27 (Fig. 4.4b), indicating that, on average, there were more than three channels in a cross-section along the course of the anabranching system. Given that tiny anabranches could not be identified from the satellite imagery, the actual An_i would be even higher. Specifically, the An_i of each reach was relatively constant with no general explicit trend over the study period (Fig. 4.4b). The most dramatic increase in An_i occurred from 2001-2009 (Period 3) due to severe erosion that significantly increased the number of anabranches in the four reaches. Regarding the spatial variability of An_i, Reaches II and III had An_i values of > 3 in all four study periods, with mean values of 3.73 and 3.54, respectively, whereas Reach IV was characterized by a lower An_i (i.e., a mean value of 2.42), which coincided with its lowest w_{to}. The mean An_i (i.e., 3.27) of the MAS was obviously higher than that of many other anabranching rivers with less complex planform structures, such as the Amazon, lower Yangtze and Orinoco Rivers, which typically develop two/three-thread patterns accompanied by single-thread sections for a significant portion (> 30%) along the rivers.

4.5.2 Lateral changes in channels

Morphological changes in the MAS exhibited a strong accretion-dominated pattern characterized by channel accretion prevailing in three of the four study periods in all four reaches (Fig. 4.5). The multiyear total A_e and A_a for the anabranching system were 12.08 and 19.19 km^2,

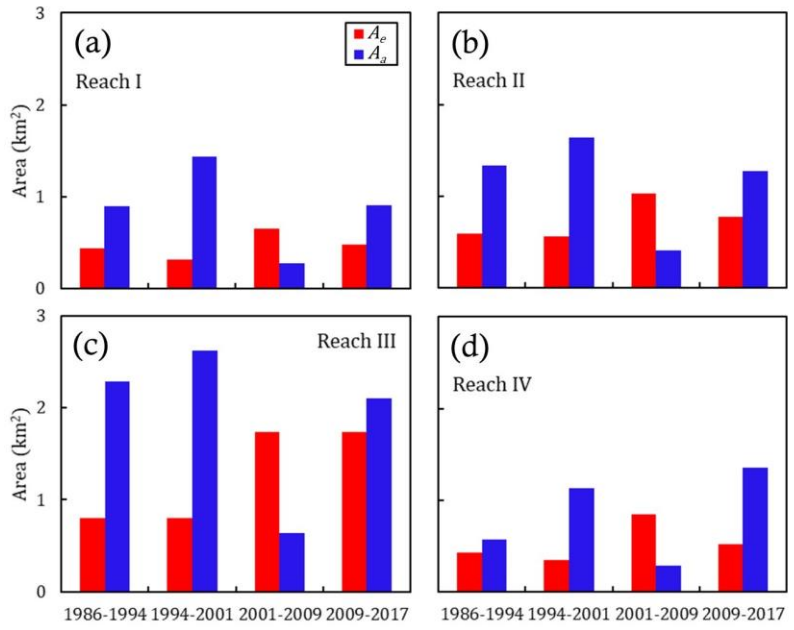

Figure 4.5 Areas of erosion (A_e) and accretion (A_a) in the four study periods of (a) Reach I, (b) Reach II, (c) Reach III, and (d) Reach IV.

respectively. In particular, the total A_a of all reaches was significantly larger than the total A_e for the first two periods, accounting for more than twice as much as the latter. The four studied reaches shared the same temporal trend in terms of the dominant morphodynamic pattern, with 2001-2009 (Period 3) being the only period in which $A_e > A_a$. This pattern coincided with the temporal pattern of w_{ac} and An_i (Fig. 4.4), demonstrating a progressively narrowing process of the anabranching channels by accretion within the system along either riverbanks or islands. It should be noted that, unlike for the other three reaches with A_e being the highest in Period 3, A_e of Reach III from 2009-2017 (Period 4) was slightly higher than that in Period 3 due to severe channel incision across islands and within floodplains. This unique change was linked to the lateral dynamics of islands, which will be discussed in the following section.

4.6 Morphological characteristics and lateral changes of islands

4.6.1 Morphological characteristics of islands

Islands in the MAS exhibited spatially variable morphological characteristics among the four studied reaches. In particular, Reach I had more rounded islands of medium-to-large sizes,

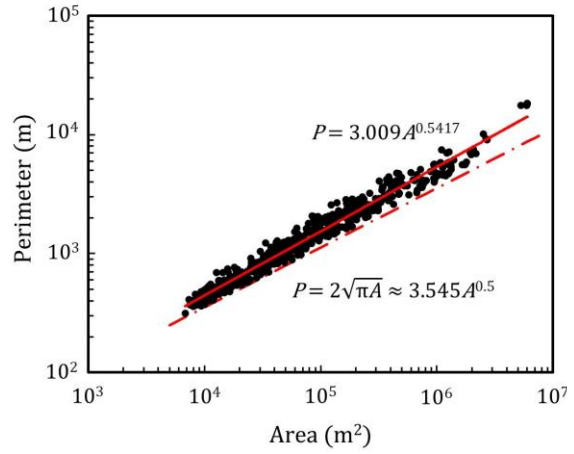

Figure 4.6 Relationship between island area and perimeter for all islands in the five studied years (1986, 1994, 2001, 2009, and 2017). The dotted line denotes the same relationship for a circle.

while Reaches II and III contained islands with highly diverse morphologies, including both very large elongated ones and smaller rounded ones. In contrast, Reach IV included much fewer islands than the other reaches, of which the sizes were comparatively small. The size and shape of these islands exhibited two general characteristics: (a) smaller islands tended to be more rounded, and larger islands tended to be more elongated, as implied by the larger exponent of the area-perimeter relationship compared to that of a circle (Fig. 4.6); (b) smaller islands were more streamlined and tended to have a lemniscate shape, indicating that they may originate from bar accretion within channels (Wyrick and Klingeman, 2011). Meanwhile, larger islands in the MAS tended to develop near channel edges and were separated from surrounding floodplains by small (narrow) anabranches, which strongly suggests floodplain incision (Leli et al., 2020). The largest island, located in Reach II (Fig. 4.1b), provides a good example of islands with such elongated morphology. With a multiyear mean area of 5.81 km^2, the island had an irregularly elongated shape and was separated from surrounding floodplains by a long, sinuous anabranch throughout the entire study period.

Reaches II and III included more large islands and higher An_i values, which suggests that the degree of channel multiplicity is controlled not only by the number of islands but also by their sizes. The multiyear mean w_{is} of islands in all reaches was 0.58 km, accounting for more than half of the mean w_{to} and demonstrating that islands were the dominant geomorphic unit in

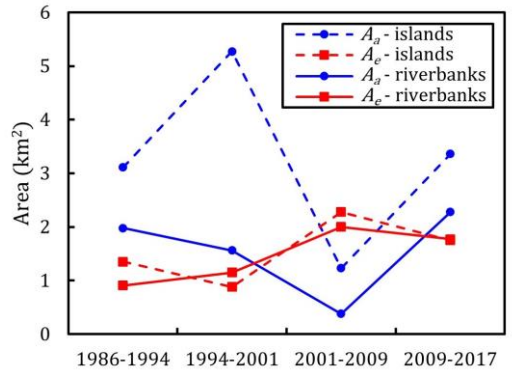

Figure 4.7 Total areas of accretion (A_a) and erosion (A_e) in all reaches based on their locations of occurrence.

the MAS. Together with An_i, these two indices may best demonstrate the complex morphological patterns of the anabranching system. Additionally, Reach IV had the lowest multiyear mean w_{is} (i.e., 0.26 km), which was consistent with its lower An_i compared to those of the other reaches. Reach III had the highest w_{is} (i.e., 0.78 km), although its corresponding mean An_i was slightly lower than that of Reach II.

For accretion that occurred within the anabranching system, the A_a value along island banks was 1.41 times greater than that measured along riverbanks (Fig. 4.7). This pattern suggests that accretion in the MAS was mainly related to island accretion and that the narrowing of active channels, as shown by temporal patterns of w_{ac} (Fig. 4.4a), was linked directly to sediment infilling of channels around islands. In particular, from 1994-2001 (Period 2), accretion on islands reached 5.27 km^2, being 2.38 times greater than that occurring along riverbanks. In contrast, erosion did not exhibit such a location preference and was distributed more evenly between islands and riverbanks (Fig. 4.7). This phenomenon indicates comparable bank strength between islands and riverbanks, even though the coarse-grained islands formed from channel bars may have less initial bank strength before vegetation encroachment. It is thus suggested that vegetation plays an important role in stabilizing these bar-formed islands.

4.6.2 Lateral changes in islands

Table 4.1: Number of islands that changed by each type of island change measured in the four study periods. The measurement of NIFa and NIFe is based on island numbers in the ending year, and that of the rest is based on island numbers in the initial year.

	1986-1994	1994-2001	2001-2009	2009-2017
EXP	52	41	32	42
SHK	12	10	47	13
CLS	24	41	11	46
CLV	3	0	12	7
NIFa	19	42	8	16
NIFe	0	0	9	4
EXTa	16	11	2	18
EXTe	1	0	5	6
CLV&CLS	1	0	1	2

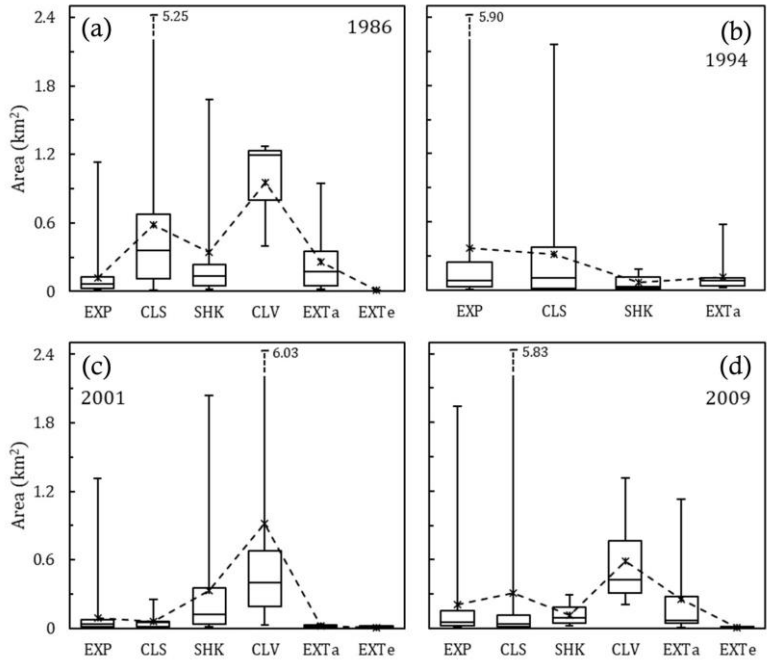

Figure 4.8 Statistical distribution (whiskers indicate the three quartiles; top and bottom bars indicate maximum and minimum values, respectively; and stars indicate mean values) of island areas in the initial year of each study period (e.g., 2009 for the 2009-2017 period) classified by types of island change.

Over the entire study period, islands in the MAS exhibited diverse patterns of lateral change (Table 4.1). EXP was very common in all four periods, accounting for approximately 40.6% of the number of islands from 1986-1994 (Period 1) and for 25.2-28.3% in other periods. Islands changed by EXP varied greatly in size with a multiyear mean value of 0.20 km^2. These areas did not show clear areal clustering over the four periods (Fig. 4.8). SHK was the most common type in the erosion group (i.e., SHK, CLV, NIFe, and EXTe), accounting for up to 37.0% of the total number of islands from 2001-2009 (Period 3) and ranging between 6.9% and 9.4% in other periods. Similarly, the sizes of islands changed by SHK varied greatly (Fig. 4.8). In addition to EXP, CLS

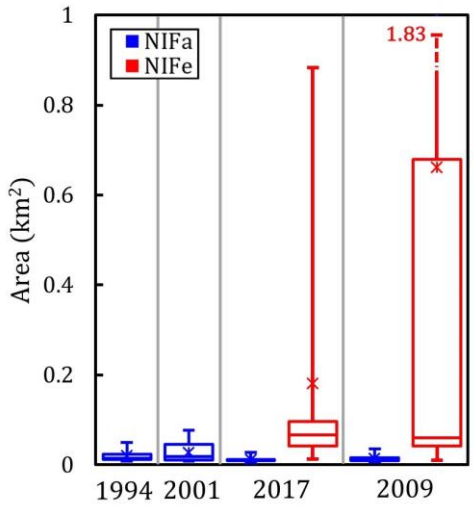

Figure 4.9 Statistical distribution of island areas between accretion-formed (NIFa) and floodplain-excised (NIFe) islands in the final year of each study period (e.g., 2009 for the 2001-2009 period).

was the most common type in the accretion group (i.e., EXP, CLS, NIFa and EXTa), accounting for approximately 18.9-30.0% of the number of islands during the entire study period except for Period 3, when only 8.7% of the islands were changed by CLS. Because EXP and CLS are accomplished by accretion, their dominance was consistent with the net accretion of the system. CLV is the opposite type of CLS and accounted for 9.4% of the number of changed islands in Period 3 and for only 0-4.5% in other periods. Compared to other types, CLV was common among large islands, with a multiyear mean area of 0.82 km^2 (Fig. 4.8).

The formation of new islands (NIF) accounted for 13.0-29.0% of the number of islands during the entire study period, with the most (i.e., 29%) island formation occurring from 1994-2001 (Period 2). Specifically, NIFa was the dominant type of NIF in all four periods except for Period 3, when NIFe slightly exceeded NIFa due to severe erosion. No NIFe occurred in the first two periods, and the dominance of NIFa in Period 2 (i.e., 42 islands) coincided with the finding that A_a was fairly large and A_e was the smallest in this period (Fig. 4.5). It is interesting to note that the areas of islands formed by NIFa were much smaller than those formed by NIFe (Fig. 4.9). The mean values of the two were 0.019 and 0.42 km^2, respectively. This finding agrees with the results of Leli et al. (2020), which implies that floodplain incision may form relatively large islands by carving new channels across floodplains, whereas considerable amounts of time are required for channel bars to develop and grow to a comparable size.

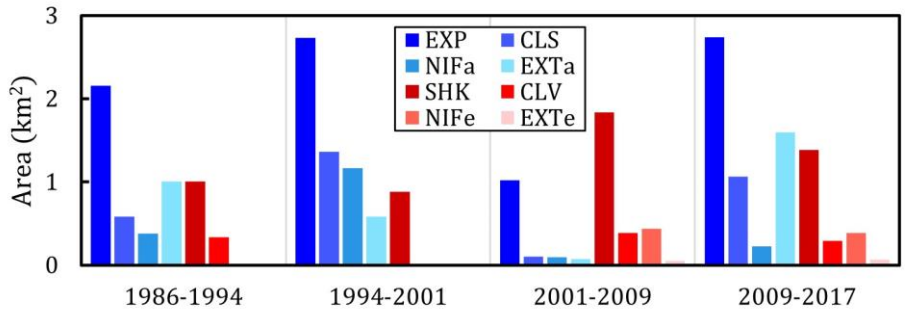

Figure 4.11 Total A_a and A_e resulting from each type of island change. The accretion group (i.e., EXP, CLS, NIFa, and EXTa) uses a blue gradient ramp, while the erosion group (i.e., SHK, CLV, NIFe, and EXTe) uses a red gradient ramp.

The proportion of islands changed by EXT ranged from 5.5-15.6% throughout the study period, and EXTa was the dominant type in all periods except for Period 3 (Table 4.1). Similar to the areal difference of islands associated with the two types of NIF, EXTe was found to occur in very small islands, whereas EXTa tended to occur in larger islands (Fig. 4.8), demonstrating that the elimination of large islands is likely accomplished through anabranch dry-up caused by accretion (the opposite of floodplain incision) rather than in-channel erosion.

By dividing A_a and A_e on islands based on types of island change, the results show that EXP and SHK contributed to the greatest areal change for accretion and erosion in the anabranching system, respectively (Fig. 4.10). The multiyear mean percentages of the area contributed by EXP to the total A_a on islands and by SHK to the total A_e on islands were 56.6 and 76.7%, respectively, implying the dominance of the two types of island change in terms of the levels of lateral change they produced. In comparison, other types (i.e., CLS, NIFa and EXTa for accretion and CLV, NIFe and EXTe for erosion) contributed much less to lateral change. Among the types of island change caused by accretion, EXTa generated relatively large areal changes from 1986-1994 (Period 1) and 2009-2017 (Period 4), which is consistent with its higher number of cases during the two periods (Table 4.1). As the two types of island change associated with

the formation and elimination of floodplain-incised anabranches, NIFe and EXTa exhibited a notable imbalance between their amounts of areal change and between their case numbers in that the total A_a resulting from EXTa was 2.93 times greater than the total A_e resulting from NIFe and that total EXTa cases were 2.62 times more common than total NIFe cases. The discrepancy indicates that the sedimentation (i.e., elimination) of floodplain-incised anabranches occurred more extensively than the creation of new anabranches by floodplain incision, suggesting a long-term trend of diminishing floodplain-incised anabranches in the MAS.

4.7 Discussion

4.7.1 Sediment-transport capacity of the MAS

The stability of anabranching channels has been a topic of considerable interest (Rhoads, 2020). While some have linked it to exogenous factors, such as riparian vegetation (e.g., Tooth et al., 2008; Jansen and Nanson, 2010, Henriques et al., 2022), others have developed and adopted a theory pertaining to flow efficiency, which relates stability to maximized sediment-transport capacity in anabranching systems with channel numbers equal to or less than four (Nanson and Huang, 1999; Huang et al., 2004; Huang and Nanson, 2004; 2007; Janson and Nanson, 2004; Huang and Chang, 2006; Eaton et al., 2010). This theory is largely derived from simplified mathematical analyses and lacks empirical evidence from measured sediment-transport capacity in natural anabranching channels (Rhoads, 2020). Moreover, by setting all channels of an anabranching system to an equal width in the modeling of sediment-transport capacity (e.g., Huang and Nanson 2007), the impact of variable widths on channel hydraulic and sediment-transport capacities has been neglected.

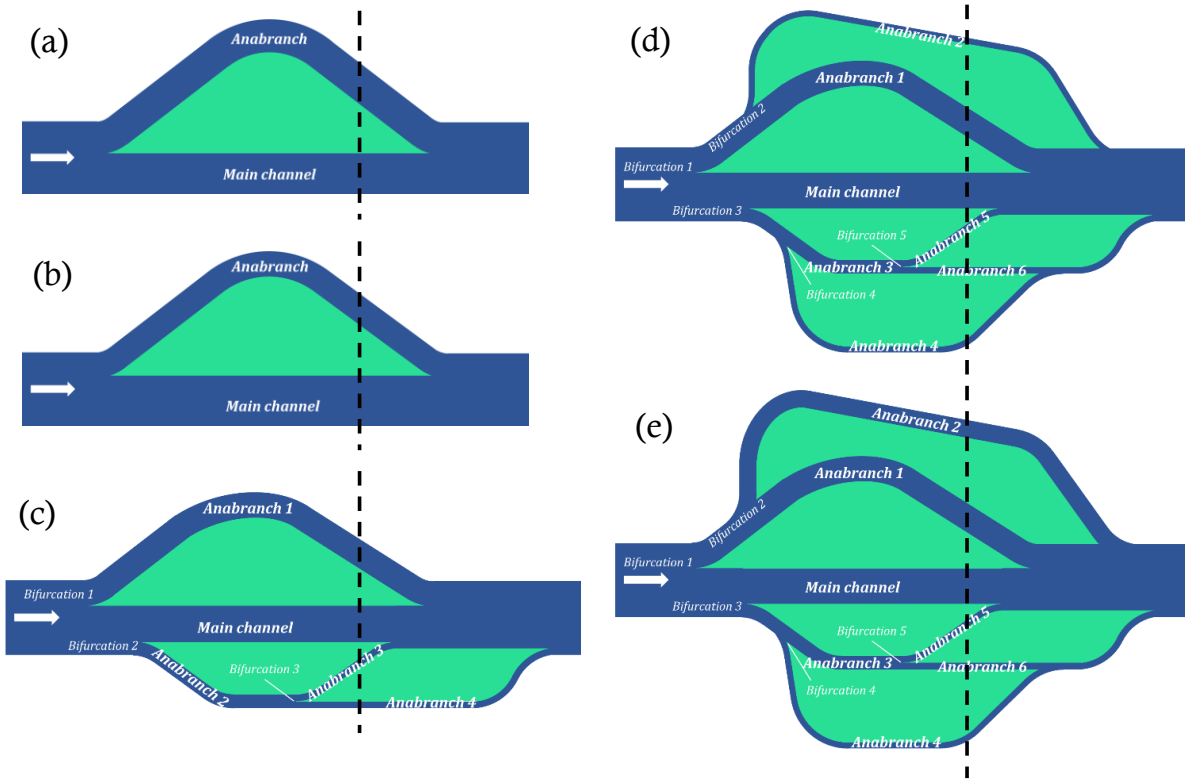

Figure 4.13 Five designed anabranching structures based on the MAS for modeling transport capacity. (a) Anabranching Structure A: a two-channel anabranching structure with bifurcation based on a width scale of 2:3; (b) Anabranching Structure B: a two-channel anabranching structure with bifurcation based on a width scale of 1:2; (c) Anabranching Structure C: a four-channel anabranching structure with bifurcations 1, 2, and 3 based on width scales of 1:2, 1:3, and 1:1, respectively; (d) Anabranching Structure D: a six-channel anabranching structure with the addition of two secondary channels (i.e., Anabranches 2 and 4) based on Anabranching Structure C. Bifurcations 1, 3, and 5 are set to width scales of 1:2, 1:3, and 1:1, respectively, and Anabranches 2 and 4 are 25 m wide; (e) Anabranching Structure E: a six-channel anabranching structure with Anabranch 2 being 50 m wide and all other properties being the same as those of Anabranching Structure D. The upstream channel width is 300 m in all five scenarios.

Using an approach that highlights the distinction of main channels from anabranches by allowing channel widths to vary, we estimated the sediment-transport capacity of the MAS under bankfull discharge using five heuristic anabranching structures with variable channel numbers and bifurcation asymmetry based on the actual morphological characteristics of the MAS (Fig. 4.11; see the supporting information section for details). The results show that the two-channel and four-channel structures (Anabranching Structures A, B, and C) have slightly higher transport capacities than the single-thread channel. Although the transport capacity of the four-channel

anabranching structure (Anabranching Structure C) is the highest of all five structures, the increased capacity accounted for < 1% of the capacity in the single-thread channel, representing a very marginal increase that possibly falls within errors induced by a variety of factors, including the use of a constant roughness coefficient, the empirical width-discharge relation, and the bedload transport equation. Similarly, in the two-channel structures (Anabranching Structures A and B), the increased transport capacity from 0.14% (Anabranching Structure A) to 0.37% (Anabranching Structure B) due to increased bifurcation asymmetry was insignificant. In contrast, the degrees of capacity reduction in the six-channel structures (i.e., Anabranching Structures D and E) were higher (1.27% and 4.18% reduction for Anabranching Structures D and E, respectively), particularly for Anabranching Structure E, in which one of the floodplain-incised anabranches (i.e., Anabranch 2) was significantly widened compared to that in Anabranching Structure D.

Although the differences in the predicted sediment transport capacities between the five possible anabranching structures and the single thread are small, the trends of decreased capacities in the six-channel structures, especially for Anabranching Structure E, suggest that anabranching structures with “excess” channels in the MAS are likely to discourage sediment transport by triggering sediment deposition in the anabranching system. Indeed, the small channels in Anabranching Structures D and E (i.e., Anabranches 2 and 4) represent floodplain-incised anabranches in the MAS, which diminished gradually over the study period. These small channels can transport very little sediment even at the bankfull stage due to their limited depths and water discharges distributed to them after bifurcations. Therefore, they largely serve as water pathways (e.g., Jansen and Nanson, 2004; Huang and Nanson, 2007) that may experience cycles of elimination (through EXTa) and re-emergence (through NIFe) over time depending on

sediment supply. When there is sufficient sediment supply under an appropriate combination of water discharge and sediment heterogeneity (Makaske et al., 2009), these small channels may be infilled to promote EXTa. When sediment supply becomes limited, erosion inevitably occurs to either reactivate previously infilled channels or carve new channels across floodplains, which both exhibit NIFe. Therefore, given that the MAS is an overloaded system with a high degree of channel multiplicity, the development of an anabranching pattern may promote sediment deposition through the accretion dynamics of islands (Nanson, 2013). However, the specific mechanisms driving this process are relevant to inter- and intra-annual changes in hydrological regimes, which remain unclear.

As a first attempt to quantitatively evaluate flow efficiency for anabranching channels based on actual morphological structures of an anabranching system, this simulation differs from "traditional" equal-width models in that it adopts variable channel widths for anabranches, which takes the important effect of channel width on river planform morphology into account (Dunne and Jerolmack, 2020). Despite the simplifications of this model, the relatively small discrepancies among the predicted transport capacities from the five simulated anabranching structures suggest that the number of channels is not necessarily a morphological condition to signify the stability of an anabranching system because channels with different widths play different roles in transporting supplied sediment from upstream through the system. Specifically, the emergence and disappearance of small anabranches are critical morphological responses to island dynamics and are further discussed in the following section.

4.7.2 Coupling hydrological variations with island-channel interactions

The results regarding lateral changes in islands and channels obtained in this study provide an opportunity to assess the interactions between islands and channels under variable hydrological regimes in the MAS. In particular, Period 2 (i.e., 1994-2001), which showed the lowest level of hydrological intensity, was associated with the strongest accretion-dominated morphological adjustment (i.e., a smaller A_e and larger A_a in Fig. 4.5). The extensive accretion in this period was accomplished mainly by EXP, followed by CLS and NIFa, which were greater than those in the other three periods (Fig. 4.10). The lack of CLV and NIFe in this period suggests that these avulsion-triggered processes are not likely to occur under low-intensity flows, which decrease the frequency of overbank flow even in channels dominated by bed aggradation (Jerolmack and Mohrig, 2007; Nanson, 2013).

Period 1 (i.e., 1986-1994) had the highest level of hydrological intensity among the four study periods (Fig. 4.3). However, the area changes in islands and channels were dominated by accretion in all four reaches (Fig. 4.5). This "mismatch" suggests that the dynamics of islands and channels were not directly controlled by extreme flows but more driven by moderate flows with higher frequency, facilitated by variability in sediment supply (Tooth and McCarthy, 2004; Draut et al., 2011; Rhoads, 2020). Under such conditions, a large amount of sediment may be transferred through the anabranching system in Period 1 due to fully mobile sediment transport (Gao, 2012) induced by very high flows and increased sediment supply caused by intensified anthropogenic impacts in the Zoige Basin (Li et al., 2015; Yu et al., 2017). Moreover, the possible bimodal property of sediment (Smith, 1996; Houssais and Lajeunesse, 2012; Dunne and Jerolmack, 2018) may force coarser components of sediment to deposit as hydraulic forces of sediment-laden flows may be reduced after bifurcations, confirming the identification of the MAS as an essentially transport-limited system. Consequently, accretion may occur around

islands in large, wider anabranches to produce NIFa and EXP, while smaller anabranches between islands/floodplains may be infilled to produce CLS and EXTa. Over the 31-year study period, sediment transport in the MAS featured net accretion (Fig. 4.5). This characteristic suggests that the MAS has been in an accreting disequilibrium state, which has been observed in some other anabranching systems (Rhoads, 2020). Along this line, future work should focus on assessing sediment supply by using systematic measures of particle size distributions in anabranching channels to better understand the spatial variability of sediment deposition.

The complex interactions between islands and channels under variable flow regimes and sediment supply in the MAS reveal that the stability of an anabranching system should not be judged by equilibrium theory based on systematic sediment balance. The MAS, while maintaining relative stability, was not identified as a graded system given its dominant trend of sediment accretion as a result of imbalanced sediment flux. Rather, its stability was characterized by relatively stable sizes and morphologies of main channels and large anabranches (i.e., at the reach scale), while small anabranches and the associated islands (i.e., at the geomorphic-unit scale) greatly exhibited dynamic patterns. With excess sediment supply, sediments incapable of being transported were "digested" within the anabranching system through deposition around islands and within small anabranches without altering the main morphological structures of the system. In a broader sense, our analysis of the dynamic interactions between islands and channels in the MAS provides new insight into how an anabranching system maintains stability under a background of excess sediment supply and the resultant slow rate of aggradation.

4.7.3 Implications for the channel-pattern continuum of multithread channels

The MAS was characterized by a high degree of channel multiplicity ($An_i > 3$) and the dominance of islands ($w_{is}/w_{to} > 0.5$). This planform structure and the morphodynamic processes that maintained its stability indicate not only the complexity of the same pattern of anabranching rivers but also the transitional nature of the two types of multithread patterns: anabranching and braided channels. In the MAS, both in- and off-channel processes were widely observed, which are typical in anabranching rivers developed elsewhere (e.g., Nanson, 2013; Leli et al., 2020; Rhoads, 2020). Our analysis of new island formation over the study periods suggests that islands formed by the in-channel process (i.e., NIFa) exceeded those formed by the off-channel process (i.e., NIFe) in terms of island numbers (Table 4.1) and the associated morphodynamic changes (i.e., areas of in-channel accretion > areas incised by anabranches within floodplains, see Fig. 4.10), although NIFe exceeded NIFa according to island size (Fig. 4.9). Therefore, both processes have been active in the MAS, resulting in the system greatly resembling wandering gravel-bed rivers (Rhoads, 2020).

Nonetheless, the unit stream power of the MAS at the bankfull stage was only 13.3 W/m^2, a value significantly lower than the lower limit signifying typical wandering gravel-bed rivers (i.e., 30 W/m^2) and within the range characteristic of anastomosing rivers (Nanson and Knighton, 1996; Burge, 2005). Meanwhile, the MAS differed from typical anastomosing rivers, as the former appears to adjust at much faster rates than the latter. Additionally, since anastomosing rivers are dominated by the avulsion process in creating anabranching patterns (Makaske, 2001; Makaske et al., 2002), active in-channel accretion in the MAS makes it further distinct from anastomosing rivers. Furthermore, large rivers (i.e., the largest rivers in the world by discharge), which are known to be fundamentally different from small and medium-sized rivers (Lewin and Ashworth, 2014), generally develop anabranching patterns and have stream

power and morphodynamic characteristics (especially for the Paraná River) similar to those of the MAS (Latrubesse, 2008; Leli et al., 2020). Therefore, although the MAS shared certain morphodynamic similarities with those of many others, it appears that the system is distinct from existing types of anabranching patterns reported previously.

Due to intense channel multiplicity, aggrading dynamics in response to excess sediment supply, and widespread island/bar excision, the MAS is similar to braided rivers in terms of morphology and dynamic processes (Ashmore, 2013, Schuurman & Kleinhans, 2015). However, what distinguishes anabranching from braided systems is the impact of vegetation on islands and the associated persistence of multithread patterns at the bankfull stage (Burge, 2006; Jansen and Nanson, 2010; Tal and Paola, 2010; Han and Brierley, 2020; Henriques et al., 2022). Compared to typical braided reaches in the Qinghai-Tibet Plateau, such as the upper Lancang and Yangtze Rivers (Li et al., 2020, Gao et al., 2022), the MAS exhibited discernably denser vegetation on islands (Fig. 4.1c). This is possibly attributable to the extensive growth of *Salix atopantha*, a willow shrub endemic to the Qinghai-Tibet Plateau, within the anabranching system, which significantly promotes the stability of fine sediments and has transformed mobile bars into more stable islands. The consistent uneven distributions of accretion (i.e., accretion mostly occurred around vegetated islands rather than along less-vegetated riverbanks) and vegetation (i.e., islands were densely vegetated with shrubs, but most floodplains only included herbaceous plants; Fig. 4.1c) further demonstrate the significant impact of vegetation on fluvial processes of multithread channels in that vegetation encroachment may initiate positive feedback by increasing the surface roughness of islands/bars, triggering the deposition of fine particles, and supporting more vegetation growth. In the braided reaches of the upper Lancang and Yangtze Rivers, the limited vegetation present is incapable of maintaining continuous bar accretion during consecutive flood

events, causing more dynamic fluvial processes to occur repetitively. Therefore, in terms of river evolution and channel planform patterns, the MAS likely developed from an initially weak braided pattern produced by flood-induced avulsions (Ferguson, 1990; Grenfell et al., 2012) and then evolved into an anabranching system under the crucial impacts of vegetation. This argument is consistent with the discernable relics of braided patterns amid extensive bars currently found within the system (Fig. 4.1c). Thus, the well-known transitional nature of channel planform morphology (Eaton et al., 2010; Nicholas, 2013; Wohl, 2019) is also observed within the multithread pattern alone, and river patterns present different planform structures but are often complicated by the coexistence of similar processes involved in rivers with different morphological planforms (Schumm, 1985; Kleinhans, 2010).

4.8 Conclusions

The Maqu Anabranching System in the Upper Yellow River exemplifies a type of anabranching river with highly complex morphological patterns characterized by a high degree of channel multiplicity and a dominance of multiple islands. Previous approaches linking anabranching stability to the number of channels mainly start from the assumption of equal channel widths, which neglects the critical role of island dynamics in influencing channels of various sizes differently. This study fills this gap by scrutinizing the morphodynamic patterns of island-channel interactions and estimating sediment-transport capacity based on five anabranching structures of variable widths for the studied anabranching system. We find that although anabranching patterns are typically deemed stable, morphological structures of the anabranching reaches exhibited dynamic and diverse temporal variations dominated by island changes, which may be classified into four paired types of changes caused by deposition and

erosion processes: (a) expansion (EXP) and shrinkage (SHK); (b) coalescence (CLS) and cleavage (CLV); (c) new island formation by accretion (NIFa) and elimination by erosion (EXTe); and (d) island elimination by anabranch accretion (EXTa) and new island formation by floodplain incision (NIFe). These processes may occur under variable hydrological conditions except for CLV and NIFe, which rely on avulsion and thus may not occur with low-magnitude flows. Among the types of island change, expansion and shrinkage contributed the greatest areal changes in terms of areas deposited or eroded, although the total depositional area was found to be significantly larger than the erosional area within the studied reach, denoting an accreting disequilibrium state of the anabranching system.

Island dynamics can result in changes in anabranch numbers within a system through the repeated formation and elimination of small floodplain-incised anabranches and minor morphological adjustments of main channels and large anabranches. The stability of this anabranching system is embodied by the sustained morphological structures of large channels. Therefore, island dynamics and the resultant dynamics of small anabranches are key to understanding the morphodynamic properties and stability of anabranching patterns. Estimations of sediment transport capacity based on the simulated anabranching structures suggest that, as a transport-limited system, the overdevelopment of anabranching channels promotes the deposition of excess sediment around islands and in nearby floodplains. This process is further facilitated by vegetation that transforms mobile bars into stable islands.

Globally, the Maqu Anabranching System resembles wandering gravel-bed rivers and some braided rivers in terms of its complex morphological structure and coexistence of in-channel accretion and floodplain excision for the formation of islands and channel bars, whereas its limited unit stream power matches that of anastomosing rivers and large anabranching rivers

across the globe. It is evident that vegetation encroachment plays a crucial role in transforming an initially unstable braided system into a more stable anabranching system. These similarities and discrepancies among multithread rivers highlight the transitional nature of alluvial channel patterns, which calls for more attention to fluvial processes that drive alluvial channel patterns.

4.9 Supplementary materials

4.9.1 Calculation of the hydrological index

We used the hydrological index to assess the overall hydrological intensity of each study period (i.e., Periods 1-4) involved in this paper. Specifically, the hydrological index calculates the weighted sum of the proportion of days with a discharge exceeding the respective reference discharges (Q_1, Q_2, Q_5, and Q_{10}) in each period using five sets of weighting criteria. They are: (a) 0.1, 0.2, 0.3, 0.4; (b) 0.1, 0.1, 0.2, 0.6; (c) 0.1, 0.15, 0.3, 0.45; (d) 0.05, 0.1, 0.35, 0.5; (e) 0.05, 0.15, 0.25, 0.55. Because there is no "standard" to be used to determine the weights, we determined them based on two principles. First, larger flows (i.e., Q_{10} compared with Q_1, Q_2 and Q_5) have larger weights, while smaller flows have smaller weights. Second, five different combinations of weights were selected to reflect the possible variations of weights.

As reported in section 4, the five weighting criteria all produce the same ranking results, with Period 1 having the greatest weighted sum, which is followed by Periods 4, 3, and 2 (Table

Table 4.3: The calculated hydrological index for the study periods using five weighting criteria introduced in section 3.2.1 (WC = weighting criterion).

	WC-a	WC-b	WC-c	WC-d	WC-e
Period 1	1.63	1.49	1.56	0.86	0.92
Period 2	0.11	0.11	0.11	0.055	0.055
Period 3	0.85	0.81	0.81	0.43	0.47
Period 4	1.42	1.32	1.32	0.76	0.83

4.2). It is therefore suggested that Period 1 has the highest overall hydrological intensity, which is followed by Periods 4, 3, and 2. Table 4.2 provides detailed results of the calculated hydrological index.

4.9.2 Estimation of sediment-transport capacity

The five simulated anabranching structures, as shown in Figure 11 of the paper, start from a 300-m wide single-thread channel and then bifurcate differently, forming (A) a two-channel structure with a bifurcation ratio (i.e., the ratio between widths of the narrower anabranch, w_n, and the wider anabranch, w_w, after a bifurcation) of 2:3 (Fig. 4.11a); (B) a two-channel structure with a bifurcation ratio of 1:2 (Fig. 4.11b); (C) a four-channel structure with three bifurcations (Bifurcations 1, 2, and 3) that have bifurcation ratios of 1:2, 1:3, and 1:1, respectively (Fig. 4.11c); (D) a six-channel structure with additional two 25-m wide anabranches (Anabranches 2 and 4) developed from the four-channel structure (Fig. 4.11d); and (E) a six-channel structure with a 50-m wide anabranch (Anabranch 2) and a 25-m wide anabranch (Anabranch 4) developed from the four-channel structure (Fig. 4.11e). Among these five structures, Anabranches 2 and 4 in the two six-channel structures reflect those created by floodplain incision, such that their adjacent wider channels remain unchanged in width after the bifurcations. Sediment-transport capacity (Q_s) of each channel in the five structures was predicted using the same shear-stress-based method adopted by Huang and Nanson (2007), and the total sediment-transport capacity of each structure was calculated as the sum of the estimated capacities of all channels at the designed transects (dotted vertical lines in Fig. 4.11). The required input discharge in the model was set as the bankfull discharge (1,328 m^3/s) at the 300-m wide, single-thread channel in all five structures, which was estimated by linking the daily

discharge at Maqu Station with the satellite image taken on the day when bankfull condition (i.e., submerged bars without overbank flow) of the MAS was present.

Water discharges of the main channels and anabranches after the single-thread channel starts to bifurcate were estimated using the discharge-width relationship proposed by Schuurman and Kleinhans (2015):

$$\frac{Q_w}{Q_n} = \left(\frac{w_w}{w_n}\right)^2 \tag{4.6}$$

where Q_w and Q_n are the discharges of the wider and narrower channels, respectively. For the floodplain-incised anabranches (i.e., Anabranches 2 and 4 in Anabranching Structures D and E in Fig. 4.11d and e), 20% of the calculated Q_n was allocated to the corresponding Q_w to reflect the fact that less discharge is diverted into these secondary channels. Channel depths (d) were then estimated using Manning's formula, assuming d approximates hydraulic radius:

$$d = \left(\frac{nQ}{w}\right)^{3/5} S^{-3/10} \tag{4.7}$$

where n is the roughness coefficient, which was set as 0.035, S is the channel gradient, which was 0.5‰, and w is the corresponding channel width. Bedload transport rate was then estimated using the relationship developed by Wong and Parker (2006):

$$q_b^* = 4.93(\tau_0^* - 0.047)^{1.6} \tag{4.8}$$

where q_b^* and τ_0^* are the dimensionless bedload transport rate per unit width and the Shields number, respectively, which are defined as:

$$q_b^* = \frac{q_b}{\sqrt{\left(\frac{\rho_s}{\rho} - 1\right) g D^3}} \tag{4.9}$$

$$\tau_0^* = \frac{RS}{\left(\frac{\rho_s}{\rho} - 1\right) D} \tag{4.10}$$

where q_b is the dimensional bedload transport rate per unit width, ρ_s and ρ are the densities of sediment and water, respectively, g is the gravitational acceleration, D is the characteristic particle size composing channel bed, which was set to be 4.5 mm, as reported in Li et al. (2013), and R is the hydraulic radius, which approximates d. The total volumetric sediment discharge (Q_s) was subsequently calculated by:

$$Q_s = q_b w \tag{4.11}$$

The estimated sediment-transport capacity of each structure was then compared with one another and with that of the upstream single-thread channel.

Results on the estimated sediment-transport capacity show that the upstream single-thread channel had a capacity of 0.103593 m^3/s. Of the five structures, Anabranching Structures A and B had total transport capacities (at the transects) of 0.103742 and 0.103976 m^3/s, respectively, which were 0.14% and 0.37% more efficient than the single-thread channel, respectively, Anabranching Structure C had the highest total transport capacity among the five structures, which was 0.104454 m^3/s, although the capacity "surplus" still accounted for < 1% (0.83%) of transport capacity in the single-thread channel. Anabranching Structures D and E, however, had transport capacities of 0.102281 and 0.099265 m^3/s, respectively, with both smaller than that of the single-thread channel by 1.27% and 4.18%, respectively. Particularly, the main channels (i.e., the widest) always transported the major portion of sediment that accounted for 71.3-82.8% of total transport capacities in the simulated anabranching structures.

Chapter 5: Conclusions

This dissertation focuses on morphological characteristics, their temporal changes, and channel-floodplain interactions of the alluvial river systems in the Zoige Basin within the Upper Yellow River watershed, eastern Qinghai-Tibet Plateau. It demonstrates the morphodynamic diversity of rivers in this high-altitude environment, highlighting the complexity of the forms and processes involved in alluvial channels. Through three main chapters that respectively focus on meandering channels (Chapter 2), oxbow lakes in the meandering river floodplain (Chapter 3), and anabranching channels (Chapter 4), the dissertation reveals multiple important findings, which help strengthen the understanding of not only the morphological characteristics of these geomorphic features, but the fluvial processes involved in their evolutionary trajectories.

In Chapter 2, I quantitatively assessed the morphological characteristics of meander bends and the pattern and rate of their lateral migration along the lower Black and White Rivers. I found that the studied meander bends migrated at relatively slow rates mainly in the form of extension, translation, and the combination of both. Their evolution was accompanied by the development of extensive compound forms and infrequent cutoffs. This is ascribed to the cohesive peat materials that built up the upper portion of channel banks, as well as the protection of the downfallen cantilever arms that inhibited bank erosion. Discrepancies in bend morphology and morphological changes between the Black and the White Rivers were caused by differences in the reach-wise channel gradient and the associated stream power. The calculated dimensionless migration rates of meander bends exhibited an envelope-type relationship with bend curvature, which is consistent with previous findings. However, the mean migration rates displayed a quasi-monotonic relationship with bend curvature. This apparent discrepancy indicates the complexity of the linkages between channel morphology (i.e., bend curvature) and

its dynamics (i.e., lateral migration rate), calling for further investigation on the inherent mechanism of meander-bend evolution that facilitates its morphological stability by developing compound forms and reducing the occurrence of cutoff and over-narrowing (i.e., bends that are highly curved with very small r_m/w, where r_m is bend radius and w is channel width) of meander bends.

Chapter 3 takes a step further from the previous chapter to examine hydrologic connectivity and morphological variation of oxbow lakes (the lacustrine phase of abandoned meander bends) under a highly variable hydrologic regime of the lower Black River. Using a probability-based index proposed here for quantifying the hydrologic connectivity of oxbow lakes, I found that the oxbow lakes had generally low hydrologic connectivity, even though their morphology underwent considerable expansion with increasing discharges in the main channel. This suggests hydrologic processes other than surface water connection as the key driving forces in controlling oxbow lake hydrology. The low hydrologic connectivity of oxbow lakes along the lower Black River was associated with the downcutting of the main channel bed. Owing to the slow migration rates of the meandering channels discovered in Chapter 2, the floodplain of the study reach had experienced inactive floodplain reworking, infrequent but pulsed sedimentation within oxbow lakes, and very limited overbank sedimentation over the floodplains. Additionally, I documented the significant impact of lateral migration of the main channel on the evolution of oxbow lakes based on remotely sensed data and cored lake deposits from the field.

Chapter 4 shifts from the meandering systems to an anabranching system in the Upper Yellow River within the Zoige Basin. It reveals the anabranching morphology that featured intensive channel multiplicity and the dominance of islands, which are distinct from the commonly observed “simple” anabranching patterns with fewer anabranches and islands in other

regions of the world. Multiple modes of island dynamics were quantitatively characterized through a spatiotemporal analysis of the anabranching system, highlighting the vital role island dynamics and their interactions with channels (i.e., anabranches) played in determining the evolutionary processes and stability of the anabranching system. Based on the actual morphological structures, this chapter proposes five heuristic anabranching structures and simulates their flow efficiency in terms of sediment-transport capacity. I found that the excess development of anabranches (i.e., > 4) cannot enhance sediment transport but rather promote deposition of excess sediment incapable of being transported through the system, particularly within the small floodplain-incised anabranches. The stability of the anabranching system is therefore maintained by comparatively stable main channels and wider anabranches, whereas the smaller floodplain-incised anabranches were prone to repeated formation and elimination depending on hydrologic conditions and sediment supply. The morphodynamic characteristics of the anabranching system also exhibited a transitional nature of channel patterns, particularly with braided patterns, corroborating existing theories of vegetation encroachment as both an impact and an outcome of fluvial processes in maintaining and adjusting channel structures.

Alluvial channel pattern has been a classical topic in fluvial geomorphology for over half a century. Yet, understanding of the underlying formative and evolutionary processes controlling channel morphology and its dynamic changes in various spatial and temporal scales remains incomplete, leading to insufficient measures for strategic management in river maintenance and restoration. Based upon previous understanding and the pristine condition of the studied rivers, this dissertation provides new insights into the morphodynamic nature of meandering and anabranching patterns, revealing the key processes and morphological properties embraced in the dynamics of these river systems. Future research is needed for further investigating and

predicting spatial patterns of meandering and anabranching evolution at the global scale, as well as their temporal patterns under the climate change. Additionally, the proposed anabranching structures for flow efficiency estimation can be significantly optimized by calibrating them using field-based hydraulic data, which are potentially useful for modeling the complex anabranching hydrodynamics. Understanding of the evolution of floodplains in relation to channel processes can also be enhanced by isotopic dating of sediment cores, which may provide implications for not only channel-floodplain interactions but the paleoenvironmental conditions of the Zoige Basin – the largest high-altitude peatland of the world.

References

Aalto, R., Lauer, J. W., & Dietrich, W. E. (2008). Spatial and temporal dynamics of sediment accumulation and exchange along Strickland River floodplains (Papua New Guinea) over decadal-to-centennial timescales. *Journal of Geophysical Research: Earth Surface*, *113*(F1).

Alber, A., Piégay, H., 2017. Characterizing and modelling river channel migration rates at a regional scale: Case study of south-east France. Journal of Environmental Management, 202, 479-493.

Amoros, C., Bornette, G., & Henry, C. P. (2000). A vegetation-based method for ecological diagnosis of riverine wetlands. *Environmental Management*, *25*(2), 211-227.

Amos, K. J., Croke, J. C., Hughes, A. O., Chapman, J., Takken, I., & Lymburner, L. (2008). A catchment-scale assessment of anabranching in the 143000 km^2 Fitzroy River catchment, north-eastern Australia. *Earth Surface Processes and Landforms*, *33*(8), 1222-1241.

Anthony, D.J., Harvey, M.D., 1991. Stage-dependent cross-section adjustments in a meandering reach of Fall River, Colorado. Geomorphology, 4(3-4), 187-203.

Ashmore, P. E. (2013), Morphology and dynamics of braided rivers, in *Treatise on Geomorphology*, vol. 9, Fluvial Geomorphology, edited by E. Wohl, pp. 289–312, Academic, San Diego, Calif.

Ashworth, P. J., & Lewin, J. (2012). How do big rivers come to be different?. *Earth-Science Reviews*, *114*(1-2), 84-107.

Bagnold, R., 1960. Some aspects of the shape of river meanders, U.S. Geol. Surv. Prof. Pap., 282E, 135–144.

Bai, Y. C., & Wang, Z. Y. (2014). Theory and application of nonlinear river dynamics. *International Journal of Sediment Research*, *29*(3), 285-303.

Beaty, C. B. (1990). Milk River in southern Alberta: a classic underfit stream. *Canadian Geographer/Le Géographe canadien*, *34*(2), 171-174.

Bertoldi, W., & Tubino, M. (2007). River bifurcations: Experimental observations on equilibrium configurations. *Water Resources Research*, *43*(10).

Bertoldi, W., Drake, N. A., & Gurnell, A. M. (2011). Interactions between river flows and colonizing vegetation on a braided river: exploring spatial and temporal dynamics in riparian vegetation cover using satellite data. *Earth Surface Processes and Landforms*, *36*(11), 1474-1486.

Bhattacharya, R., Hausmann, S., Hubeny, J. B., Gell, P., & Black, J. L. (2016). Ecological response to hydrological variability and catchment development: insights from a shallow oxbow lake in Lower Mississippi Valley, Arkansas. *Science of the Total Environment*, *569*, 1087-1097.

Blanckaert, K., Graf, W.H., 2001. Mean flow and turbulence in open-channel bend. Journal of Hydraulic Engineering, 127(10), 835-847.

Bracken, L. J., Wainwright, J., Ali, G. A., Tetzlaff, D., Smith, M. W., Reaney, S. M., & Roy, A. G. (2013). Concepts of hydrological connectivity: Research approaches, pathways and future agendas. *Earth-Science Reviews*, *119*, 17-34.

Brice, J.C. (1974). Evolution of meander loops. Geological Society of America Bulletin, 85(4), 581-586.

Brizga, S. O., & Finlayson, B. L. (1990). Channel avulsion and river metamorphosis: the case of the Thomson River, Victoria, Australia. *Earth Surface Processes and Landforms*, *15*(5), 391-404.

Burge, L. M. (2005). Wandering Miramichi rivers, New Brunswick, Canada. *Geomorphology*, *69*(1-4), 253-274.

Burge, L. M. (2006). Stability, morphology and surface grain size patterns of channel bifurcation in gravel–cobble bedded anabranching rivers. *Earth Surface Processes and Landforms*, *31*(10), 1211-1226.

Carling, P., Jansen, J., & Meshkova, L. (2014). Multichannel rivers: their definition and classification. *Earth Surface Processes and Landforms*, 39(1), 26-37.

Casado, A., Peiry, J.L., Campo, A.M. (2016). Geomorphic and vegetation changes in a meandering dryland river regulated by a large dam, Sauce Grande River, Argentina. Geomorphology, 268, 21-34.

Chang, H.H. (1984). Analysis of river meanders. Journal of Hydraulic Engineering, 110(1), 37-50.

Chen, F. H., Bloemendal, J., Zhang, P. Z., & Liu, G. X. (1999). An 800 ky proxy record of climate from lake sediments of the Zoige Basin, eastern Tibetan Plateau. *Palaeogeography, Palaeoclimatology, Palaeoecology*, *151*(4), 307-320.

Chow, V.T., Maidment, D.R., Mays, L.W. (1988). Applied hydrology McGraw-Hill International editions. New York, USA.

Church, M., & Ferguson, R. I. (2015). Morphodynamics: Rivers beyond steady state. *Water Resources Research*, *51*(4), 1883-1897.

Citterio, A., & Piégay, H. (2009). Overbank sedimentation rates in former channel lakes: characterization and control factors. *Sedimentology*, *56*(2), 461-482.

Constantine, J. A., & Dunne, T. (2008). Meander cutoff and the controls on the production of oxbow lakes. *Geology*, *36*(1), 23-26.

Constantine, J. A., Dunne, T., Ahmed, J., Legleiter, C., & Lazarus, E. D. (2014). Sediment supply as a driver of river meandering and floodplain evolution in the Amazon Basin. *Nature Geoscience*, *7*(12), 899-903.

Constantine, J. A., Dunne, T., Piégay, H., & Mathias Kondolf, G. (2010). Controls on the alluviation of oxbow lakes by bed-material load along the Sacramento River, California. *Sedimentology*, *57*(2), 389-407.

Czuba, J. A., David, S. R., Edmonds, D. A., & Ward, A. S. (2019). Dynamics of surface-water connectivity in a low-gradient meandering river floodplain. *Water Resources Research*, *55*(3), 1849-1870.

Darby, S. E., Alabyan, A. M., & Van de Wiel, M. J. (2002). Numerical simulation of bank erosion and channel migration in meandering rivers. *Water Resources Research*, *38*(9), 2-1.

Davis, W. M. (1913). Meandering valleys and underfit rivers. *Annals of the Association of American Geographers*, *3*(1), 3-28.

Dembkowski, D. J., & Miranda, L. E. (2011). Comparison of fish assemblages in two disjoined segments of an oxbow lake in relation to connectivity. *Transactions of the American Fisheries Society*, *140*(4), 1060-1069.

Dépret, T., Riquier, J., & Piégay, H. (2017). Evolution of abandoned channels: Insights on controlling factors in a multi-pressure river system. *Geomorphology*, *294*, 99-118.

Dieras, P. L. (2013). *The persistence of oxbow lakes as aquatic habitats: an assessment of rates of change and patterns of alluviation* (Doctoral dissertation, Cardiff University).

Dieras, P. L., Constantine, J. A., Hales, T. C., Piégay, H., & Riquier, J. (2013). The role of oxbow lakes in the off-channel storage of bed material along the Ain River, France. *Geomorphology*, *188*, 110-119.

Dietrich, W. E., Day, G., & Parker, G. (1999). The Fly River, Papua New Guinea: Inferences about river dynamics, floodplain sedimentation and fate of sediment. *Varieties of Fluvial Form*, 345-376.

Dietrich, W.E., 1987. Mechanics of flow and sediment transport in river bends. In River Channels: Environment and Process (Vol. 18, pp. 179-227). Oxford: Blackwell.

Dietrich, W.E., Smith, J.D., Dunne, T. (1979). Flow and sediment transport in a sand bedded meander. *The Journal of Geology*, 87(3), 305-315.

Donovan, M., Belmont, P., & Sylvester, Z. (2021). Evaluating the relationship between meander-bend curvature, sediment supply, and migration rates. *Journal of Geophysical Research: Earth Surface*, *126*(3), e2020JF006058.

Donovan, M., Belmont, P., Notebaert, B., Coombs, T., Larson, P., & Souffront, M. (2019). Accounting for uncertainty in remotely-sensed measurements of river planform change. *Earth-Science Reviews*, *193*, 220-236.

Downward, S. R., Gurnell, A. M., & Brookes, A. (1994). A methodology for quantifying river channel planform change using GIS. *IAHS Publications-Series of Proceedings and Reports-Intern Assoc Hydrological Sciences*, *224*, 449-456.

Draut, A. E., Logan, J. B., & Mastin, M. C. (2011). Channel evolution on the dammed Elwha River, Washington, USA. *Geomorphology*, *127*(1-2), 71-87.

Dudgeon, D., Arthington, A. H., Gessner, M. O., Kawabata, Z. I., Knowler, D. J., Lévêque, C., ... & Sullivan, C. A. (2006). Freshwater biodiversity: importance, threats, status and conservation challenges. *Biological reviews*, *81*(2), 163-182. Li, X. Z., Chen, Z. J., Fan, X. C., & Cheng, Z. J. (2018). Hydropower development situation and prospects in China. *Renewable and Sustainable Energy Reviews*, *82*, 232-239.

Dunne, K. B., & Jerolmack, D. J. (2018). Evidence of, and a proposed explanation for, bimodal transport states in alluvial rivers. *Earth Surface Dynamics*, *6*(3), 583-594.

Dunne, K. B., & Jerolmack, D. J. (2020). What sets river width?. *Science Advances*, *6*(41), eabc1505.

Eaton, B. C., Millar, R. G., & Davidson, S. (2010). Channel patterns: Braided, anabranching, and single-thread. *Geomorphology*, 120(3-4), 353-364.

Ebisemiju, F.S. (1994). The sinuosity of alluvial river channels in the seasonally wet tropical environment: case study of river Elemi, southwestern Nigeria. *Catena*, 21(1), 13-25.

Erskine, W., McFadden, C., & Bishop, P. (1992). Alluvial cutoffs as indicators of former channel conditions. *Earth Surface Processes and Landforms*, *17*(1), 23-37.

Ferguson, R. I. (1990). Understanding braiding processes in gravel-bed rivers: progress and unsolved problems, in *Braided Rivers*, edited by J. L. Best and C. S. Bristow, pp. 73-87, Geological Society Special Publication, London, UK.

Ferguson, R.I. (1975). Meander irregularity and wavelength estimation. *Journal of Hydrology*, 26(3-4), 315-333.

Finotello, A., D'Alpaos, A., Lazarus, E.D., Lanzoni, S. (2019). High curvatures drive river meandering: COMMENT. *Geology*, 47(10), 485.

Fisk, H.N. (1947). *Fine grained alluvial deposits and their effects on Mississippi River activity*. Vols 1 & 2. Mississippi River Commission, Vicksburg, MS.

Freeman, M. C., Pringle, C. M., & Jackson, C. R. (2007). Hydrologic connectivity and the contribution of stream headwaters to ecological integrity at regional scales 1. *JAWRA Journal of the American Water Resources Association*, *43*(1), 5-14.

Frias, C. E., Abad, J. D., Mendoza, A., Paredes, J., Ortals, C., & Montoro, H. (2015). Planform evolution of two anabranching structures in the U pper P eruvian A mazon R iver. *Water Resources Research*, *51*(4), 2742-2759.

Friend, P. F., & Sinha, R. (1993). Braiding and meandering parameters. *Geological Society, London, Special Publications*, *75*(1), 105-111.

Frothingham, K.M., Rhoads, B.L., 2003. Three‐dimensional flow structure and channel change in an asymmetrical compound meander loop, Embarras River, Illinois. Earth Surface Processes and Landforms: The Journal of the British Geomorphological Research Group, 28(6), 625-644.

Gagliano, S. M., & Howard, P. C. (1984). The neck cutoff oxbow lake cycle along the Lower Mississippi River. In *River Meandering* (pp. 147-158). ASCE.

Gao, P. (2012). Validation and implications of an energy-based bedload transport equation. *Sedimentology*, *59*(6), 1926-1935.

Gao, P., Li, Z., & Yang, H. (2021). Variable discharges control composite bank erosion in Zoige meandering rivers. *Catena*, *204*, 105384. https://doi.org/10.1016/j.catena.2021.105384

Gao, P., Li, Z., You, Y., Zhou, Y., & Piégay, H. (2022). Assessing functional characteristics of a braided river in the Qinghai-Tibet Plateau, China. *Geomorphology*, *403*, 108180.

Gautier, E., Brunstein, D., Vauchel, P., Roulet, M., Fuertes, O., Guyot, J. L., ... & Bourrel, L. (2007). Temporal relations between meander deformation, water discharge and sediment fluxes in the floodplain of the Rio Beni (Bolivian Amazonia). *Earth Surface Processes and Landforms*, *32*(2), 230-248.

Gautier, E., Dépret, T., Cavero, J., Costard, F., Virmoux, C., Fedorov, A., ... & Brunstein, D. (2021). Fifty-year dynamics of the Lena River islands (Russia): Spatio-temporal pattern of large periglacial anabranching river and influence of climate change. *Science of the Total Environment*, *783*, 147020.

Gilvear D, Bryant R. 2016. Analysis of remotely sensed data for fluvial geomorphology and river science. In Tools in Fluvial Geomorphology, Kondolf G.M., Piégay, H. (eds). John Wiley & Sons: Chichester, UK, pp. 103-132.

Gilvear, D., Winterbottom, S., & Sichingabula, H. (2000). Character of channel planform change and meander development: Luangwa River, Zambia. *Earth Surface Processes and Landforms*, *25*(4), 421-436.

Glińska-Lewczuk, K. (2009). Water quality dynamics of oxbow lakes in young glacial landscape of NE Poland in relation to their hydrological connectivity. *Ecological Engineering*, *35*(1), 25-37.

Gregory, K. J. (2006). The human role in changing river channels. *Geomorphology*, *79*(3-4), 172-191.

Grenfell, M., Aalto, R., & Nicholas, A. (2012). Chute channel dynamics in large, sand-bed meandering rivers. *Earth Surface Processes and Landforms*, *37*(3), 315-331.

Güneralp, İ., Marston, R.A. (2012). Process-form linkages in meander morphodynamics: Bridging theoretical modeling and real world complexity. *Progress in Physical Geography*, 36(6), 718-746.

Güneralp, İ., Rhoads, B.L. (2009). Empirical analysis of the planform curvature-migration relation of meandering rivers. *Water Resources Research*, 45(9).

Guo, X., Chen, D., Parker, G. (2019). Flow directionality of pristine meandering rivers is embedded in the skewing of high-amplitude bends and neck cutoffs. *Proceedings of the National Academy of Sciences*, 116(47), 23448-23454.

Guo, X., Gao, P., & Li, Z. (2021). Morphological characteristics and changes of two meandering rivers in the Qinghai-Tibet Plateau, China. *Geomorphology*, *379*, 107626.

Guo, X., Gao, P., & Li, Z. (2023). Morphodynamic characteristics of a complex anabranching system in the Qinghai-Tibet Plateau and the implications for anabranching stability. *Journal of Geophysical Research: Earth Surface*, 128, e2022JF006788.

Gurnell, A. M., Downward, S. R., & Jones, R. (1994). Channel planform change on the River Dee meanders, 1876–1992. *Regulated Rivers: Research & Management*, *9*(4), 187-204.

Han, J., Zhang, W., Yuan, J., & Fan, Y. (2018). Channel evolution under changing hydrological regimes in anabranching reaches downstream of the Three Gorges Dam. *Frontiers of Earth Science*, *12*(3), 640-648.

Han, M., & Brierley, G. (2020). Channel geomorphology and riparian vegetation interactions along four anabranching reaches of the Upper Yellow River. *Progress in Physical Geography: Earth and Environment*, 44(6), 898-922.

He, Q., Walling, D. E., & Owens, P. N. (1996). Interpreting the 137Cs profiles observed in several small lakes and reservoirs in southern England. *Chemical Geology*, *129*(1-2), 115-131.

Henriques, M., McVicar, T. R., Holland, K. L., & Daly, E. (2022). Riparian vegetation and geomorphological interactions in anabranching rivers: A global review. *Ecohydrology*, *15*(2), e2370.

Henshaw, A. J., Gurnell, A. M., Bertoldi, W., & Drake, N. A. (2013). An assessment of the degree to which Landsat TM data can support the assessment of fluvial dynamics, as revealed by changes in vegetation extent and channel position, along a large river. *Geomorphology*, *202*, 74-85.

Hickin, E.J. (1978). Mean flow structure in meanders of the Squamish River, British Columbia. *Canadian Journal of Earth Sciences*, 15(11), 1833-1849.

Hickin, E.J., Nanson, G.C. (1975). The character of channel migration on the Beaton River, Northeast British Columbia, Canada. *Geological Society of America Bulletin*, 86, 487–494.

Hickin, E.J., Nanson, G.C. (1984). Lateral migration rates of river bends. *Journal of Hydraulic Engineering*, 110(11), 1557-1567.

Hooke, J. M. (1995). River channel adjustment to meander cutoffs on the River Bollin and River Dane, northwest England. *Geomorphology*, *14*(3), 235-253.

Hooke, J. M. (2013). River meandering. In J. F. Shroder (Ed.), *Treatise on geomorphology* (Vol. 9, pp. 260–288). Academic Press.

Hooke, J.M. (1984). Changes in river meanders: a review of techniques and results of analyses. *Progress in Physical Geography*, 8(4), 473-508.

Hooke, J.M. (1997). Styles of channel change. In: Thorne, C.R., Hey, R.D., Newson, M.D. (Eds.), *Applied Fluvial Geomorphology for River Engineering and Management*. John Wiley & Sons, Chichester, 237–268.

Hooke, J.M. (2007). Complexity, self-organization and variation in behaviour in meandering rivers. *Geomorphology*, 91, 236–258.

Hooke, J.M., Harvey, A.M. (1983). Meander changes in relation to bend morphology and secondary flows. *Modern and ancient fluvial systems*, 121-132.

Hooke, J.M., Yorke, L. (2010). Rates, distributions and mechanisms of change in meander morphology over decadal timescales, River Dane, UK. *Earth Surface Processes and Landforms*, 35(13), 1601-1614.

Houssais, M., & Lajeunesse, E. (2012). Bedload transport of a bimodal sediment bed. *Journal of Geophysical Research: Earth Surface*, *117*(F4). https://doi.org/10.1029/2012JF002490

Howard, A.D. (1992). Modeling channel migration and floodplain sedimentation in meandering streams. In: Carling, P.A., Petts, G.E. (Eds.), *Lowland Floodplain Rivers: Geomorphological Perspectives*. John Wiley & Sons Ltd., Chichester, UK, pp. 1–41.

Howard, A.D., Knutson, T.R. (1984). Sufficient conditions for river meandering: A simulation approach. *Water Resources Research*, 20(11), 1659-1667.

Hu, C., Fang, C., & Cao, W. (2015). Shrinking of Dongting Lake and its weakening connection with the Yangtze River: analysis of the impact on flooding. *International Journal of Sediment Research*, *30*(3), 256-262.

Hu, G., Dong, Z., Lu, J., & Yan, C. (2015). The developmental trend and influencing factors of aeolian desertification in the Zoige Basin, eastern Qinghai–Tibet Plateau. *Aeolian Research*, *19*, 275-281.

Huang, H. Q., & Chang, H. H. (2006). Scale independent linear behavior of alluvial channel flow. *Journal of Hydraulic Engineering*, *132*(7), 722-730.

Huang, H. Q., & G. C. Nanson (2004), Maximum flow efficiency, in *Encyclopedia of Geomorphology*, edited by A. S. Goudie, pp. 654– 655, Routledge, London.

Huang, H. Q., & Nanson, G. C. (2007). Why some alluvial rivers develop an anabranching pattern?. *Water Resources Research*, *43*(7).

Huang, H. Q., Chang, H. H., & Nanson, G. C. (2004). Minimum energy as the general form of critical flow and maximum flow efficiency and for explaining variations in river channel pattern. *Water Resources Research*, *40*(4). https://doi.org/10.1029/2003WR002539

Hudson, P. F., Heitmuller, F. T., & Leitch, M. B. (2012). Hydrologic connectivity of oxbow lakes along the lower Guadalupe River, Texas: The influence of geomorphic and climatic controls on the "flood pulse concept". *Journal of Hydrology*, *414*, 174-183.

Hudson, P.F., Kesel, R.H. (2000). Channel migration and meander-bend curvature in the lower Mississippi River prior to major human modification. *Geology*, 28(6), 531-534.

Hughes, M. L., McDowell, P. F., & Marcus, W. A. (2006). Accuracy assessment of georectified aerial photographs: implications for measuring lateral channel movement in a GIS. *Geomorphology*, *74*(1-4), 1-16.

Ielpi, A., Lapôtre, M. G. A., Finotello, A., & Roy-Léveillée, P. (2023). Large sinuous rivers are slowing down in a warming Arctic. *Nature Climate Change*.

Ielpi, A., Lapôtre, M. G., Gibling, M. R., & Boyce, C. K. (2022). The impact of vegetation on meandering rivers. *Nature Reviews Earth & Environment*, *3*(3), 165-178.

Ielpi, A., Lapôtre, M.G. (2019). Barren meandering streams in the modern Toiyabe Basin of Nevada, USA, and their relevance to the study of the pre-vegetation rock record. *Journal of Sedimentary Research*, 89(5), 399-415.

Ikeda, S., Parker, G., Sawai, K. (1981). Bend theory of river meanders. Part 1. Linear development. *Journal of Fluid Mechanics*, 112, 363-377.

Ishii, Y., & Hori, K. (2016). Formation and infilling of oxbow lakes in the Ishikari lowland, northern Japan. *Quaternary International*, *397*, 136-146.

Jain, V., & Sinha, R. (2004). Fluvial dynamics of an anabranching river system in Himalayan foreland basin, Baghmati river, north Bihar plains, India. *Geomorphology*, 60(1-2), 147-170.

Jansen, J. D., & Nanson, G. C. (2004). Anabranching and maximum flow efficiency in Magela Creek, northern Australia. *Water Resources Research*, 40(4). https://doi.org/10.1029/2003WR002408

Jansen, J. D., & Nanson, G. C. (2010). Functional relationships between vegetation, channel morphology, and flow efficiency in an alluvial (anabranching) river. *Journal of Geophysical Research: Earth Surface*, 115(F4). https://doi.org/10.1029/2010JF001657

Jerolmack, D. J., & Mohrig, D. (2007). Conditions for branching in depositional rivers. *Geology*, *35*(5), 463-466.

Junk, W. J., Bayley, P. B., & Sparks, R. E. (1989). The flood pulse concept in river-floodplain systems. *Canadian special publication of fisheries and aquatic sciences*, *106*(1), 110-127.

Kleinhans, M. G. (2010). Sorting out river channel patterns. *Progress in physical geography*, *34*(3), 287-326.

Kleinhans, M. G., Ferguson, R. I., Lane, S. N., & Hardy, R. J. (2013). Splitting rivers at their seams: bifurcations and avulsion. *Earth Surface Processes and Landforms*, 38(1), 47-61.

Kleinhans, M. G., van Dijk, W. M., van de Lageweg, W. I., Hoyal, D. C., Markies, H., van Maarseveen, M., ... & Cheshier, N. (2014). Quantifiable effectiveness of experimental scaling of river-and delta morphodynamics and stratigraphy. *Earth-Science Reviews*, *133*, 43-61.

Knighton, A. D., & Nanson, G. C. (1993). Anastomosis and the continuum of channel pattern. *Earth Surface Processes and Landforms*, *18*(7), 613-625.

Kobus, S., Glińska-Lewczuk, K., Sidoruk, M., Skwierawski, A., Obolewski, K., Timofte, C. M., & Sowiński, P. (2016). Effect of hydrological connectivity on physicochemical properties of bottom sediments of floodplain lakes-a case study of the Łyna River, Northern Poland. *Environmental Engineering & Management Journal (EEMJ)*, *15*(6), 1237-1246.

Komar, P. D. (1983). Shapes of streamlined islands on Earth and Mars: Experiments and analyses of the minimum-drag form. *Geology*, *11*(11), 651-654.

Kong, D., Latrubesse, E. M., Miao, C., & Zhou, R. (2020). Morphological response of the Lower Yellow River to the operation of Xiaolangdi Dam, China. *Geomorphology*, 350, 106931.

Konsoer, K. M., Richards, G., & Edwards, B. (2016). Planform evolution of neck cutoffs on elongate meander loops, White River, Arkansas, USA. In *River Flow* (pp. 11-14).

Konsoer, K.M., Rhoads, B.L., Langendoen, E.J., Best, J.L., Ursic, M.E., Abad, J.D., Garcia, M.H. (2016). Spatial variability in bank resistance to erosion on a large meandering, mixed bedrock-alluvial river. *Geomorphology*, 252, 80-97.

Lan, J., Wang, T., Chawchai, S., Cheng, P., Yu, K., Yan, D., ... & Xu, H. (2020). Time marker of ^{137}Cs fallout maximum in lake sediments of Northwest China. *Quaternary Science Reviews, 241*, 106413. https://doi.org/10.1016/j.quascirev.2020.106413

Lancaster, S.T., Bras, R.L. (2002). A simple model of river meandering and its comparison to natural channels. *Hydrological Processes,* 16(1), 1-26.

Lane, E.W. (1957). A Study of the Shape of Channels Formed by Natural Streams Flowing in Erodible Materials. *Missouri Rivers Division Sediment Series No 9*. US Army Engineer division, Missouri River, Corps of engineers, Omaha, NE. 106 pp.

Lane, S. N., Richards, K. S., & Chandler, J. H. (1996). Discharge and sediment supply controls on erosion and deposition in a dynamic alluvial channel. *Geomorphology*, 15(1), 1-15.

Latrubesse, E. M. (2008). Patterns of anabranching channels: The ultimate end-member adjustment of mega rivers. *Geomorphology*, 101(1-2), 130-145.

Latrubesse, E. M. (2015). Large rivers, megafans and other Quaternary avulsive fluvial systems: A potential “who's who” in the geological record. *Earth-Science Reviews*, 146, 1-30.

Latrubesse, E. M., & Franzinelli, E. (2005). The late Quaternary evolution of the Negro River, Amazon, Brazil: Implications for island and floodplain formation in large anabranching tropical systems. *Geomorphology*, 70(3-4), 372-397.

Latrubesse, E. M., Arima, E. Y., Dunne, T., Park, E., Baker, V. R., d’Horta, F. M., ... & Stevaux, J. C. (2017). Damming the rivers of the Amazon basin. *Nature*, *546*(7658), 363-369.

Lea, D. M., & Legleiter, C. J. (2016). Refining measurements of lateral channel movement from image time series by quantifying spatial variations in registration error. *Geomorphology*, *258*, 11-20.

Lehner, B., Liermann, C. R., Revenga, C., Vörösmarty, C., Fekete, B., Crouzet, P., ... & Wisser, D. (2011). High-resolution mapping of the world's reservoirs and dams for sustainable river-flow management. *Frontiers in Ecology and the Environment*, *9*(9), 494-502.

Leli, I. T., Stevaux, J. C., & Assine, M. L. (2020). Origin, evolution, and sedimentary records of islands in large anabranching tropical rivers: The case of the Upper Paraná River, Brazil. *Geomorphology*, *358*, 107118.

Leopold, L. B., & Wolman, M. G. (1957). *River channel patterns: braided, meandering, and straight.* US Government Printing Office.

Leopold, L.B., Wolman, M.G. (1960). River meanders. *Geological Society of America Bulletin*, 71, 769–793.

Lewin, J., & Ashworth, P. J. (2014). Defining large river channel patterns: alluvial exchange and plurality. *Geomorphology*, *215*, 83-98.

Lewin, J., & Brewer, P. A. (2001). Predicting channel patterns. *Geomorphology*, *40*(3-4), 329-339.

Li, B., Yu, Z., Liang, Z., Song, K., Li, H., Wang, Y., ... & Acharya, K. (2014). Effects of climate variations and human activities on runoff in the Zoige alpine wetland in the eastern edge of the Tibetan Plateau. *Journal of Hydrologic Engineering*, *19*(5), 1026-1035.

Li, X., Li, Z., Hu, X., & Tian, S. (2017). Analysis on morphological features of oxbow lakes along Heihe River in Zoige Basin. *Advances in Science and Technology of Water Resources*, *37*(6), 19-24. (in Chinese)

Li, Z. W., Wang, Z. Y., Brierley, G., Nicoll, T., Pan, B. Z., & Li, Y. F. (2015). Shrinkage of the Ruoergai Swamp and changes to landscape connectivity, Qinghai-Tibet Plateau. *Catena*, *126*, 155-163.

Li, Z., & Gao, P. (2019a). Channel adjustment after artificial neck cutoffs in a meandering river of the Zoige basin within the Qinghai-Tibet Plateau, China. *Catena*, *172*, 255-265.

Li, Z., & Gao, P. (2019b). Impact of natural gullies on groundwater hydrology in the Zoige peatland, China. *Journal of Hydrology: Regional Studies*, *21*, 25-39.

Li, Z., & Gao, P. (2020). Characterizing spatially variable water table depths in a disturbed Zoige peatland watershed. *Journal of Hydro-environment Research*, *29*, 70-79.

Li, Z., Gao, P., Hu, X., Yi, Y., Pan, B., & You, Y. (2020). Coupled impact of decadal precipitation and evapotranspiration on peatland degradation in the Zoige basin, China. *Physical Geography*, *41*(2), 145-168.

Li, Z., Gao, P., You, Y. (2018). Characterizing hydrological connectivity of artificial ditches in Zoige Peatlands of Qinghai-Tibet Plateau. *Water*, 10(10), 1364.

Li, Z., Lu, H., Gao, P., You, Y., & Hu, X. (2020). Characterizing braided rivers in two nested watersheds in the Source Region of the Yangtze River on the Qinghai-Tibet Plateau. *Geomorphology*, *351*, 106945.

Li, Z., Wang, Z., Pan, B., Du, J., Brierley, G., Yu, G. A., & Blue, B. (2013). Analysis of controls upon channel planform at the first great bend of the upper Yellow River, Qinghai-Tibet Plateau. *Journal of Geographical Sciences*, 23(5), 833-848.

Li, Z., Yu, G.A., Brierley, G.J., Wang, Z. and Jia, Y. (2017). Migration and cutoff of meanders in the hyperarid environment of the middle Tarim River, northwestern China. *Geomorphology*, 276, 116-124.

Li, Z., Gao, P., You, Y., Finotello, A. & Ielpi, A. (2023) Delayed neck cutoff in the meandering Black River of the Qinghai–Tibet plateau. *Earth Surface Processes and Landforms*, 1– 12.

Liu, X., Huang, H. Q., & Nanson, G. C. (2016). The morphometric variation of islands in the middle and lower Yangtze River: a variational analytical explanation. *Geomorphology*, 261, 273-281.

Liu, Y., Wang, X., Su, Q., Yi, S., Miao, X., Li, Y., & Lu, H. (2021). Late Quaternary terrace formation from knickpoint propagation in the headwaters of the Yellow River, NE Tibetan Plateau. *Earth Surface Processes and Landforms*, *46*(14), 2788-2806.

Liverpool, T. B., & Edwards, S. F. (1995). Dynamics of a meandering river. *Physical review letters*, *75*(16), 3016.

Magdaleno, F., Fernández-Yuste, J.A. (2011). Meander dynamics in a changing river corridor. *Geomorphology*, 130(3-4), 197-207.

Makaske, B. (2001). Anastomosing rivers: a review of their classification, origin and sedimentary products. *Earth-Science Reviews*, 53(3-4), 149-196.

Makaske, B., Smith, D. G., & Berendsen, H. J. (2002). Avulsions, channel evolution and floodplain sedimentation rates of the anastomosing upper Columbia River, British Columbia, Canada. *Sedimentology*, *49*(5), 1049-1071.

Makaske, B., Smith, D. G., Berendsen, H. J., de Boer, A. G., van Nielen-Kiezebrink, M. F., & Locking, T. (2009). Hydraulic and sedimentary processes causing anastomosing morphology of the upper Columbia River, British Columbia, Canada. *Geomorphology*, *111*(3-4), 194-205.

Markham, A.J., & Thorne, C.R., 1992. Geomorphology of gravel-bed river bends. Dynamics of gravel-bed rivers, 433-450.

Mason, J., & Mohrig, D. (2019). Differential bank migration and the maintenance of channel width in meandering river bends. *Geology*, *47*(12), 1136-1140.

Mendoza, A., Abad, J. D., Frias, C. E., Ortals, C., Paredes, J., Montoro, H., ... & Soto Cortés, G. (2016). Planform dynamics of the Iquitos anabranching structure in the Peruvian Upper Amazon River. *Earth Surface Processes and Landforms*, 41(7), 961-970.

Mertes, L. A., Dunne, T., & Martinelli, L. A. (1996). Channel-floodplain geomorphology along the Solimões-Amazon river, Brazil. *Geological Society of America Bulletin*, *108*(9), 1089-1107.

Meshkova, L. V., & Carling, P. A. (2013). Discrimination of alluvial and mixed bedrock–alluvial multichannel river networks. *Earth Surface Processes and Landforms*, *38*(11), 1299-1316.

Micheli, E.R., Kirchner, J.W. and Larsen, E.W. (2004). Quantifying the effect of riparian forest versus agricultural vegetation on river meander migration rates, Central Sacramento River, California, USA. *River Research and Applications*, 20(5), 537-548.

Miranda, L. E. (2005). Fish assemblages in oxbow lakes relative to connectivity with the Mississippi River. *Transactions of the American Fisheries Society*, *134*(6), 1480-1489.

Morais, E.S., Rocha, P.C., Hooke, J., 2016. Spatiotemporal variations in channel changes caused by cumulative factors in a meandering river: The lower Peixe River, Brazil. Geomorphology, 273, 348-360.

Morón, S., Edmonds, D. A., & Amos, K. (2017). The role of floodplain width and alluvial bar growth as a precursor for the formation of anabranching rivers. *Geomorphology*, 278, 78-90.

Mueller, E.R., & Pitlick, J. (2014). Sediment supply and channel morphology in mountain river systems: 2. Single thread to braided transitions. *Journal of Geophysical Research: Earth Surface, 119*, 1516 - 1541.

Nanson, G. C. (2013). Anabranching and anastomosing rivers. In J. F. Shroder (Ed.), *Treatise on geomorphology* (Vol. 9, pp. 330–345). Academic Press.

Nanson, G. C., & Huang, H. Q. (1999). Anabranching rivers: divided efficiency leading to fluvial diversity. In A. J. Miller and A. Gupta (editors), *Varieties of Fluvial Form*, 7, 477-494, John Wiley & Sons, Inc.

Nanson, G. C., & Huang, H. Q. (2017). Self-adjustment in rivers: Evidence for least action as the primary control of alluvial-channel form and process. *Earth Surface Processes and Landforms*, *42*(4), 575-594.

Nanson, G. C., & Knighton, A. D. (1996). Anabranching rivers: their cause, character and classification. *Earth Surface Processes and Landforms*, 21(3), 217-239.

Nanson, G.C. (1980). Point bar and floodplain formation of the meandering Beatton River, northeastern British Columbia, Canada. *Sedimentology*, 27(1), 3-29.

Nanson, G.C., Hickin, E.J. (1983). Channel migration and incision on the Beatton river. *Journal of Hydraulic Engineering*, 109(3), 327-337.

Nicholas, A. P. (2013). Modelling the continuum of river channel patterns. *Earth Surface Processes and Landforms*, *38*(10), 1187-1196.

Nicholas, A. P., Ashworth, P. J., Smith, G. S., & Sandbach, S. D. (2013). Numerical simulation of bar and island morphodynamics in anabranching megarivers. *Journal of Geophysical Research: Earth Surface*, 118(4), 2019-2044.

Nicoll, T. J., & Hickin, E. J. (2010). Planform geometry and channel migration of confined meandering rivers on the Canadian prairies. *Geomorphology*, *116*(1-2), 37-47.

Nicoll, T., Brierley, G., & Yu, G. A. (2013). A broad overview of landscape diversity of the Yellow River source zone. *Journal of Geographical Sciences*, *23*(5), 793-816.

Ollero, A. (2010). Channel changes and floodplain management in the meandering middle Ebro River, Spain. *Geomorphology*, 117(3-4), 247-260.

Osterkamp, W. R. (1998). Processes of fluvial island formation, with examples from Plum Creek, Colorado and Snake River, Idaho. *Wetlands*, *18*(4), 530-545.

Palmer, M. A., Bernhardt, E. S., Allan, J. D., Lake, P. S., Alexander, G., Brooks, S., ... & Sudduth, E. (2005). Standards for ecologically successful river restoration. *Journal of applied ecology*, *42*(2), 208-217.

Park, E. (2020). Characterizing channel-floodplain connectivity using satellite altimetry: Mechanism, hydrogeomorphic control, and sediment budget. *Remote Sensing of Environment*, *243*, 111783.

Park, E., & Latrubesse, E. M. (2017). The hydro-geomorphologic complexity of the lower Amazon River floodplain and hydrological connectivity assessed by remote sensing and field control. *Remote Sensing of Environment*, *198*, 321-332.

Parker, G., Diplas, P., Akiyama, J. (1983). Meander bends of high amplitude. *Journal of Hydraulic Engineering*, 109(10), 1323-1337.

Perucca, E., Camporeale, C., Ridolfi, L. (2007). Significance of the riparian vegetation dynamics on meandering river morphodynamics. *Water Resources Research*, 43(3).

Phillips, J. D. (2013). Hydrological connectivity of abandoned channel water bodies on a coastal plain river. *River Research and Applications*, *29*(2), 149-160.

Poff, N. L., Allan, J. D., Bain, M. B., Karr, J. R., Prestegaard, K. L., Richter, B. D., ... & Stromberg, J. C. (1997). The natural flow regime. *BioScience*, *47*(11), 769-784.

Qiu, P., Wu, N., Luo, P., Wang, Z., & Li, M. (2009). Analysis of dynamics and driving factors of wetland landscape in Zoige, Eastern Qinghai-Tibetan Plateau. *Journal of Mountain Science*, *6*(1), 42-55.

Rhoads, B. L. (2020). *River dynamics: Geomorphology to support management*. Cambridge University Press.

Richards, D., & Konsoer, K. (2020). Morphologic adjustments of actively evolving highly curved neck cutoffs. *Earth Surface Processes and Landforms*, *45*(4), 1067-1081.

Richards, D., Konsoer, K., Langendoen, E., Ursic, M., & Constantine, J. (2022). Depositional patterns of slowly plugging neck cutoffs from core analysis and estimates of bedload transport, White River, Arkansas. *Sedimentology*, *69*(2), 568-591.

Riquier, J., Piégay, H., Lamouroux, N., & Vaudor, L. (2017). Are restored side channels sustainable aquatic habitat features? Predicting the potential persistence of side channels as aquatic habitats based on their fine sedimentation dynamics. *Geomorphology*, *295*, 507-528.

Rokni, K., Ahmad, A., Selamat, A., & Hazini, S. (2014). Water feature extraction and change detection using multitemporal Landsat imagery. *Remote Sensing*, *6*(5), 4173-4189.

Rosgen, D. L. (1994). A classification of natural rivers. *Catena*, *22*(3), 169-199.

Rowland, J. C., Lepper, K., Dietrich, W. E., Wilson, C. J., & Sheldon, R. (2005). Tie channel sedimentation rates, oxbow formation age and channel migration rate from optically stimulated luminescence (OSL) analysis of floodplain deposits. *Earth Surface Processes and Landforms: The Journal of the British Geomorphological Research Group*, *30*(9), 1161-1179.

Rowland, J. C., Shelef, E., Pope, P. A., Muss, J., Gangodagamage, C., Brumby, S. P., & Wilson, C. J. (2016). A morphology independent methodology for quantifying planview river change and characteristics from remotely sensed imagery. *Remote Sensing of Environment*, *184*, 212-228.

Rowland, J. C., Dietrich, W. E., Day, G., and Parker, G. (2009), Formation and maintenance of single-thread tie channels entering floodplain lakes: Observations from three diverse river systems, *J. Geophys. Res.*, 114, F02013. https://doi.org/10.1029/2008JF001073

Rust B. (1978). A classification of alluvial channel systems. In *Fluvial Sedimentology*. Canadian Society of Petroleum Geologists: Calgary, Canada; 187–198.

Sambrook Smith, G. H. (1996). Bimodal fluvial bed sediments: origin, spatial extent and processes. *Progress in Physical Geography*, *20*(4), 402-417.

Schumm, S. A. (1985). Patterns of alluvial rivers. Annual Review of Earth and Planetary *Sciences*, 13(1), 5-27.

Schuurman, F., & Kleinhans, M. G. (2015). Bar dynamics and bifurcation evolution in a modelled braided sand-bed river. *Earth Surface Processes and Landforms*, *40*(10), 1318-1333.

Schwendel, A., Aalto, R., Nicholas, A., & Parsons, D. (2018). Fill characteristics of abandoned channels and resulting stratigraphy of a mobile sand-bed river floodplain. *Fluvial Meanders and Their Sedimentary Products in the Rock Record*, 251-272.

Schwendel, A.C., Nicholas, A.P., Aalto, R.E., Sambrook Smith, G.H., Buckley, S. (2015). Interaction between meander dynamics and floodplain heterogeneity in a large tropical sand‐bed river: the Rio Beni, Bolivian Amazon. *Earth Surface Processes and Landforms*, 40(15), 2026-2040.

Schwenk, J., Khandelwal, A., Fratkin, M., Kumar, V., Foufoula-Georgiou, E. (2017). High spatiotemporal resolution of river planform dynamics from Landsat: The RivMAP toolbox and results from the Ucayali river. *Earth and Space Science* (Hoboken, N.J.), 4(2), 46-75.

Seminara, G. (2006). Meanders. *Journal of Fluid Mechanics*, 554, 271- 297.

Shen, Z., Aeschliman, M., & Conway, N. (2021). Paleodischarge reconstruction using oxbow lake sediments complicated by shifting hydrological connectivity. *Quaternary International*, *604*, 75-81.

Simon, A., Collison, A.J. (2002). Quantifying the mechanical and hydrologic effects of riparian vegetation on streambank stability. *Earth surface Processes and Landforms*, 27(5), 527-546.

Singh, K. V., Setia, R., Sahoo, S., Prasad, A., & Pateriya, B. (2015). Evaluation of NDWI and MNDWI for assessment of waterlogging by integrating digital elevation model and groundwater level. *Geocarto International*, *30*(6), 650-661.

Słowik, M. (2018). The formation of an anabranching planform in a sandy floodplain by increased flows and sediment load. *Earth Surface Processes and Landforms*, 43(3), 623-638.

Smith, C. E. (1998). Modeling high sinuosity meanders in a small flume. *Geomorphology*, *25*(1-2), 19-30.

Smith, D. G., & Smith, N. D. (1980). Sedimentation in anastomosed river systems; examples from alluvial valleys near Banff, Alberta. *Journal of Sedimentary Research*, 50(1), 157-164.

Srivastava, G. S., I. B. Singh, and A. K. Kulshrestha (2014), Geomorphic and Tectonic features of Punjab-Haryana Plain as identified from Digital Elevation Model and surface profiles, *Himalayan Geology*, *35*(2), 97-109.

Stølum, H. H. (1996). River meandering as a self-organization process. *Science*, *271*(5256), 1710–1713.

Stølum, H. H. (1998). Planform geometry and dynamics of meandering rivers. *Geological Society of America Bulletin*, *110*(11), 1485-1498.

Surian, N., & Rinaldi, M. (2003). Morphological response to river engineering and management in alluvial channels in Italy. *Geomorphology*, *50*(4), 307-326.

Sylvester, Z., Durkin, P., & Covault, J. A. (2019). High curvatures drive river meandering. *Geology*, *47*(3), 263-266.

Szewczyk, L., Grimaud, J. L., Cojan, I., & Piegay, H. (2022). Bedload infilling and depositional patterns in chute cutoffs channels of a gravel-bed river: The Ain River, France. *Earth Surface Processes and Landforms*, *47*(2), 459-476.

Tal, M., & Paola, C. (2010). Effects of vegetation on channel morphodynamics: results and insights from laboratory experiments. *Earth Surface Processes and Landforms*, *35*(9), 1014-1028.

Thorne CR. (1991). Bank erosion and meander migration of the Red and Mississippi Rivers, USA. Hydrology for the Water Management of Large River Basins: 20th General Assembly of the

International Union of Geodesy and Geophysics, Vienna. International Association of Hydrological Sciences, 301-313.

Thorne, C. R., Hey, H. D., & Newson, M. D. (1997). *Applied Fluvial Geomorphology for River Engineering and Management*. John Wiley & Sons: New York.

Toonen, W. H., Kleinhans, M. G., & Cohen, K. M. (2012). Sedimentary architecture of abandoned channel fills. *Earth Surface Processes and Landforms*, *37*(4), 459-472.

Tooth, S., & McCarthy, T. S. (2004). Anabranching in mixed bedrock-alluvial rivers: the example of the Orange River above Augrabies Falls, Northern Cape Province, South Africa. *Geomorphology*, *57*(3-4), 235-262.

Tooth, S., & Nanson, G. C. (1999). Anabranching rivers on the Northern Plains of arid central Australia. *Geomorphology*, 29(3-4), 211-233.

Tooth, S., Jansen, J. D., Nanson, G. C., Coulthard, T. J., & Pietsch, T. (2008). Riparian vegetation and the late Holocene development of an anabranching river: Magela Creek, northern Australia. *Geological Society of America Bulletin*, 120(7-8), 1021-1035.

U.S. Geological Survey, 2022, Landsat TM and OLI imagery, accessed at URL https://earthexplorer.usgs.gov/.

Van den Berg, J. H. (1995). Prediction of alluvial channel pattern of perennial rivers. *Geomorphology*, 12(4), 259-279.

Van Dijk, W. M., Van de Lageweg, W. I., & Kleinhans, M. G. (2012). Experimental meandering river with chute cutoffs. *Journal of Geophysical Research: Earth Surface*, *117*(F3).

Vayssière, A., Castanet, C., Gautier, E., Virmoux, C., Depret, T., Gandouin, E., Develle, A.L., Mokadem, F., Saulnier-Copard, S., Sabatier, P. and Carcaud, N. (2020). Readjustments of a sinuous river during the last 6000 years in northwestern Europe (Cher River, France): From an active meandering river to a stable river course under human forcing. *Geomorphology*, *370*, 107395.

Wainwright, J., Turnbull, L., Ibrahim, T. G., Lexartza-Artza, I., Thornton, S. F., & Brazier, R. E. (2011). Linking environmental regimes, space and time: Interpretations of structural and functional connectivity. *Geomorphology*, *126*(3-4), 387-404.

Wang, B., Smith, L. C., Yang, X., Pavelsky, T. M., Altenau, E. H., Gleason, C. J., ... & Bates, P. D. (2022). Remote sensing of broad-scale controls on large river anabranching. *Remote Sensing of Environment*, *281*, 113243.

Wang, D., Li, Z., Li, Z., Pan, B., Tian, S., & Nie, X. (2020). Environmental gradient relative to oxbow lake-meandering river connectivity in Zoige Basin of the Tibetan Plateau. *Ecological Engineering*, *156*, 105983. https://doi.org/10.1016/j.ecoleng.2020.105983

Wang, D., Ma, Y., Liu, X., Huang, H. Q., Huang, L., & Deng, C. (2019). Meandering-anabranching river channel change in response to flow-sediment regulation: Data analysis and model validation. *Journal of Hydrology*, *579*, 124209.

Wang, J., Pan, B., Zhang, G., Cui, H., Cao, B., & Geng, H. (2013). Late Quaternary glacial chronology on the eastern slope of Gongga Mountain, eastern Tibetan Plateau, China. *Science China Earth Sciences*, *56*(3), 354-365.

Wang, N., Zha, X., Huang, C., Zhang, Y., Zhou, Y., Pang, J., ... & Chai, J. (2023). Age and causes of the Yellow River dissecting the Zoige Basin in the eastern Tibetan Plateau, China. *Science of The Total Environment*, *857*, 159481. https://doi.org/10.1016/j.scitotenv.2022.159481

Weihaupt, J. G. (1977). Morphometric definitions and classifications of oxbow lakes, Yukon River Basin, Alaska. *Water Resources Research*, *13*(1), 195-196.

Wende, R., & Nanson, G. C. (1998). Anabranching rivers: ridge-form alluvial channels in tropical northern Australia. *Geomorphology*, *22*(3-4), 205-224.

Winterbottom, S. J. (2000). Medium and short-term channel planform changes on the Rivers Tay and Tummel, Scotland. *Geomorphology*, *34*(3-4), 195-208.

Wohl, E. (2005). Compromised rivers: understanding historical human impacts on rivers in the context of restoration. *Ecology and Society*, *10*(2).

Wohl, E. (2019). Forgotten legacies: understanding and mitigating historical human alterations of river corridors. *Water Resources Research*, *55*(7), 5181-5201.

Wohl, E., Lane, S. N., & Wilcox, A. C. (2015). The science and practice of river restoration. *Water Resources Research*, *51*(8), 5974-5997.

Wolfe, B. B., Hall, R. I., Last, W. M., Edwards, T. W., English, M. C., Karst-Riddoch, T. L., ... & Palmini, R. (2006). Reconstruction of multi-century flood histories from oxbow lake sediments, Peace-Athabasca Delta, Canada. *Hydrological Processes: An International Journal*, *20*(19), 4131-4153.

Wong, M., & Parker, G. (2006). Reanalysis and correction of bed-load relation of Meyer-Peter and Müller using their own database. *Journal of Hydraulic Engineering*, *132*(11), 1159-1168.

Wren, D. G., Davidson, G. R., Walker, W. G., & Galicki, S. J. (2008). The evolution of an oxbow lake in the Mississippi alluvial floodplain. *Journal of Soil and Water Conservation*, *63*(3), 129-135.

Wyrick, J. R., & Klingeman, P. C. (2011). Proposed fluvial island classification scheme and its use for river restoration. *River Research and Applications*, *27*(7), 814-825.

Xia, J., Deng, S., Lu, J., Xu, Q., Zong, Q., & Tan, G. (2016). Dynamic channel adjustments in the Jingjiang Reach of the Middle Yangtze River. *Scientific reports*, *6*(1), 1-10.

Xu, H. (2006). Modification of normalised difference water index (NDWI) to enhance open water features in remotely sensed imagery. *International Journal of Remote Sensing*, *27*(14), 3025-3033.

Yang, C., Cai, X., & Wang, X. (2017). Remote sensing of hydrological changes in Tian-e-zhou oxbow lake, an ungauged area of the Yangtze River basin. *Remote Sensing*, *10*(1), 27. https://doi.org/10.3390/rs10010027

Yang, H., Li, Z., Lu, Y., Liu, H., & Zuo, L. (2023). Modelling of cantilever bank failure for peat-type meander bends in the source region of the Yellow River. *International Journal of Sediment Research*, *38*(3), 421-431.

Yao, T., Bolch, T., Chen, D., Gao, J., Immerzeel, W., Piao, S., ... & Zhao, P. (2022). The imbalance of the Asian water tower. *Nature Reviews Earth & Environment*, *3*(10), 618-632.

Yousefi, S., Pourghasemi, H.R., Hooke, J., Navratil, O., Kidová, A. (2016). Changes in morphometric meander parameters identified on the Karoon River, Iran, using remote sensing data. *Geomorphology*, 271, 55-64.

Yu, G. A., Brierley, G., Huang, H. Q., Wang, Z., Blue, B., & Ma, Y. (2014). An environmental gradient of vegetative controls upon channel planform in the source region of the Yangtze and Yellow Rivers. *Catena*, 119, 143-153.

Yu, K. F., Lehmkuhl, F., & Falk, D. (2017). Quantifying land degradation in the Zoige Basin, NE Tibetan Plateau using satellite remote sensing data. *Journal of Mountain Science*, *14*(1), 77-93.

Zeng, M., Zhu, C., Song, Y., Ma, C., & Yang, Z. (2017). Paleoenvironment change and its impact on carbon and nitrogen accumulation in the Z oige wetland, northeastern Qinghai-Tibetan Plateau over the past 14,000 years. *Geochemistry, Geophysics, Geosystems*, *18*(4), 1775-1792.

Zhang, W., Yi, Y., Song, K., Kimball, J. S., & Lu, Q. (2016). Hydrological response of alpine wetlands to climate warming in the eastern Tibetan Plateau. *Remote Sensing*, *8*(4), 336.

Zhou, T., & Zhang, W. (2021). Anthropogenic warming of Tibetan Plateau and constrained future projection. *Environmental Research Letters*, *16*(4), 044039.

Zinger, J.A., Rhoads, B.L., Best, J.L., Johnson, K.K. (2013). Flow structure and channel morphodynamics of meander bend chute cutoffs: A case study of the Wabash River, USA. *Journal of Geophysical Research: Earth Surface*, 118(4), 2468-2487.

Zolezzi, G., Seminara, G. (2001). Downstream and upstream influence in river meandering. Part 1. General theory and application to overdeepening. *Journal of Fluid Mechanics*, 438(13), 183-211.

Xiwei Guo

Ph.D. Candidate of Geography and the Environment, Syracuse University
Email: xguo18@syr.edu

Education

Syracuse University
Doctor of Philosophy in Geography expected 2023

University of Texas, Austin
Master of Arts in Geography 2017

University of Colorado, Boulder
Bachelor of Arts in Geography 2015
Minor: Atmospheric and Oceanic Sciences

Research Projects

Doctoral Dissertation since 2017
"Morphodynamic Diversity of Alluvial River Systems in the Upper Yellow River Watershed, Qinghai-Tibet Plateau"

Master's Thesis 2015-2017
"Morphodynamics of large anabranching rivers: the case of Madeira River, Brazil"

Undergraduate Research Project 2014-2015
"*Impact of largescale fire and bark beetle outbreak on local streams in southern Colorado*"

Teaching Experiences

Instructor 2023

- The Natural Environment
- River Environments

Department of Geography and the Environment
Syracuse University

Teaching Assistant 2017-2022

- Geographic Information Systems
- Environmental Remote Sensing
- The Natural Environment

Department of Geography and the Environment
Syracuse University

Teaching Assistant 2016-2017

- Environmental Geographic Information System
- Process Geomorphology
- Geography of Latin America

- The Natural Environment
- Human Geographies

Department of Geography and the Environment
University of Texas, Austin

Research Assistant 2015
Department of Geography and the Environment
University of Texas, Austin

Publications

Guo, X., Gao, P., & Li, Z. (2023). Hydrologic connectivity and morphologic variation of oxbow lakes in an alpine pristine fluvial system. *Journal of Hydrology*, 129768.

Guo, X., Gao, P., & Li, Z. (2023). Morphodynamic Characteristics of a Complex Anabranching System in the Qinghai-Tibet Plateau and the Implications for Anabranching Stability. *Journal of Geophysical Research: Earth Surface*, *128*(2), e2022JF006788.

Guo, X., Gao, P., & Li, Z. (2021). Morphological characteristics and changes of two meandering rivers in the Qinghai-Tibet Plateau, China. *Geomorphology*, *379*, 107626.

Academic Presentation

Guo, X., Gao, P., & Li, Z. (2022). Inferring Channel-floodplain Connection from Morphological Variations of Oxbow Lakes in the Zoige Basin, Northeastern Qinghai-Tibet Plateau. *American Geophysical Union (AGU) Fall Meeting*. Chicago, IL, USA

Guo, X. & Gao, P. (2022). Channel adjustment, island dynamics, and hydraulic efficiency of a high-order anabranching system in the Upper Yellow River, Qinghai-Tibet Plateau. *American Association of Geographers (AAG) Annual Meeting.* Online

Guo, X. & Gao, P. (2019). Morphological characteristics of alpine meandering channels in Qinghai-Tibet Plateau, China. *American Association of Geographers (AAG) Annual Meeting.* Washington D.C., USA

Guo, X. & Latrubesse, M. E. (2018). Morphodynamics of large anabranching rivers: the case of the Madeira River, Brazil. *American Association of Geographers (AAG) Annual Meeting*, New Orleans, LA, USA

Guo, X. (2016). Complexity of channel patterns: understanding anabranching channel from meandering and braided channels. *Association of American Geographers (AAG) Annual Meeting*, San Francisco, CA, USA

Grants/Awards

University Graduate Fellowship 2022
Syracuse University

Roscoe Martin Grant for Graduate Research 2022
Syracuse University

Summer Dissertation Fellowship 2022
Syracuse University

Moynihan Research Grant 2020
Syracuse University

Roscoe Martin Grant for Graduate Research 2019
Syracuse University

Roscoe Martin Grant for Graduate Research 2017
Syracuse University

Veselka Endowed Fellowship for Field Research 2016
University of Texas, Austin

Professional Development Award 2016
University of Texas, Austin

Undergraduate Research Opportunities Program Grant 2015
University of Colorado, Boulder

International Student of the Year 2014
University of Colorado, Boulder

Membership

- American Association of Geographers
- American Geophysical Union

Languages

- Mandarin Chinese (native)
- English (fluent)

Other Services

President, Chinese Students and Scholars Association 2013-2014
University of Colorado, Boulder

Student Member, Student Group Funding Board of Student Government 2013-2014
University of Colorado, Boulder